

**CZECH TECHNICAL  
UNIVERSITY  
IN PRAGUE**

**FACULTY OF  
MECHANICAL  
ENGINEERING**



**DOCTORAL  
THESIS**

**2018**

**JAKUB  
HORVÁTH**



CZECH TECHNICAL UNIVERSITY  
IN PRAGUE

FACULTY OF MECHANICAL ENGINEERING



INSTITUTE OF MATERIALS ENGINEERING

# **The structural stability of creep resistant austenitic steels SUPER 304H and Tp 347HFG**

**Study program: Mechanical engineering**

**Study field: Materials engineering**

## **DOCTORAL THESIS**

AUTHOR

Ing. JAKUB HORVÁTH, IWE

SUPERVISOR

Doc. Ing. JIŘÍ JANOVEC, CSc.

CONSULTANT

---

## Acknowledgements

I would like to thank to my supervisor Mr. Jiří Janovec for thesis leading and kind consultation. Thanks also to Mr. Josef Čmakal and UJP PRAHA a.s. for providing exposed test material. The main acknowledgments are for my parents Mr. Ladislav Horváth and MRs. Růžena Horváthová for their excellent support and providing opportunity for study. I would like to thank my loved ones and friends for their patience.

---

Declaration

I declare that I have developed this Ph.D. thesis on my own, using listed literature and documents and on the basis of consultations and under the guidance of the supervisor.

In Prague: 3.9.2018

.....  
Ing. Jakub Horváth, IWE  
Signature

---

## Abstract

The sigma phase precipitation can cause serious problems with application of creep resistant austenitic steels. This thesis deals with the SUPER 304H structural stability especially with the sigma phase precipitation. Degraded state of the steel SUPER 304H was reached by an isothermal laboratory exposition. Used exposition temperatures were 650, 675 and 700°C. Maximal exposition time was  $2,45 \times 10^4$  hours. The sigma phase precipitation was confirmed by using various experimental methods (SEM, TEM, EBSD, EDS). Precipitation mechanism and morphology were documented and described. The main part of the thesis was quantification of the sigma phase precipitation and its mathematical description. Equations describing fraction area and precipitation rate of the sigma phase for the steel SUPER 304H are summarised by the thesis. Those equations were extended by using Fick's laws and diffusion equations for steel Tp 347HFG. The thesis documents influence of the sigma phase precipitation on mechanical properties of the steel SUPER 304H and discusses applicability of this steel.

## Keywords:

Structural stability, Sigma phase, SUPER 304H, Tp 347HFG, Modelling

# Content

|         |   |    |
|---------|---|----|
| 1       | Introduction.....   | 4  |
| 1.1     | Current need of reaching the thesis goals .....                                   | 8  |
| 2       | Theoretical part.....   | 12 |
| 2.1     | The creep resistant steels .....  | 12 |
| 2.1.1   | Requirements for creep resistant steels.....                                      | 13 |
| 2.1.2   | The creep resistant steels grouping .....   | 13 |
| 2.1.3   | The austenitic creep resistant steels for USC power plants application....        | 14 |
| 2.1.4   | The alloying elements used for increasing creep resistivity.....                  | 15 |
| 2.1.5   | The precipitates causing embrittlement in austenitic creep resistant steels ..... | 18 |
| 2.2     | The specific austenitic steels from group 18/9 for USC power plants .....         | 23 |
| 2.2.1   | SUPER 304H.....   | 23 |
| 2.2.2   | TP 347HFG.....  | 26 |
| 2.2.3   | The similarity and differences of both steels.....                                | 27 |
| 2.3     | The austenitic 18/9 creep resistant steels structural stability .....             | 30 |
| 2.3.1   | The mechanical properties changes caused by instability .....                     | 33 |
| 2.3.2   | The transformation kinetics .....   | 36 |
| 2.3.2.1 | The applied parameters equations for the degradation description .                | 36 |
| 2.3.3   | The structural constitution modelling.....  | 39 |
| 2.3.3.1 | The basis of commercially used modelling methods .....                            | 43 |
| 3       | The thesis goals.....   | 47 |
| 4       | Methodology .....   | 48 |
| 4.1     | Used experimental materials .....   | 48 |
| 4.2     | The laboratory isothermally ageing .....  | 49 |
| 4.3     | Preparation of the experimental samples .....                                     | 50 |
| 4.3.1   | Preparation.....  | 50 |
| 4.3.2   | Mechanical processing.....  | 50 |
| 4.3.3   | Etching .....   | 51 |
| 4.4     | Description of the used experimental methods .....                                | 51 |
| 4.4.1   | The structural changes study methodology .....                                    | 51 |
| 4.4.1.1 | Optical microscopy .....  | 51 |
| 4.4.1.2 | Scanning electron microscopy (SEM).....   | 52 |
| 4.4.1.3 | Transmission electron microscopy (TEM).....                                       | 53 |
| 4.4.1.4 | The energy dispersive spectroscopy (EDS).....                                     | 54 |
| 4.4.1.5 | The electron backscattered diffraction (EBSD).....                                | 54 |
| 4.4.2   | Mechanical properties testing methods.....  | 55 |

---

|         |   |     |
|---------|---|-----|
| 4.4.2.1 | The tensile test.....   | 55  |
| 4.4.2.2 | The Charpy pendulum impact test.....  | 56  |
| 4.5     | The precipitation and structural modelling.....                                       | 56  |
| 5       | Experimental part.....  | 60  |
| 5.1     | The electron microscopy.....  | 60  |
| 5.1.1   | The sigma phase particles identification.....   | 60  |
| 5.1.2   | The sigma phase precipitation morphology.....   | 70  |
| 5.1.3   | The correlation between the electron and the optical microscopy.....                  | 72  |
| 5.2     | The optical microscopy.....   | 75  |
| 5.2.1   | Evolving of the sigma phase morphology during aging for steel SUPER 304H.....         | 76  |
| 5.2.2   | Evolving of the precipitation kinetics.....   | 81  |
| 5.3     | The mechanical properties testing.....  | 83  |
| 5.3.1   | Tensile testing.....  | 83  |
| 5.3.2   | V notch pendulum testing.....   | 83  |
| 6       | Experimental results discussion.....  | 87  |
| 6.1     | The sigma phase verification and extension for optical microscopy quantification..... | 87  |
| 6.2     | The sigma phase precipitation morphology.....   | 88  |
| 6.3     | The precipitation kinetics curves.....  | 89  |
| 6.4     | Influence of the precipitation to the mechanical properties.....                      | 90  |
| 6.5     | The modelling and achieved results comparison.....                                    | 90  |
| 6.5.1   | Tp 347HFG precipitation rate transformation verification.....                         | 94  |
| 6.6     | The practical application of the thesis results.....                                  | 96  |
| 6.6.1   | The degradation prediction.....   | 96  |
| 6.6.2   | The state of degradation.....   | 96  |
| 6.6.3   | Information for future production of the next steels generation.....                  | 97  |
| 7       | Summary.....  | 98  |
| 7.1     | Meet the thesis goal.....   | 98  |
| 7.2     | The main conclusion description.....  | 99  |
| 7.3     | The practical application recommendation.....   | 99  |
| 7.4     | Proposal of further experimental work on the problem.....                             | 100 |
| 8       | Bibliography.....   | 101 |
| 8.1     | Thesis bibliography.....  | 101 |
| 8.2     | Authors publications.....   | 109 |
| 8.2.1   | Impact and WoS publications.....  | 109 |
| 8.2.2   | Indexed and other publications.....   | 110 |
| 9       | Lists.....  | 113 |
| 9.1     | List of the abbreviations and variables.....  | 113 |

---

**9.2 List of the tables.....116**  
**9.3 List of the figures .....117**



# 1 Introduction

The Czech Republic electricity production development since 2007 to 2016 is summarized by the first graph (Fig. 1). The electricity production figure provides information that most exploited source of energy in the Czech Republic is coal. Fig. 1 also shows long term stability of energy production by coal combusting.

Czech Republic energy production divided into group by the primary energy source is plot in Fig. 2. The source data plotted in the pie chart are from year 2016. Energy made from coal is marked with green colour. In the year 2016 about 55 percent of the Czech total energy production was covered by the coal power plants.

Those two graphs describe the energy production situation in The Czech Republic, but the situation is the same for the industrially developed countries.

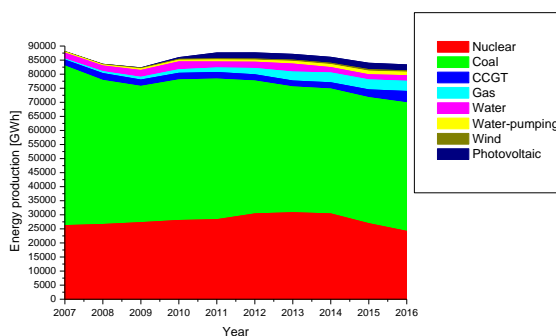


Fig. 1 The electricity production development in the Czech Republic since year 2007 to 2016 [1]

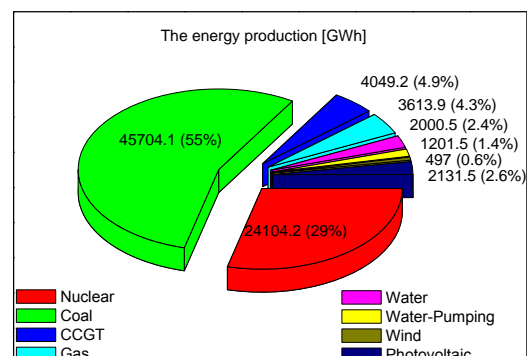


Fig. 2 The constitution of energy production by source in the Czech Republic in year 2016 [1]

The electricity production situation and expected development up to the year 2018 in Japan is described by Fig. 3. The annual energy production from coal is about 22%. It is a half time lower production in comparison with the Czech Republic. Difference is caused by bad availability of primary source (coal) on the island. On the other hand, combusting of coal and natural gas is based on the same physical principal. It means that heat cycle powerplants in Japan hold about 54% of total annual electricity production.

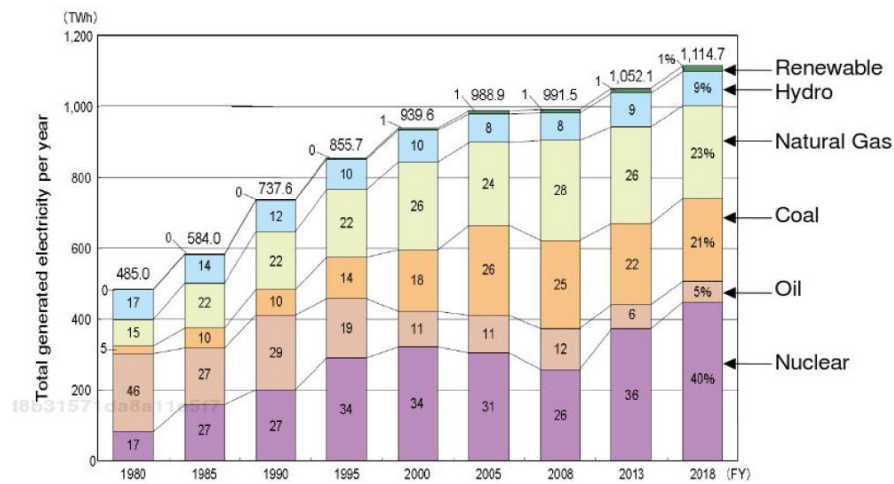


Fig. 3 Annual power generation in Japan [2]

On global scale, it can be said that energy production is based on thermal cycle powerplants. The thermal cycle powerplants cover coal, gas and oil combustion [3]. The global energy production statistics made by the International Energy Agency is plotted in the following graph (Fig. 4). The energy production statistics confirms leader position of coal like a primary energy source. The future prediction suggests continuous increase in the coal-based energy production (Fig. 4).

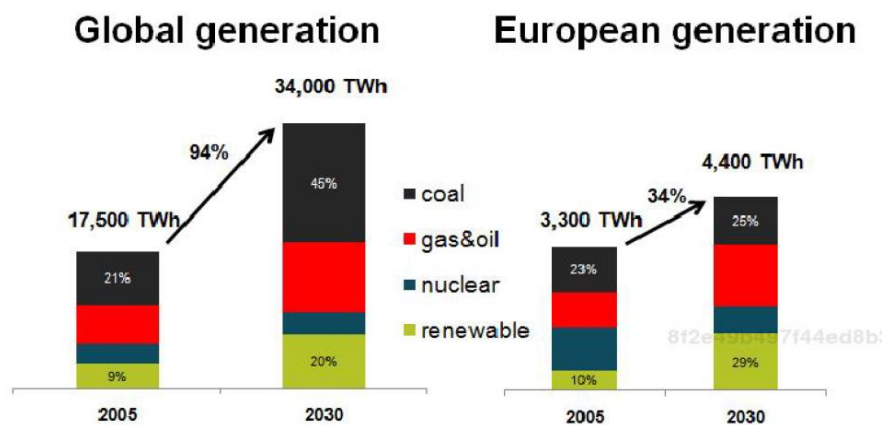


Fig. 4 IEA predictions for the development of power production divided on primary fuels [4]

If we considered the coal not to be renewable source of the energy it is necessary to pay attention to make the best use of this resource. That is motivation for increasing the efficiency of coal powerplants. In case of the heat cycle power plants the higher efficiency means better operation ecology.

Possible way how to increase the power plant efficiency and at the same time the operating ecology is by getting to the higher steam operation condition. Steam operating conditions are pressure and temperature of the steam.

The heat power plants are based on the Rankin-Claus heat cycle. The heat cycle efficiency is directly proportional to the lower and the higher cycle temperature. The fact about the efficiency increasing is historically known so there is continuously effort in reaching higher cycle temperature and pressure.

The influence on the power plant effectivity by reaching higher operating steam parameters was published in [2]. The article summarized case study of the four case-model differences by steam parameter for 500MW power plant. Parameters for each case study part are summarized in Fig. 5. Calculated thermal efficiency of each model parameters power plants is summarized in Fig. 6.

In fact, the difference between parameters (Fig. 5) is just the difference in the USC power plants group. Case D can be marked like the USC power plant with lower working parameters; on the other hand, Case A can be marked like the A-USC power plant. Increase in the complex thermal efficiency is considerable (increase by 12 %) and definitely very interesting for future production of energy from coal.

|        |  |           |
|--------|--|-----------|
| Case A | Double Reheat                            |           |
|        | Main Steam Pressure                      | 35 MPa    |
|        | Main Steam Temperature                   | 700 deg-C |
|        | 1 <sup>st</sup> Reheat Steam Temperature | 720 deg-C |
|        | 2 <sup>nd</sup> Reheat Steam Temperature | 720 deg-C |
| Case B | Single Reheat                            |           |
|        | Main Steam Pressure                      | 25 MPa    |
|        | Main Steam Temperature                   | 700 deg-C |
|        | Reheat Steam Temperature                 | 720 deg-C |
| Case C | Single Reheat                            |           |
|        | Main Steam Pressure                      | 24.1 MPa  |
|        | Main Steam Temperature                   | 610 deg-C |
|        | Reheat Steam Temperature                 | 720 deg-C |
| Case D | Single Reheat                            |           |
|        | Main Steam Pressure                      | 25 MPa    |
|        | Main Steam Temperature                   | 600 deg-C |
|        | Reheat Steam Temperature                 | 600 deg-C |

Fig. 5 Four case study parameters set up for the 500MW power plant [2]

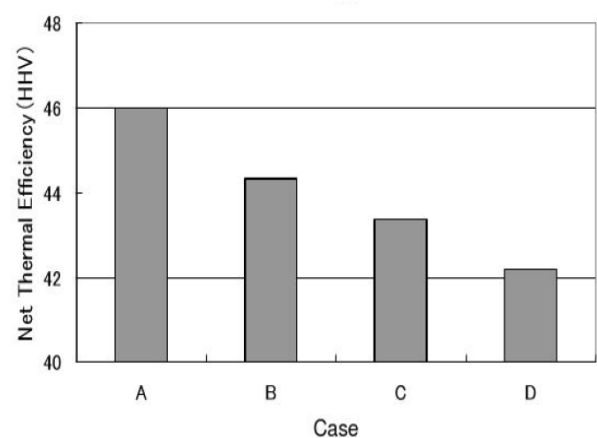


Fig. 6 Estimate thermal efficiency for parameters listed in Fig. 5 [2]

The increase in efficiency is considerable in lower costs of produced energy. EPRI economy analysis considering the beneficial of higher steam parameters is presented in [5]. Powerplants divided into groups sorted by operation parameters published in report [5] are summarized in Fig. 7.

|                    | Sub-critical | Supercritical | Current USC | A-USC |
|--------------------|--------------|---------------|-------------|-------|
| SH Temperature, °C | 541          | 582           | 604         | 680   |
| SH pressure, bar   | 179          | 262           | 276         | 352   |
| RH temperature, °C | 541          | 582           | 604         | 700   |
| RH pressure, bar   | 35.9         | 57.9          | 65.5        | 73.5  |

Fig. 7 Design parameters for the power plants examined in EPRI's 2008 study [5]

The same grouping like in Fig. 7 is used for economy analysis summarized in Fig. 8. The analysis considers the coal price, power plant capital cost, dispatch cost Etc. Analysis was made for power plant situated in Kenosha, Wisconsin. Position of the powerplant ensure relatively cheap and easy to transport coal. According data in Fig. 8 the relatively low delivered cost of coal and with no charges for CO<sub>2</sub> emission does not have A-USC plants cost-of-electricity advantage over the other cases.

|                         | Sub-critical | Supercritical | Current USC | A-USC |
|-------------------------|--------------|---------------|-------------|-------|
| Capital cost, \$/kW     | 1780         | 1800          | 1840        | 1990  |
| Coal cost, \$/GJ        | 1.71         | 1.71          | 1.71        | 1.71  |
| Cost of Electricity*    |              |               |             |       |
| Capital, \$/MWh         | 28.9         | 29.3          | 29.9        | 32.3  |
| O&M, \$/MWh             | 8.1          | 8.1           | 8.2         | 8.6   |
| Fuel, \$/MWh            | 17.0         | 15.9          | 15.7        | 14.4  |
| Total, \$/MWh           | 54.0         | 53.3          | 53.7        | 55.3  |
| Dispatch cost, \$/MWh** | 18.6         | 17.4          | 17.1        | 15.7  |

Fig. 8 Key economic results from A-USC study – Assumes no cost penalty for CO<sub>2</sub> emission [5]

Previous case is acceptable just in case of the low-price coal and without including price of CO<sub>2</sub> production permit.

Following case study published in the other EPRI document [6] includes price of the coal and CO<sub>2</sub> production permits costs. The economic analysis was applied to the schematic coal power plant with installed capacity 750 MW.

The benefit overview reached by increasing of power plant working parameters [6]:

- The steam parameters (A-USC): Temperature 750°C and Pressure 35 MPa
- Efficiency of complex power plant operating under steam parameters listed previously: 45 % (Average subcritical boiler efficiency is about 37 %)
  - With double steam reheating efficiency of 47 % can be reached
  - Money save for coal per year will be 16,4 mil. \$ (that is equal with 330 mil. \$ save during of all the power plant lifetime)
- Decrease of pollution production from 0,85 to 0,67 ton/MWh
  - The drop of CO<sub>2</sub> emission is by 22% (700 000 ton CO<sub>2</sub>/year)
  - It means money save for emission allowances

## **1.1 Current need of reaching the thesis goals**

The last part of chapter 1 (Introduction) documents economic benefits of upgoing to the USC steam parameters. The increment of working parameters is continuous process strongly influenced by available construction materials. Each parameters increment is in connection with the use of the new modification or new materials. Working conditions of the last generation of the USC or A-USC power plants are at the edge of possible steel usage.

Getting to the higher steam parameters is a world-wide effort. Diagram of the continually increasing power plant working parameters in USA is shown in Fig. 9. State in the Mid-Europe (Germany) is documented in Fig. 10. Asian part of the world working steam parameters development is demonstrated by China in Fig. 11 and by Japan in Fig. 12.

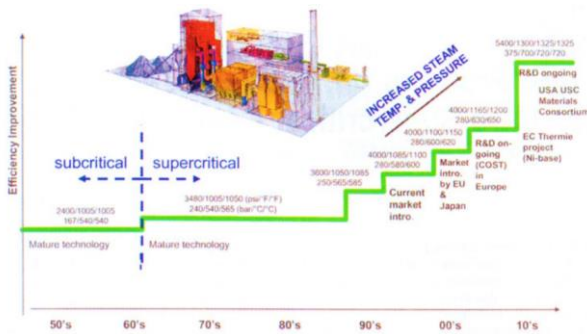


Fig. 9 The scheme of steam working parameters development in USA [6]

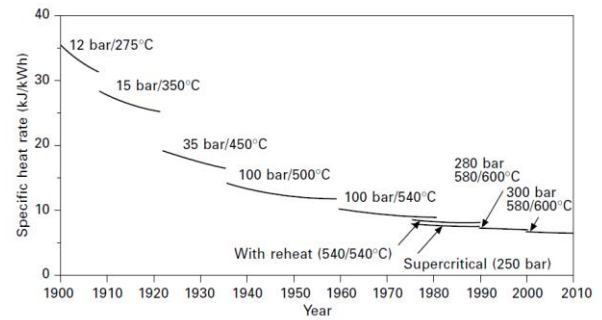


Fig. 10 Heat rate of steam power plants in Germany as a function of steam parameters since the year 1900 [7]

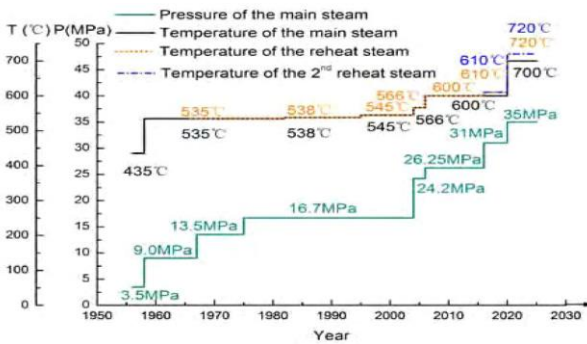


Fig. 11 Steam parameter evolution of Chinese fossil power plants [8]

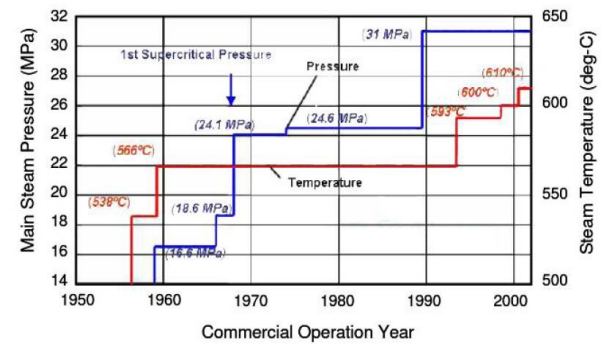


Fig. 12 Trends in steam condition in Japan [2]

Until now, we have mentioned just positives of operating under higher conditions (USC), but there are negatives too. Higher steam operation temperature means higher material thermal load. Higher thermal load can cause series problems by faster material degradation. Second increasing steam parameter is pressure. Higher operation pressure means higher material tension. In case of the creep resistant steels used for the heat exchanging surfaces it causes extreme acceleration of creep process and microstructure degradation. We need to find proper materials, which will be suitable to operate all the projected power plant lifetime under those steam conditions. Creep resistant austenitic steels application can be cost-effective choice for last generation of superheaters.

General requirements to austenitic steel in the superheater application are corrosion resistance, exfoliation resistance and sufficient creep resistance. In literature ([6][9]) steels SUPER 304H and Tp 347HFG are categorized like suitable

for this type of application. Both steels were designed especially for superheaters and reheaters. Producers of these types of steel are Sumitomo Corporation and Manesman. Producers and developers are the same organisations. It is first problem with steels application, because properties of those steels are guaranteed by their producer based on relatively short time examination.

Both steels were developed by chemical composition modification of the classic corrosion resistant steel AISI 304. Both steels are relatively newly developed. Steel Tp 347HFG was developed in the early 1980s [7]. Steel SUPER 304H was developed in 2000s [7]. Available tested mechanical properties are just from short time testing. Creep properties and structural stability are measured just partially. Longer creep properties are extrapolated. Extrapolation is definitely useful, but there can be some differences caused by microstructural changes which can occur under the exposition. The same problem was documented in case of the martensitic steels grade. Finally measured mechanical properties were approximately two times lower than the extrapolated.

Both SUPER 304H and Tp 347HFG are type 18/9 (18% chromium and 9% nickel) complexly alloyed creep resistant austenitic steels. The alloying elements are added for improving steels creep resistance. The alloying elements are in case of steel SUPER 304H 0,4% Nb, 0,1% N a 3,0% Cu and carbon content is optimised at value of 0,1% [7]. Steel Tp 347HFG hase higher content of Ni (about 11%) and is modified by 0,9 % Nb [7]. It is possible to categorised those steels like complex-alloyed. The relatively high content of alloying elements leads to thermodynamic instability of those steels. The instability causes phase precipitations during the thermal exposition.

In literature [10] conditions for precipitation of the brittle phases in austenitic steels according to their chemical composition are listed. Steels SUPER 304H and Tp 347HFG meet the conditions. There is a possibility for precipitation of the brittle phases, which deteriorates steel mechanical

properties. It was shown in literature [11], [12], [13] that precipitation of the brittle phases really occurs in those steels under the heat exposition.

Motivation for this thesis is to provide the information about creep resistant 18/9 steels group instability (especially by using group representatives Tp 347HFG and SUPER 304H) and its influence on the mechanical properties and to improve application possibility for those steels usage under USC parameters. Second motivation is to research how to influent precipitation rate by the modification of those steels chemical composition or by the manufacturing process.



## 2 Theoretical part

The thesis theoretical part summarizes information about creep resistant steels with focus on the austenitic steels and its application. Last section of theoretical part summarizes information about structural modelling and methods of modelling.

### 2.1 The creep resistant steels

The most general definition of a creep resistant steel is steel which is resistant to plastic flow under constant stress and elevated temperature. [14][15]

Fig. 13 illustrates creep deformation dependence on time. There are marked primary, secondary and tertiary creep regions. Usually creep resistant steels during their lifetime operate in the secondary creep region. As it seen from Fig. 13 with increasing temperature the secondary creep region is getting smaller. Continuously effort of increasing steam operation temperature and pressure is documented in chapter 1.1. Getting to higher operating temperatures finally means smaller range of the secondary creep range. The newly developed materials like steep SUPER 304H and Tp 347HFG exhibit better creep behaviour in comparison with previous material generation.

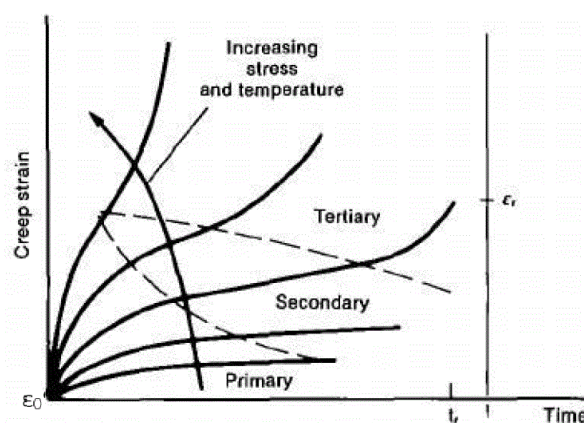


Fig. 13 Schematic illustration of creep curve changes with increasing stress and temperature [15]

The creep resistivity is not only one crucial property of this group of steels. There are other degradation processes and steel requirements.

### **2.1.1 Requirements for creep resistant steels**

Creep-resistant steels for use in thermal power plants must be capable of satisfying the specific requirements established for dependable and economic operation. All phases of development and testing must therefore be specifically aligned to the following requirements [7]:

High thermal efficiency, operational capability in the medium and peak load ranges, life expectancy of at least 200 000 h, high availability, long intervals between overhauls, short overhaul periods, short manufacturing times, competitive production costs for the steam plant and electric power.

These requirements mean that the application of newly developed steels must not involve any additional risks, implying [7]:

That long-time creep testing up to 100 000 h is needed to predict reliably the creep strength for 200 000 h (which means that the tests must be started with a large number of specimens, because at the outset of the tests a prediction cannot be made about the stress level which will be reached after a test period of 100 000 h. A long test period should also be scheduled if a research project is only due to last for 3–5 years), satisfactory oxidation resistance, high ductility of the steels under conditions of creep stressing, high fracture toughness of the steels in a new condition and following prolonged operational stressing, satisfactory production of the new steels in terms of melting, casting, forging, hot forming and welding.

### **2.1.2 The creep resistant steels grouping**

The creep resistant steels are divided into the groups by the steel microstructure. Fig. 14 illustrates increase of the creep resistance through the last century. In figure (Fig. 14) both steels SUPER 304H and Tp 347HFG are marked and other steels grouped by microstructure.

These groups are [7]:

- Ferritic (include martensitic and bainitic)
- Meta-stable austenite
- Stable austenite

Steels SUPER 304H and Tp 347HFG are members of the last group of the stable austenitic steels.

Ferritic steels are applied for boiler water walls and low heat exposed power plant parts. Martensitic steels like P91 are used for thick wall components like steam drivers or stem headers. Meta stable austenitic steels were applied for the low exposed (or older) heat exchanger surfaces for steam reheating. Last group of stable austenitic steels are used for construction of superheaters and reheaters of USC power plants. [7][16]

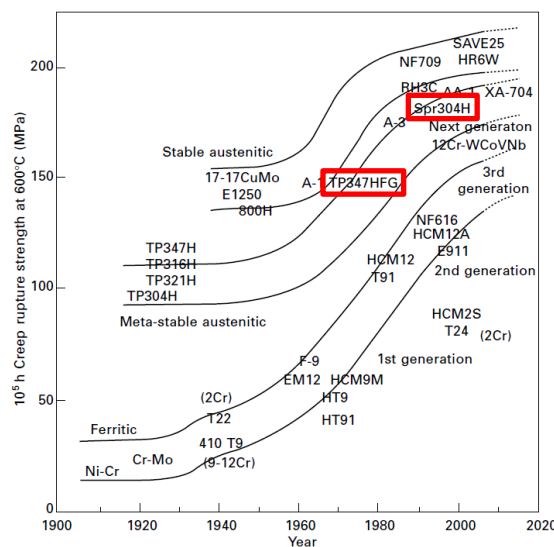


Fig. 14 Historical improvement in creep rupture strength of boiler steels [7]

### 2.1.3 The austenitic creep resistant steels for USC power plants application

Complex design of the heat power plant must be cost effective. With consideration of the austenitic steels price, application must be for most heat exposed parts like superheaters and reheaters (Fig. 15).

| Component                            | 1100°F/1100°F               | 1150°F/1150°F               | 1200°F/1200°F               | 1300°F/1300°F <sup>(2)</sup>                      | 1350°F/1400°F <sup>(3)</sup>       |
|--------------------------------------|-----------------------------|-----------------------------|-----------------------------|---|------------------------------------|
| SH Outlet Header/<br>Main steam pipe | P91, P92, E911              | P92, P122, E911,<br>SAVE 12 | NF12,<br>CCA617             | Nimonic263,<br>CCA617                             | IN740                              |
| RH Outlet Header/RH pipe             | P91, P92, E911              | P91, P92, E911              | Same as above               | Nimonic263  | IN740                              |
| SH panels (4)                        | Super304H,<br>HR3C, 347HFG  | Super304H,<br>HR3C, 347HFG  | NF 709, Cr 30A              | Super304H,<br>Sanicro25, HR3C,<br>Super304H, 310N | IN617<br>347HFG                    |
| Finish SH (4)                        | Super 304H, HR3C,<br>347HFG | HR6W,<br>HR120, HR3C        | IN617                       | IN617, IN740                                      | IN740                              |
| Primary RH (4)                       | Super304H, HR3C,<br>347HFG  | Super304H, H<br>R3C, 347HFG | NF709, Cr 30A,<br>Super304H | Sanicro 25, HR 3C,<br>Super304H                   | 304H,<br>347HFG                    |
| Finish RH (4)                        | Super304H, HR3C,<br>347HFG  | Super304H,<br>HR3C, 47HFG   | IN617                       | IN617, IN740                                      | Haynes 230,<br>Super304H,<br>HR120 |
| Economizer                           | SA 210C                     | SA 210C                     | SA 210C                     | SA 210C   | SA 210C                            |
| Lower waterwall                      | T11, T12, T22               | T22                         | T22                         | T23   | T23                                |
| Upper waterwall                      | T 23, HCM12                 | T23, HCM12                  | HCM12, T23                  | Ti B1010, 7Cr Mo V<br>T23, HCM12                  | T92, HCM12                         |

1: Steam pressure of 4500 psi is assumed for this table; 2: Based on European AD700 Project; 3: Based on DOE/OCD/O Project; 4: For corrosive, high sulfur low NOx conditions SH/RH and waterwall tubes may require weld overlay or cladding with IN72 (42% Cr). Table 1 is for general information only, and does not include all the nuances considered by the designer. The service condition listed in each column represents the maximum conditions of exposure.

Fig. 15 Bill of Materials for various components of USC and A-USC coal-fired power plant boiler steam condition[9]

## 2.1.4 The alloying elements used for increasing creep resistivity

Increasing of creep resistance through the evolved steel generation illustrated in Fig. 14 has another connection. Each of creep resistant steels generation has higher content of alloying elements than previous ones.

For group of stable austenitic steels various ways for creep resistance improving were used. Scheme for austenitic steels is displayed in Fig. 16.

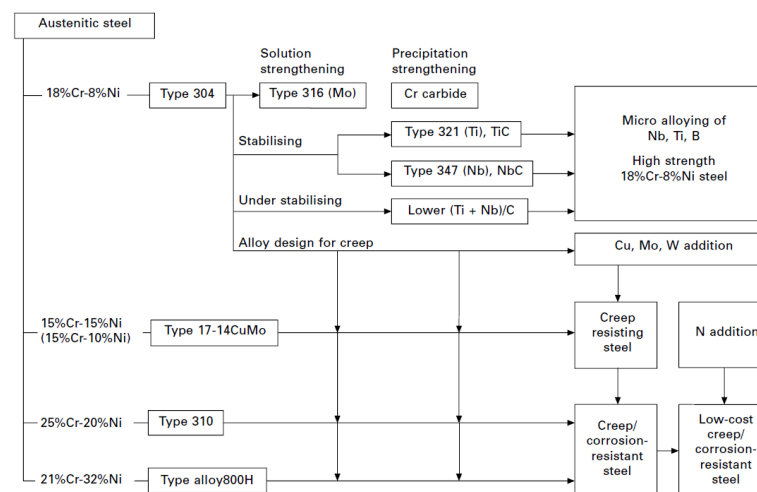


Fig. 16 General concept of alloy design for austenitic heat-resistant steels [7]

Alloying elements used for creep resistant increasing are Mo, Nb, Ti, V, W, N, B, Co [16].

Changes of mechanical properties are affected by many factors. Precipitation processes, changes at grain boundaries and grain coarsening mainly influence mechanical properties [16]. All the processes closely relate to the type and content of alloying elements. Following elements groups are set according to the type of interaction in the steel.

Dividing of the influence of elements [6],[16]:

- Interstitial elements, secondary phase precipitation – C, N
- Dissolving in steel matrix (matrix distortion - hardening) – Mo, W, V, Co
- Stabilizing elements by precipitation carbonitrides – Ti, Nb, Ta, Zr
- Elements ingoing to secondary phases – Cr, V, Nb,

The alloying elements influence:

Cr Ferritic area stable element, ensures steel corrosion resistance, over temperature 500°C precipitation of the chromium carbide  $M(Cr)_{23}C_6$ , if there are suitable conditions can precipitate like sigma phase ( $\sigma$  phase)

Ni Austenitic area stable element, dissolving in the steel matrix, influence to maximal solubility of carbon in matrix, higher nickel content decrease carbon solubility [16]

Nb Alloying by niobium stabilized austenitic steels by reacting with carbon and decreasing the sigma phase precipitation rate [16]. Maximal benefit for creep rupture strength have alloying by 0,7 % [16]. The beneficial effect of alloying Nb is presented in Fig. 17

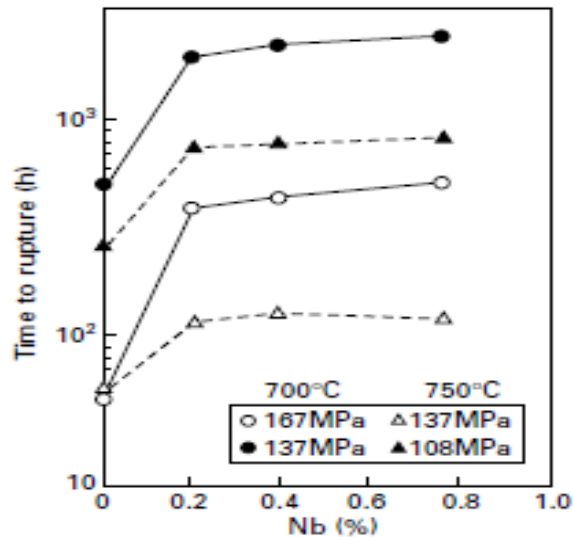


Fig. 17 Effect of Nb on creep rupture strength of 18Cr-8Ni steels [7]

C and N Interstitial elements, precipitation of secondary phases, significant influence on creep rupture strength, precipitation of carbides or carbo-nitrides, precipitation causes decreasing of interstitial hardening, on the other hand increases steel precipitation hardening

Ti Stabilising steel by reacting with carbon, fine titanium carbides precipitation decreases or avoids precipitation rate of chromium carbides at the grain boundaries, stabilisation influence to the steel is lower than by niobium. Ti and Nb combined contribution to creep resistance illustrate Fig. 18

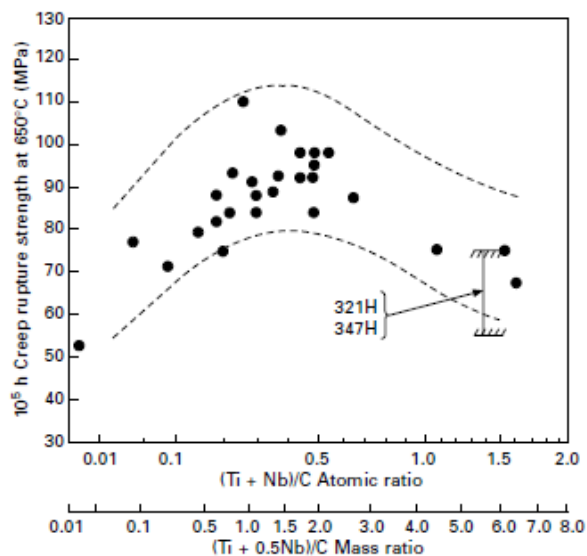


Fig. 18 Effect of (Ti + Nb)/C ratio on creep rupture strength of 18Cr10NiNbTi steel [7]

B Partially precipitates in  $M_{23}C_6$  carbides and partially at the interface between carbide-matrix [6], boron atomic size (0,095 nm) leads to high interstitial hardening of steel, another possibilities of placing the boron atoms are grain boundary defect areas [16], which decrease sliding of grain boundaries during creep exposition, lower grain boundaries movability provides steel creep resistance, boron affects precipitation of carbides and sigma phase at grain boundaries [16], benefit of boron alloying to steel creep resistance is documented over content of 0,0005%, usual range of boron alloying is 0,005 to 0,07% [16]. Maximal boron content in steels is set as the beginning of the boron particles precipitation.

Cu Precipitation hardening by fine disperses Cu rich phases [6]. Copper alloying influence to properties of steel SUS 304H is described in [17]. Benefit of alloying is increasing of steel creep resistance. There is information about increasing of stress corrosion cracking resistance by copper alloying. The beneficial effect of alloying Cu is presented in Fig. 19

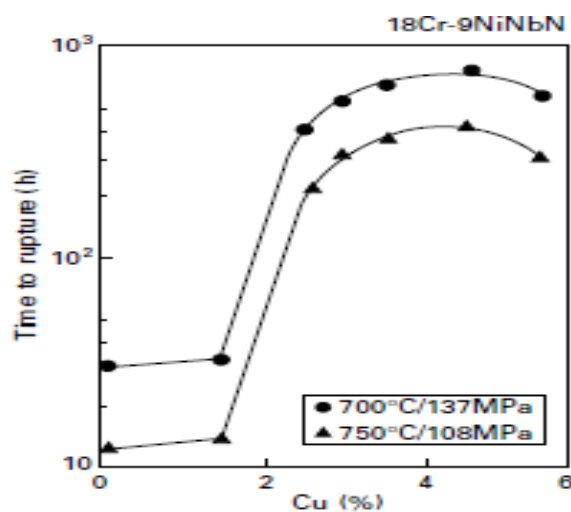


Fig. 19 Effect of Cu on creep rupture strength of 18Cr-8Ni steels [7]

### 2.1.5 The precipitates causing embrittlement in austenitic creep resistant steels

Embrittlement of the austenitic steels from group 18/9 is in general caused by precipitation of the intermetallic phase. Name of those precipitation groups is the sigma phase. The sigma phase precipitates in Fe-Cr system. Precipitation of a sigma phase leads to the serious alloy embrittlement.

The sigma phase early precipitation stages were first time identification in year 1907 [10].

The sigma phase may precipitate in several variations, depending on the chemical composition of the steel. Fig. 20 illustrates different chemical composition of the sigma phase and its lattice parameters.

| Alloy                 | Lattice parameter (Å)                          | Composition of phase (wt%) |       |       |       |     | Formula            |
|-----------------------|--|----------------------------|-------|-------|-------|-----|--------------------|
|                       |  | Fe                         | Cr    | Ni    | Mo    | Si  |                    |
| Fe-Cr                 | $a_0 = 8.799, c_0 = 4.544$                     |                            |       |       |       |     | Fe-Cr              |
| Fe-Mo                 | $a_0 = 9.188, c_0 = 4.812$                     |                            |       |       |       |     | Fe-Mo              |
| 17Cr-11Ni-2Mo-0.4Ti   | —  |                            | 30    | 4.3   | 9     | 0.8 | $(FeNi)_x(CrMo)_y$ |
| 17Cr-11Ni-0.9Mo-0.5Ti | —  |                            | 33    | 4.5   | 5.4   | 0.7 |                    |
| Type 316              | $a_0 = 8.28 \sim 8.38, c_0 = 4.597 \sim 4.599$ | 55                         | 29    | 5     | 11    | —   |                    |
| Type 316L             | $a_0 = 9.21, c_0 = 4.78$                       |                            |       |       |       |     |                    |
| 20Cr-25-34Ni-6.5-8Mo  | $a_0 = 8.87, c_0 = 4.61$                       | 35/37                      | 17/26 | 15/21 | 21/28 | —   |                    |
| 25Cr-20Ni             | —  | 40                         | 46    | 9.4   | —     | 3   |                    |

Fig. 20 The sigma phase lattice parameters depending on the chemical composition [10]

Both steels SUPER 304H and Tp 347HFG have average base of alloying elements ratio 18/9. Precipitation diagram for alloy with 19 % Cr and 9% Ni is plotted in Fig. 21. Letters B, H, E mean: B: initial precipitation, H: intermediate stage, E: final precipitation stage.

The diagram indicates beginning of the sigma phase precipitation after 100 expose hours at 600 °C. This time is several orders of magnitude lower than the power plant projected lifetime. So, it will be necessary to creates same prediction model of sigma phase precipitation.

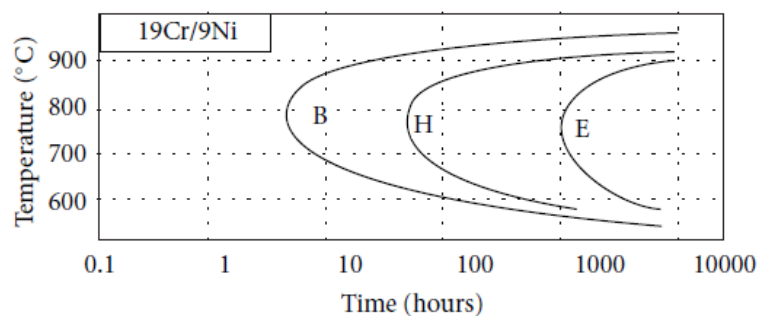


Fig. 21 The sigma phase precipitation time – temperature dependence for system 19/9 [10]

The precipitation diagram shown in Fig. 21 was published for base constitution of austenitic steel. Both SUPER 304H and TP 347HFG are alloyed by



other elements like copper, niobium etc. Those alloying elements will influence the sigma phase precipitation.

Fig. 22 displays a scheme of the initial sigma phase precipitation stage. Precipitation begins at grain boundaries near to the high chromium regions. Next stages are illustrated for steel AISI 316L in Fig. 23. Fig. 23 documents precipitation occurrence not just at grains triple intercourses, but inside the grains too. Austenite degradation in meaning of delta ferrite formation is shown in Fig. 23, too. Delta ferrite regions accelerate the sigma phase precipitation. Highly alloyed austenitic steels like SUPER 304H or Tp 347HFG are alloyed by austenitic stabilized elements. This type of alloying ensures fully austenitic structure during heat exposition. Fully stable austenite means slower sigma phase precipitation.

According to the published precipitation mechanism it is clear that precipitation process is driven by diffusion. Diffusion in solids is described by Fick's laws. Precipitation process is firstly precipitation of chromium carbides and lately carbides transformation into the sigma phase. This process is driven by carbon and chromium diffusion.

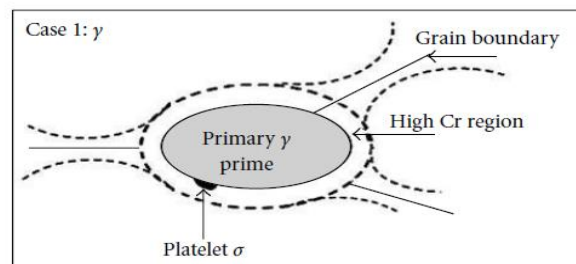


Fig. 22 *The sigma phase precipitation scheme [10]*

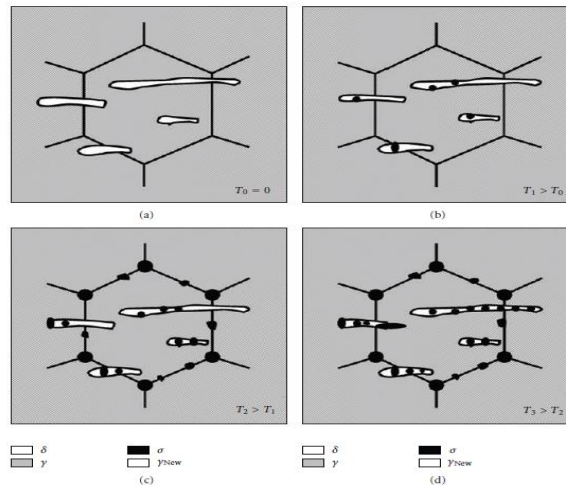


Fig. 23 Progress of the sigma phase precipitation in steel AISI 316L [10]

Sigma phase precipitation is influenced by many factors like chemical composition of steel, ageing time/temperature, additional steel deformation. Higher deformation rate leads to precipitation accelerating.

Phase nucleation can be homogenous or heterogenous [16]. The sigma phase precipitates preferably in chromium rich areas. Chromium content in ferrite is higher than in austenite. Precipitation will firstly start in ferrite regions. Fig. 24 displays precipitation rate in ferrite, austenite 18/10 and austenite 18/13Nb. The austenitic steel with no delta ferrite dissolve chromium carbides first. Chromium carbides dissolving causes a chromium rich area. This area is a preferable start point for sigma phase precipitation [16]. Slowing down of the sigma phase precipitation rate caused by N alloying is described in [18]. Similar information was published in [10]. Slowing down of precipitation rate is caused by prior carbides and carbo-nitrides precipitation and then sigma phase.

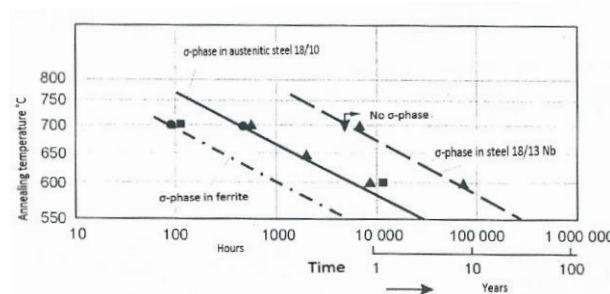


Fig. 24 The sigma phase precipitation curves for various modification of austenitic steels [16]

Beginning of precipitation processes is dependent on original material microstructure (Fig. 24). Ferritic matrix is more susceptible for sigma phase precipitation in comparison with austenite. There is lots of information listed about meta-stable steels but just a little information about sigma phase precipitation in fully stabilized austenite. No information about sigma phase precipitation is published for complex alloyed systems like SUPER 304H. The sigma phase precipitation processes for steel SUPER 304H will be definitely slower.

The precipitated volume fraction of sigma phase in various types of alloys is shown in Fig. 25. Graphs confirm that other alloying elements influence sigma phase precipitation rate. Category including the steels SUPER 304H and Tp 347HFG is austenitic complexly alloyed steels. The main word is complexly. Here is place to make model of sigma phase precipitation.

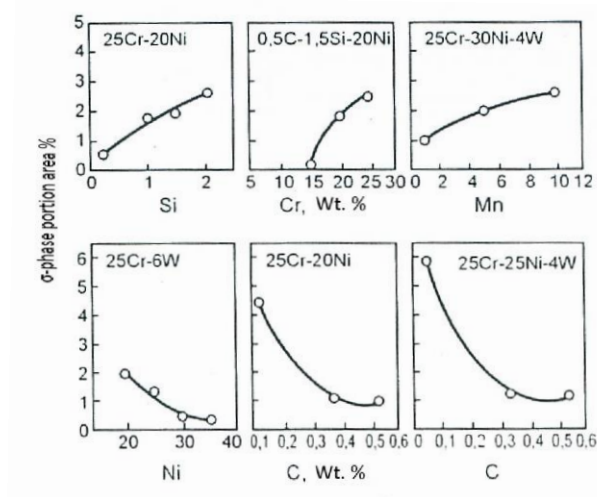


Fig. 25 The influence of Si, Cr, Mn, Ni and C content to sigma phase precipitation (annealing 1250°C and exposition 1000 hours/ 850°C) [16]

Fig. 25 summarized influence of alloying elements in high chromium and nickel austenitic steel. On the other hand, there is no information about influence of copper which is nowadays used like alloying element in complexly alloyed steels like SUPER 304H. That is missing information.

The sigma phase precipitation influence to the mechanical properties obtained from short time testing is well known and is significant ([12][13][16]). On the other hand, creep rupture strength influence is probably low ([16][19]).

Combination of sigma phase precipitation and missing information about interaction between sigma phase and for example copper (alloyed in SUPER 304H for increasing of creep resistivity) may lead to changes in creep rupture strength.

## **2.2 The specific austenitic steels from group 18/9 for USC power plants**

The sub-chapter 2.2 summarizes literature information about the two examined creep resistant steels SUPER 304H and Tp 347HFG. Mechanical properties, physical properties and chemical composition are listed. Last part summarizes difference between both steels which are crucial for the precipitation examination and optionally for modelling.

### **2.2.1 SUPER 304H**

Steel SUPER 304H is relatively newly developed. It means that in literature there is just a little information about this steel. SUPER 304H is fine grain (ASTM G 8-10) complexly alloyed steel from group of austenitic steels 300 (according ASTM). The ratio of base alloying elements is 18/9 (18% chromium and 9% nickel). Copper, nitrogen, boron and aluminium are used like alloying elements. The carbon content is optimized in range 0,07 – 0,13 %. Copper improves creep resistance by fine dispersion coherent precipitates. Nitrogen with carbon precipitated like chromium carbonitride inside grains. Precipitation of carbonitrides inside grains reduces chromium carbides precipitation possibility on the grain boundaries. [7]

Normative steel specification is summarised by [20].

Literature [21] and [22] shows application of austenitic steels to the superheaters loops. Operation conditions are temperature in range of 640-650 °C and pressure 30 MPa. On the basis of strength calculations and acceptable calculated wall thickness listed in [22] steels SUPER 304H, Tp 347HFG and HR3C are acceptable for those operation parameters.

Polish Institute for Ferrous Metallurgy research activities were focused on the steels SUPER 304H and HR3C. Unfortunately, in [22] it is listed that diameters of tubes were 42,4 and 51 mm and hardness of the welding joints didn't overstep 260HV.

### Chemical composition

The chemical composition according to the DMV datasheet of steel SUPER 304H is presented in Tab. 1.

**Tab. 1** Chemical composition in mass % according ASME Case 2328-1 [23]

|        | C    | Si   | Mn   | P    | S    | Cr    | Ni    | Nb(Cd) | Cu   | N    | Al    | B     |
|--------|------|------|------|------|------|-------|-------|--------|------|------|-------|-------|
| % min. | 0,07 |      |      |      |      | 17,00 | 7,50  | 0,30   | 2,50 | 0,05 | 0,003 | 0,001 |
| %max.  | 0,13 | 0,30 | 1,00 | 0,04 | 0,01 | 19,00 | 10,50 | 0,60   | 3,50 | 0,12 | 0,030 | 0,010 |

### Mechanical properties

Mechanical properties published in DMV datasheet are shown in Tab. 2.

**Tab. 2** Mechanical properties according ASME Code Case 2328-1 [23]

|                  | MPa | ksi |
|------------------|-----|-----|
| Y.S. min.        | 235 | 34  |
| U.T.S. min.      | 590 | 85  |
| E in 2'' min., % | 35  |     |

According to the [23] the impact strength KV in longitude direction is 85J (Average value from 3 specimens. The average value may fall short only with one specimen, and only by max. 30%).

### Creep

In literature there is information about accelerated creep tests of SUPER 304H steel [24]. Steel was tested without measurement of elongation. Testing conditions were tension of 150 and 180 MPa with combination of 650, 675, 700, 725 and 750 °C. The set of results is summarized in Tab. 3. Graphical interpretation of results is plot in the charts in Fig. 26 and Fig. 27.

Tab. 3 Creep rupture strength of steel SUPER 304H [24]

| Testing tension $\sigma_b$ (MPa) | Testing temperature $T_b$ (°C) |      |     |     |     |
|----------------------------------|--------------------------------|------|-----|-----|-----|
|                                  | 650                            | 675  | 700 | 725 | 750 |
|                                  | Time to rupture $t_z$ (h)      |      |     |     |     |
| 150                              | (10000)                        | 8330 | 250 | 484 | 111 |
| 180                              | 6770                           | 1805 | 430 | 103 | 22  |

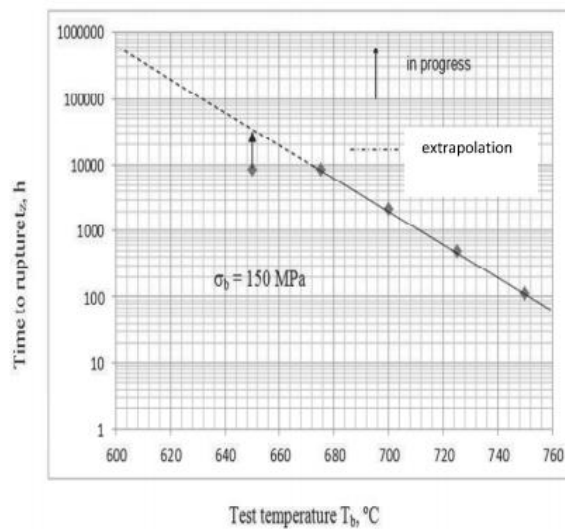


Fig. 26 Time to rupture – temperature diagram for tension of 150 MPa [24]

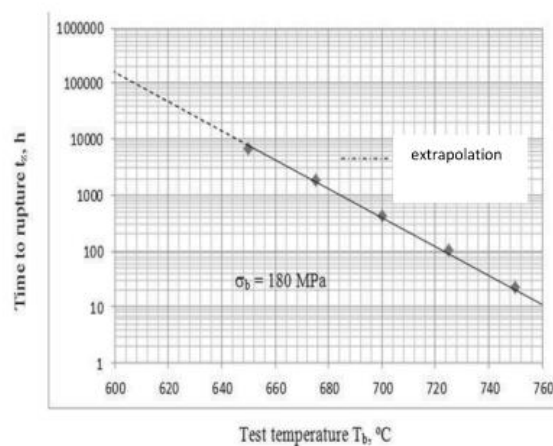


Fig. 27 Time to rupture – temperature diagram for tension of 180 MPa [24]

The results presented in [24] are in agreement with requirements of ASME Code Case 2328-1 (Boiler and pressure vessel code). Values over 10000 hours are just extrapolated.

Average preliminary creep strength values for 10,000 h and 100,000 h are summarized in Tab. 4. The lower scale band can be estimated as 20% lower than average values. [23]

Tab. 4 Creep rupture strength of steel SUPER 304H by [23]

| Temp. °C        | 600 | 610 | 620 | 630 | 640 | 650 | 660 | 670 | 680 | 690 | 700 | 710 | 720 | 730 | 740 | 750 |
|-----------------|-----|-----|-----|-----|-----|-----|-----|-----|-----|-----|-----|-----|-----|-----|-----|-----|
| 10,000h<br>MPa  | 240 | 222 | 206 | 192 | 174 | 160 | 146 | 134 | 124 | 114 | 101 | 92  | 84  | 76  | 68  | 61  |
| 100,000h<br>MPa | 182 | 165 | 152 | 139 | 126 | 116 | 105 | 96  | 86  | 78  | 68  | 61  | 54  | 48  | 42  | 37  |

### 2.2.2 Tp 347HFG

Austenitic creep resistant steel Tp 347HFG has the base alloying elements ratio 18/12. For increasing steel creep resistance Nb in combination with higher C content is alloyed. Alloying of Nb+C provides the niobium carbonitrides precipitation. In steel mark HFG means high fine grain. Grain size of Tp 347 HFG is ASTM G 7-10. [25]

#### Chemical composition

The chemical composition of steel Tp 347HFG found in literature is listed in Tab. 5.

Tab. 5 Tp 347HFG chemical composition in Wt. % [25]

| C    | Si  | Mn   | P     | S     | C     | Mo | Ni    | Ti | Nb   |
|------|-----|------|-------|-------|-------|----|-------|----|------|
| 0,09 | 0,4 | 0,15 | 0,026 | 0,001 | 18,21 | -  | 11,34 | -  | 0,88 |

Chemical composition published in Tp 347HFG datasheet [26] is summarized in Tab. 6.

Tab. 6 Chemical composition in mass % according ASME SA-213/SA-213M [26]

|        | C    | Si   | Mn   | P    | S    | Cr    | Ni    | Nb +Ta |
|--------|------|------|------|------|------|-------|-------|--------|
| % min. | 0,06 |      |      |      |      | 17,00 | 9,00  | 8 x C  |
| %max.  | 0,10 | 0,75 | 2,00 | 0,04 | 0,03 | 20,00 | 13,00 | 1,00   |

### Mechanical properties

Base mechanical properties are summarized in Tab. 7.

Tab. 7 Mechanical properties according ASME SA-213/SA-213M [26]

|                  | MPa | ksi |
|------------------|-----|-----|
| Y.S. min.        | 205 | 30  |
| U.T.S. min.      | 550 | 80  |
| E in 2'' min., % | 35  |     |

The impact strength KV in longitudinal direction is min. 85 J (Average value from 3 specimens. The average value may fall short only with one specimen, and only by max. 30 %). [26]

### Creep

Average preliminary creep strength values for 10,000 h and 100,000 h are summarized in Tab. 8. The lower scale band can be estimated as 20% lower than average values. [26]

Tab. 8 The creep values of steel Tp 347HFG by [26]

| Temp. °C     | 600 | 610 | 620 | 630 | 640 | 650 | 660 | 670 | 680 | 690 |
|--------------|-----|-----|-----|-----|-----|-----|-----|-----|-----|-----|
| 10,000h MPa  | 215 | 197 | 182 | 168 | 155 | 142 | 130 | 119 | 108 | 99  |
| 100,000h MPa | 159 | 145 | 134 | 120 | 109 | 100 | 90  | 81  | 72  | 65  |

## 2.2.3 The similarity and differences of both steels

Steel SUPER 304H is modern and more complex alloyed in comparison with Tp 347HFG. It is consistent with higher creep resistance of SUPER 304H in comparison with a Tp 347HFG (Fig. 28). Both steels were created by continuously



modifications of origin AISI 302 and are members of the stable austenitic steels group 18/9 (Fig. 28). It means that base alloying elements ratio is 18% chromium and 9% nickel. In fact, this categorization can be quite confusing because SUPER 304H average nickel content is 9% and Tp 347HFG 10% (Fig. 29).

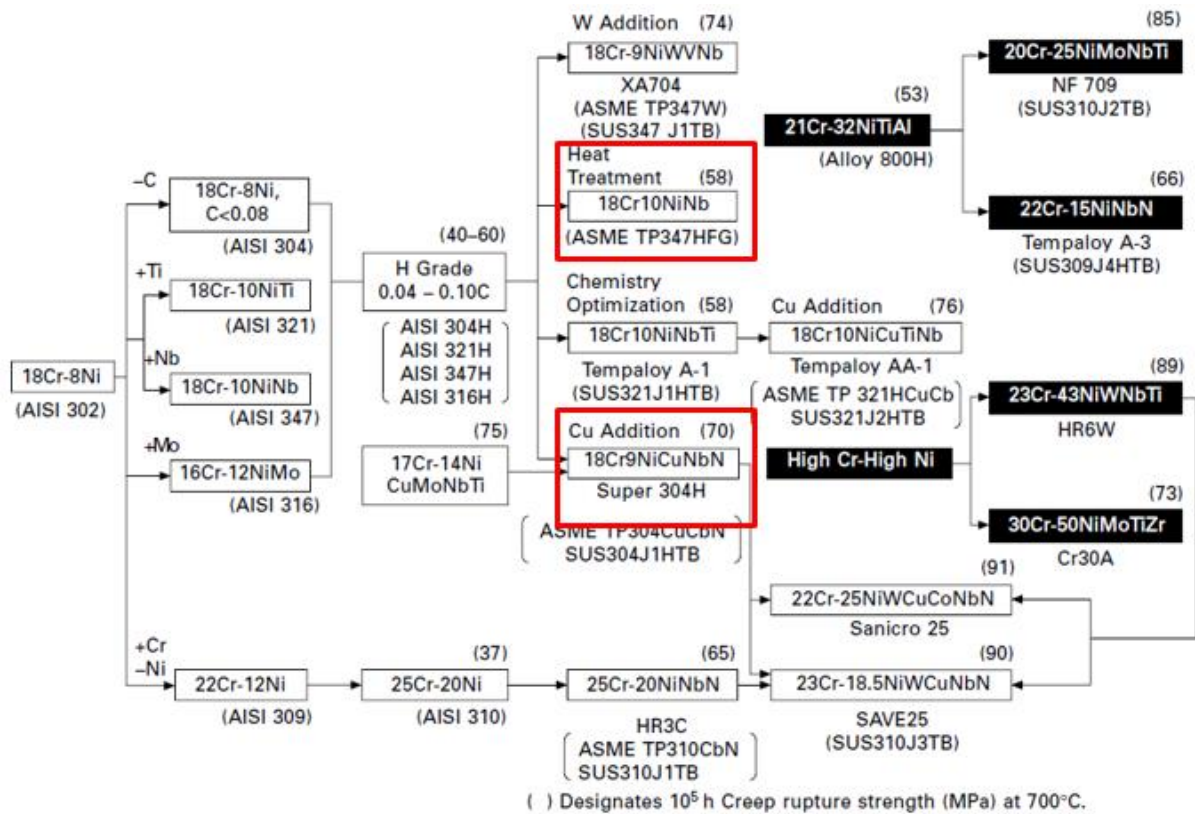


Fig. 28 Development progress of austenitic boiler steels [7]

| Steels     | Chemical composition (mass%) |                  |      |     |     |      |      |     |    |      |      |        |             |
|------------|------------------------------|------------------|------|-----|-----|------|------|-----|----|------|------|--------|-------------|
|            | C                            | Si               | Mn   | Ni  | Cr  | Mo   | W    | V   | Nb | Ti   | B    | Others |             |
| 18%Cr-8%Ni | TP304H                       | 18Cr-8Ni         | 0.08 | 0.6 | 1.6 | 8.0  | 18.0 | -   | -  | -    | -    | -      | -           |
|            | TP316H                       | 16Cr-12NiMo      | 0.08 | 0.6 | 1.6 | 12.0 | 16.0 | 2.5 | -  | -    | -    | -      | -           |
|            | TP321H                       | 18Cr-10NiTi      | 0.08 | 0.6 | 1.6 | 10.0 | 18.0 | -   | -  | -    | 0.50 | -      | -           |
|            | TP347H                       | 18Cr-10NiNb      | 0.08 | 0.6 | 1.6 | 10.0 | 18.0 | -   | -  | 0.80 | -    | -      | -           |
|            | TP347HFG                     | 18Cr-10NiNb (FG) | 0.08 | 0.6 | 1.6 | 10.0 | 18.0 | -   | -  | 0.80 | -    | -      | -           |
|            | Tempaloy A-1                 | 18Cr-10NiNbTi    | 0.12 | 0.6 | 1.6 | 10.0 | 18.0 | -   | -  | 0.10 | 0.08 | -      | -           |
|            | Super304H                    | 18Cr-9NiCuNbN    | 0.10 | 0.2 | 0.8 | 9.0  | 18.0 | -   | -  | 0.4  | -    | -      | 3.0Cu, 0.1N |

Fig. 29 Nominal chemical composition of austenitic steels for boilers [7]

Summarization of the mechanical and creep performed properties in the chapters 2.2.1 and 2.2.2 in general shows that SUPER 304H has superior properties than Tp 347HFG. This result is caused partially by mechanical processing of the steels and mainly by their chemical composition. Comparison of the steels chemical composition is summarized in Fig. 30.

| SUPER 304H |        |       | Tp 347HFG |        |       |
|------------|--------|-------|-----------|--------|-------|
|            | % min. | %max. |           | % min. | %max. |
| C          | 0,07   | 0,13  | C         | 0,06   | 0,10  |
| Si         |        | 0,30  | Si        |        | 0,75  |
| Mn         |        | 1,00  | Mn        |        | 2,00  |
| P          |        | 0,04  | P         |        | 0,04  |
| S          |        | 0,01  | S         |        | 0,03  |
| Cr         | 17,00  | 19,00 | Cr        | 17,00  | 20,00 |
| Ni         | 7,50   | 10,50 | Ni        | 9,00   | 13,00 |
| Nb(Cd)     | 0,30   | 0,60  | Nb +Ta    | 8 x C  | 1,00  |
| Cu         | 2,50   | 3,50  |           |        |       |
| N          | 0,05   | 0,12  |           |        |       |
| Al         | 0,003  | 0,030 |           |        |       |
| B          | 0,001  | 0,010 |           |        |       |

Fig. 30 The chemical composition comparison [23][26]

First difference is in content of base alloying elements (Cr and Ni). Influence of chromium and nickel alloying in binary system is presented in Fig. 31. Most interesting part is over 30 % of chromium where sigma phase region is. According to the information summarized in subchapter 2.1.5 sigma phase can precipitate under this chromium content during heat exposition. The sigma phase precipitation rate will be strongly dependant on carbon and chromium content (initial state of sigma phase precipitation). After beginning of precipitation the precipitation rate will be driven by diffusivity of chromium, iron and nickel.

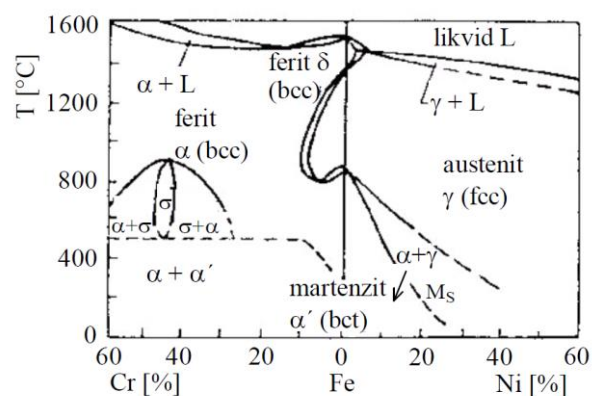


Fig. 31 Double binary diagram Fe-Cr and Fe-Ni [27]

The second difference in chemical composition is complex alloying for increasing steel creep resistance. For increasing SUPER 304H steel creep resistance is alloyed Cu, N, Al and B (boron increases mechanical properties too). Cu alloying into steel SUPER 304H may ensure nanoprecipitation of Cu coherent particles, which may slow creep processes. All of those alloying elements will influence sigma phase precipitation rate just by their content. Precipitation processes for steel SUPER 304H will be probably slower than for Tp 347 HFG.

A question is, how stable the steels under long term heat exposition will be.

### **2.3 The austenitic 18/9 creep resistant steels structural stability**

The information about heat exposition influence on the steel SUPER 304H is presented in [11][13][19][24]. In general influence of heat exposition on the austenitic steels is:

- Grain coarsening
- Slowly generating of corrosion layers
- The microstructure changes

Linearly oriented niobium carbo-nitrides are only precipitates in the original state of steel [11]. Microstructure changes caused by heat exposition (650 and 700 °C) up to 3000 hours are describe in [24]. Documented microstructure changes are changed of niobium particles size and chromium carbides ( $\text{Cr}_{23}\text{C}_6$ ) precipitation. Unfortunately, time of 3000 hours is quite low for microstructure changes assumption.

Initial state of steel SUPER 304H (Fig. 32) can be correlated with state after 3000 hours at the temperature of 700°C (Fig. 33).

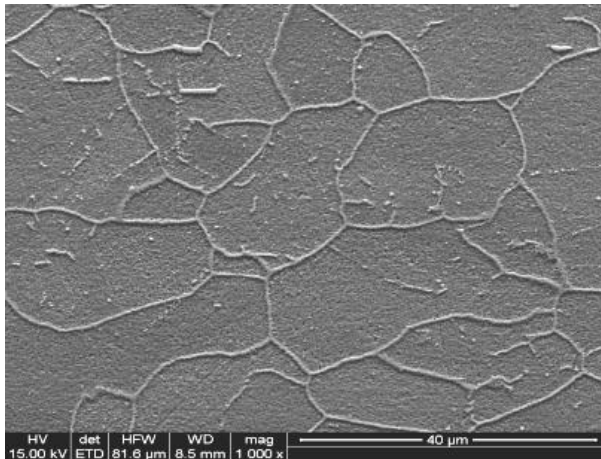


Fig. 32 *The initial state of steel SUPER 304H [24]*

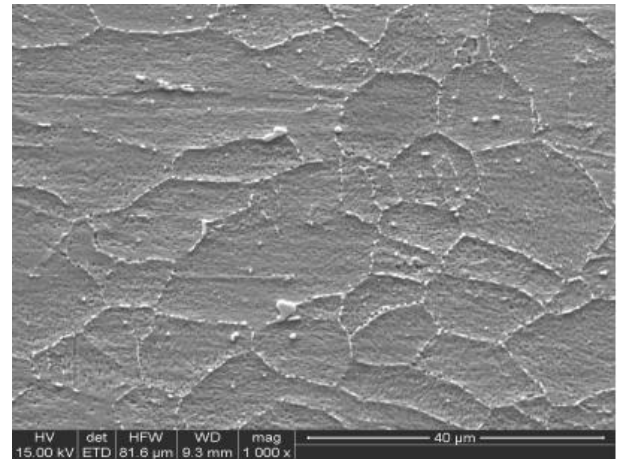


Fig. 33 *Microstructure of steel SUPER 304H after 3000 hours of ageing at 700°C [24]*

It was mentioned that 3000 hours of ageing is quite low for some predictions. It will be necessary to have a look to the state after 15000 or more hours of ageing. After longer expose time, sigma phase precipitation can occur in microstructure of SUPER 304H steel.

The sigma phase precipitation system for austenitic steel 316H is published in [28]. Transformation  $M_{23}C_6$  – laves phase – sigma phase is documented. Precipitation of the laves phase in this system is very implausible. Probably it is bad identification during EBSD. Fig. 34 and Fig. 35 present the sigma phase experimental documentation for steel type 316H after thermal exposition.

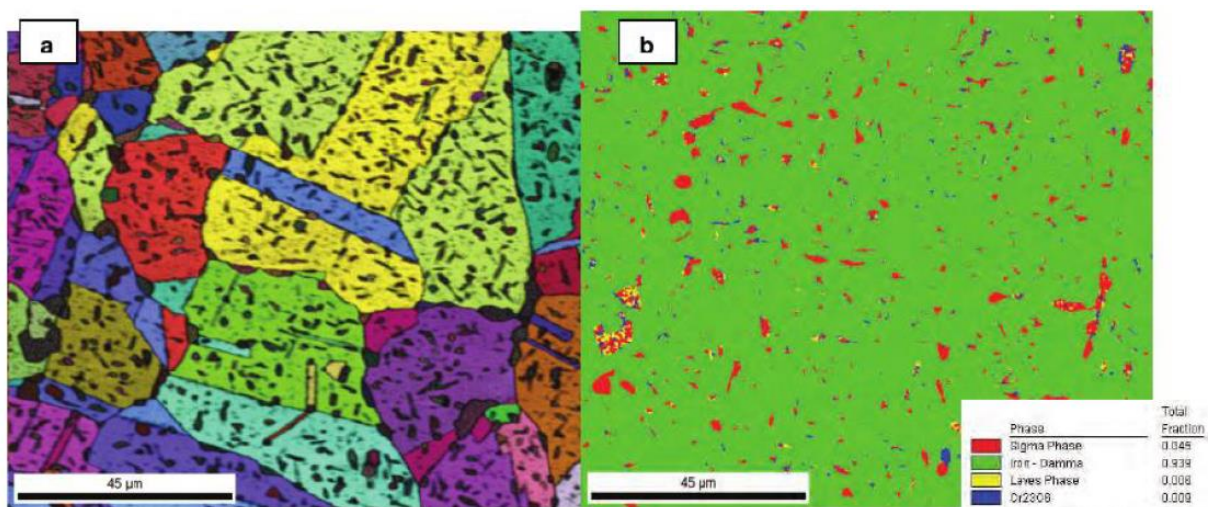


Fig. 34 *EBSD orientation map and phase map of type 316H [28]*

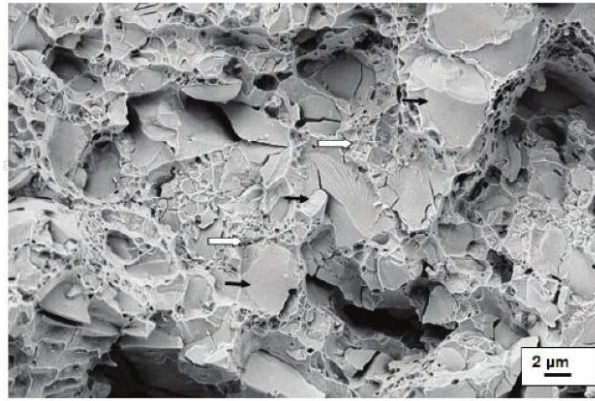


Fig. 35 Fraction surface of type 316H steel with black pointed sigma phase [28]

Precipitation of the sigma phase for steel type Tp 347HFG after laboratory exposition up to 10 000 hours is present in [25]. The sigma phase microstructure in austenitic matrix of Tp 347HFG is shown in Fig. 36. Total measured area fraction is displayed in Fig. 37.

Presented results are very beneficial like information about sigma phase precipitation. On the other hand, exposition temperature is absolutely out of range suitable for those material applications. There will be necessary to repeat this experiment but with using of lower temperature and longer time of exposition.

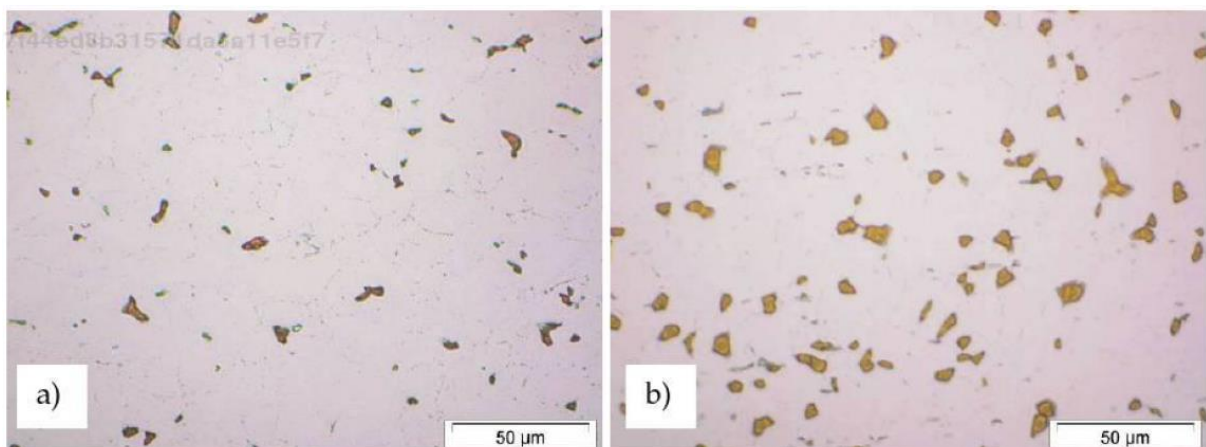


Fig. 36 Sigma phase in 347HFG after a) 5 000 hours and b) 10 000 hours of aged 750°C [25]

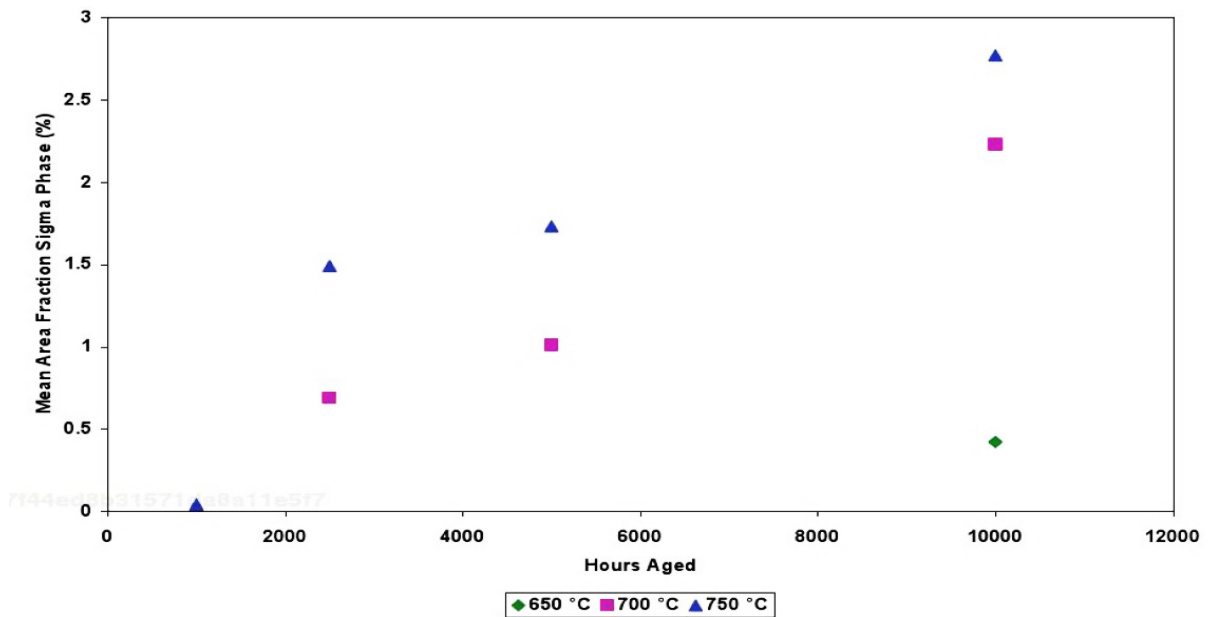


Fig. 37 Area fraction of the sigma phase in 347 HFG stainless steel [25]

### 2.3.1 The mechanical properties changes caused by instability

It is definitely possible to state that alloy chemical composition has an influence on the mechanical properties.

Tab. 9 documents copper additional influence on the mechanical properties of SUPER 304H. Higher copper content reduces all the conventional mechanical properties. The most significant difference is between three and five percent. It is interesting because possible copper content is 2,5 – 3,5 %. As we have mentioned above copper might increase creep resistance. Difference of the copper content will have influence not just on the mechanical properties, but on the creep resistance, too. This gives possible space to model behaviour of steel.

Tab. 9 Mechanical properties of SUPER 304H by copper content [17]

| Cu content | $R_e$ | $R_m$ | Elongation | Fracture toughness   |
|------------|-------|-------|------------|----------------------|
| %          | MPa   | MPa   | %          | MPa*m <sup>1/2</sup> |
| 0          | 362   | 734   | 66         | 45,8                 |
| 1          | 350   | 714   | 60         | 46,0                 |
| 3          | 300   | 618   | 61         | 49,7                 |
| 5          | 290   | 624   | 46         | 47,8                 |

The following table (Tab. 10) documents the mechanical properties changes caused by short time of ageing. Ageing temperatures were 600, 700 and 800 °C. Six hundred degree of Celsius is lower than projected operation conditions, on the other hand seven hundred is slightly higher and eight hundred is over projected working parameters. In all three cases, mechanical properties were documented. Maximal aging time was three hours, which is really short time in comparison with projected lifetime of the power plant. Short time changes aren't negligible. Those results raise two questions:

- How fast will the change be during the longer-term exposition
- What will changes caused by in-technological superheater operating be like

Tab. 10 SUS 304H mechanical properties after short them aging [29]

| Temperature (°C) | Property       | Unit | Aging time (hrs.) |       |       |       |
|------------------|----------------|------|-------------------|-------|-------|-------|
|                  |                |      | 0                 | 1     | 2     | 3     |
| RT               | R <sub>m</sub> | MPa  | 668,8             |       |       |       |
|                  | R <sub>e</sub> | MPa  | 273,0             |       |       |       |
|                  | A              | %    | 59,0              |       |       |       |
| 600              | R <sub>m</sub> | MPa  |                   | 661,9 | 639,0 | 610,0 |
|                  | R <sub>e</sub> | MPa  |                   | 219,2 | 216,5 | 213,0 |
|                  | A              | %    |                   | 56,6  | 57,3  | 58,1  |
| 700              | R <sub>m</sub> | MPa  |                   | 617,8 | 597,8 | 578,5 |
|                  | R <sub>e</sub> | MPa  |                   | 214,4 | 201,3 | 191,7 |
|                  | A              | %    |                   | 55,4  | 56,5  | 57,1  |
| 800              | R <sub>m</sub> | MPa  |                   | 615,0 | 597,0 | 577,8 |
|                  | R <sub>e</sub> | MPa  |                   | 211,7 | 200,6 | 191,0 |
|                  | A              | %    |                   | 55,1  | 55,3  | 56,6  |

SUPER 304H mechanical properties measurements after exposition 1000 and 3000 hours are presented in [24]. Exposition temperatures were 650 and 700°C. The changes caused by exposition are significant in case of tension strengths but enormous in case of impact strength.

Result of the tension strength testing is that hardening effect of precipitation and its degradation of mechanical properties are balanced.

Elongation of steel SUPER 304H after heat exposition decreases. This state is caused by precipitation of sigma phase which is highly brittle. Brittle phase content leads to the decrease of the possible elongation.

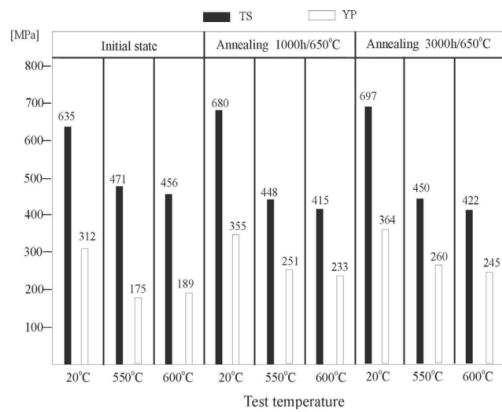


Fig. 38 Yield and ultimate strengths for exposed material. Exposition parameters 650°C, exposition time 1000 and 3000 hours [24]

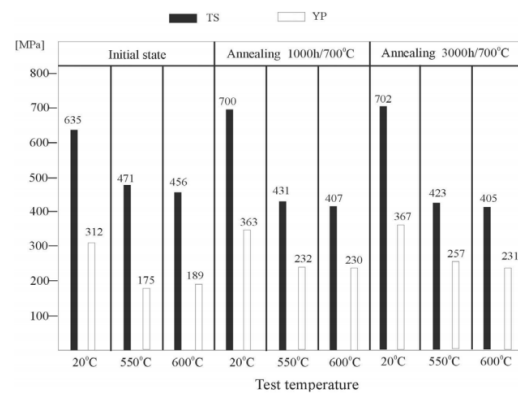


Fig. 39 Yield and ultimate strengths for exposed material. Exposition parameters 700°C, exposition time 1000 and 3000 hours [24]

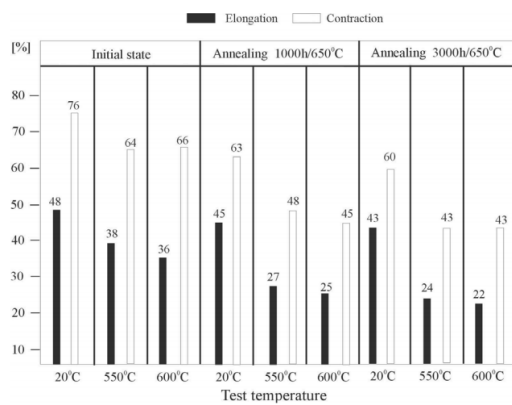


Fig. 40 Elongation of exposed material. Exposition parameters 650°C, exposition time 1000 and 3000 hours [24]

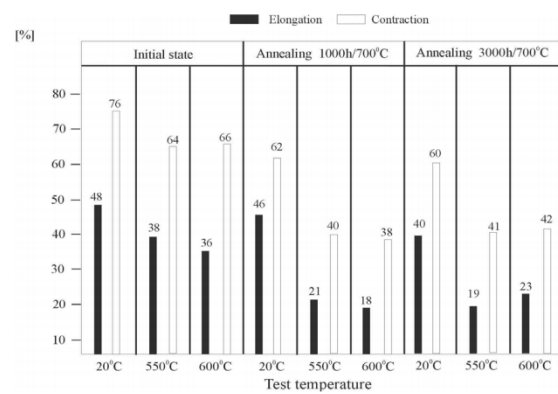


Fig. 41 Elongation of exposed material. Exposition parameters 700°C, exposition time 1000 and 3000 hours [24]

The most markantable change is drop of impact strength (Fig. 42). Steel embrittlement can cause problems during the lifetime of the superheater or by forming and developing of the cracking caused by welding into brittle degradet superheater steel.



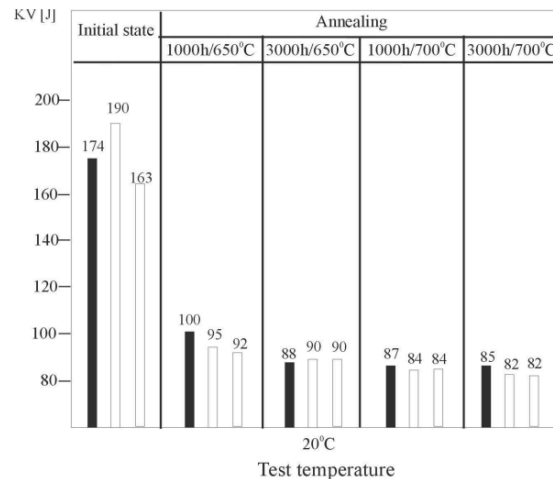


Fig. 42 The impact strength of initial and exposed steel [24]

### 2.3.2 The transformation kinetics

Description of the transformation (or precipitation) kinetics is strongly dependent on many factors. The most important (with higher influence) are:

- Chemical composition
- Exposition time
- Temperature of heat exposition
- Applied tension

The equations which get together two or more of named parameters were historically accepted and still used for the kinetics description.

#### 2.3.2.1 The applied parameters equations for the degradation description

The temperature and time of heat exposition can be combined into one parameter by the equations referred in this subchapter (Eq. (1) - Eq. (3)). Three of possible parametrisations are shown below. For each type of parametrization schematic figure presenting constant stress lines is added (Fig. 43 - Fig. 45).

Larson-Miller parameter [15]

$$LMP = T(K_1 + \log t_r) \quad \text{Eq. (1)}$$

LMP – Larson-Miller parameter

$K_1$  – constant depend on material (range 10-40, average value about 20)

$T$  – Temperature

$t_r$  – Time to rupture

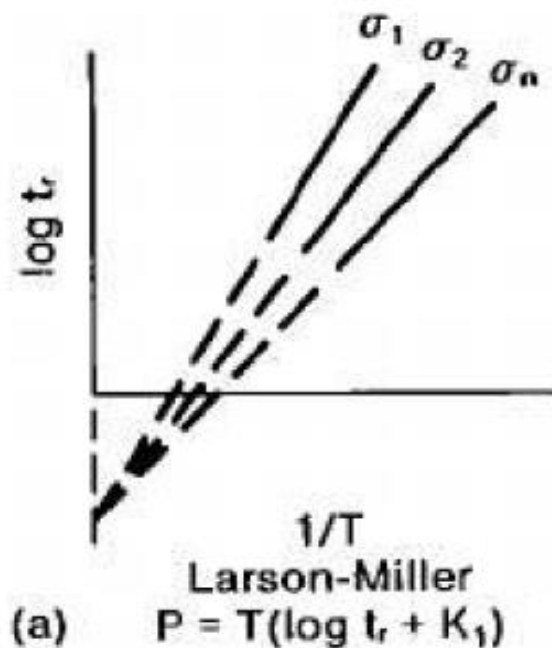


Fig. 43 Schematic representation of constant stress lines for Larson-Miller parameter [15]

Orr-Sherby-Dorn parameter [15]

$$\log A_2 = \log t_r - \frac{B_2}{2,3T} \quad \text{Eq. (2)}$$

$A_2$  – Material constant

$B_2$  – Material constant

$t_r$  – Time to rupture

$T$  – Temperature

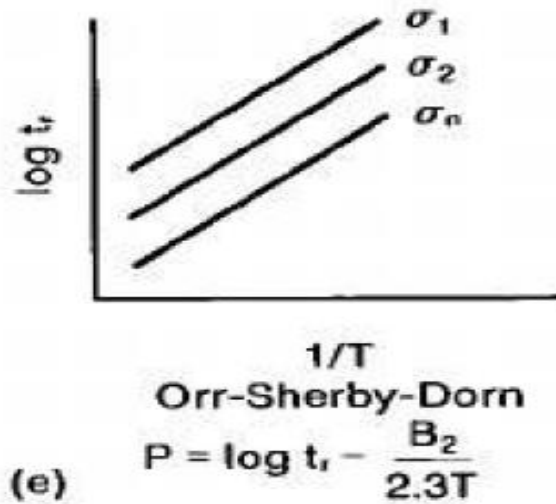


Fig. 44 Schematic representation of constant stress lines for Orr-Sherby-Dorn parameter [15]

Manson-Haferd parameter [15]

$$t_r = A_3 \exp(-B_3 T) \tag{Eq. (3)}$$

$t_r$  – Time to rupture

$B_3$  – Material constant

$A_3$  – Material constant

$T$  – Temperature

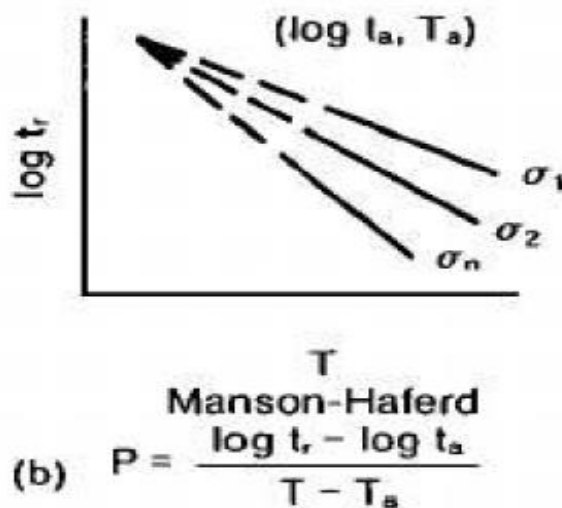


Fig. 45 Schematic representation of constant stress lines for Manson-Haferd parameter [15]

For degradation description in experimental part of this thesis Larson – Miller construction will be used.

### 2.3.3 The structural constitution modelling

Precipitation predictions based on the experiments, like creep tests and laboratory heat exposition, need extremely long time. Those long-term experiments are not just of long duration but are extremely expensive, too. Possibility for prediction in shorter time is to model microstructure changes and precipitation processes.

Information about microstructure changes prediction for steels SUPER 304H and Tp 347HFG is too low or none in literature. Specific constants and general information about sigma phase precipitation in different alloys are published but this information is unfortunately nearly useless.

The sigma phase precipitation in duplex stainless steel is analysed in [30]. Description of precipitation process is shown and described by CALPHAD approach. Scheme of precipitation is plotted in Fig. 46. The longest time used in [30] is about 100 hours. This is too low for our application.

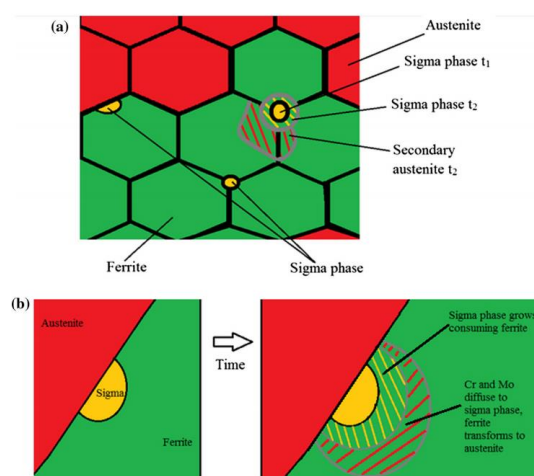


Fig. 46 The sigma phase precipitation scheme in stainless duplex steel[30]

Mathematical background of precipitation is listed in [31]. Unfortunately, this article is also about duplex steels. Model is based on Avrami type of equations.

Article [28] presents modelling of precipitation phases in steel 316H based on Monte Carlo random sampling. This method considered inter-granular and intra-granular precipitation. On the other hand, model considered just average

calculated values. Results of modelling are shown in Fig. 47. Meaning of single charts is:

- Inter granular  $M_{23}C_6$  carbide size at 750°C
- Inter granular  $M_{23}C_6$  carbide volume fraction at 750°C
- Inter granular sigma phase precipitation size at 750°C
- Simulated volume fraction for different phases at 750°C

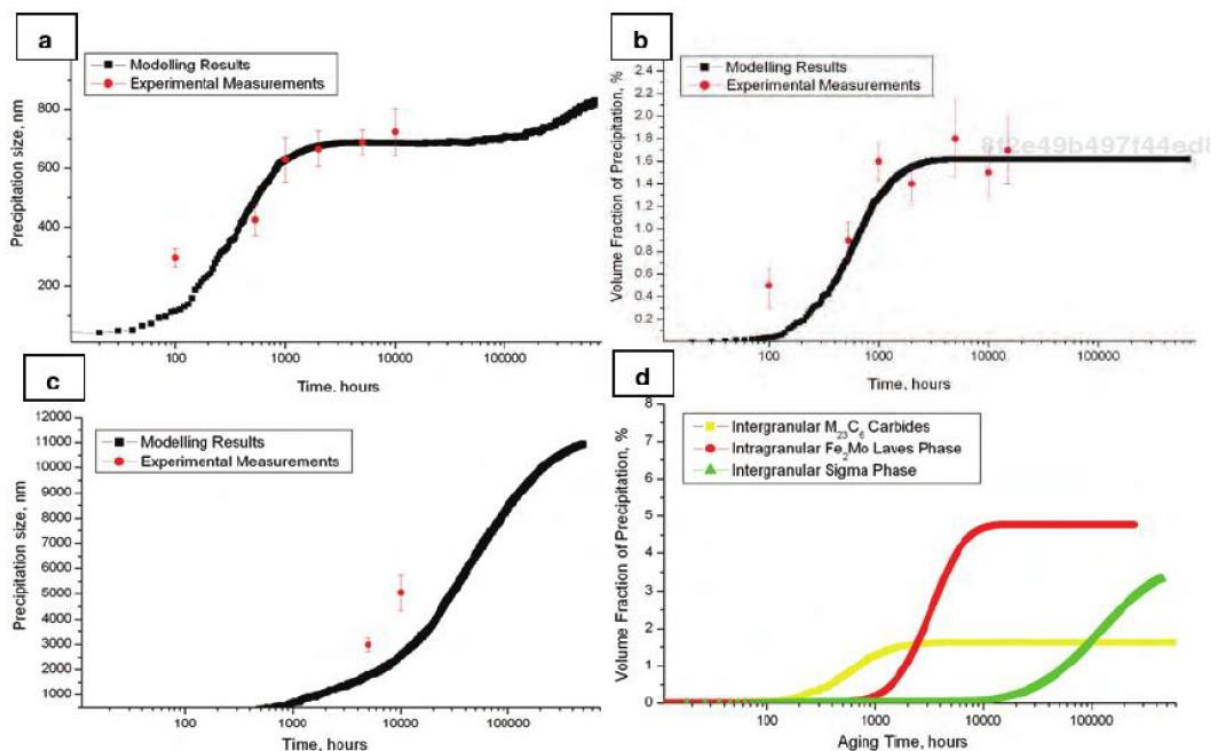


Fig. 47 Results of modelling for steel type 316H[28]

Thermodynamic calculations for steel type Tp 347HFG by Thermo-Calc software is presented in article [25]. This software simulated just stable state of precipitation and is strongly influenced by inputs databases. That can cause high inaccuracy of modelling. Simulated results are presented in Fig. 48. In conclusions of the article it is mentioned that precipitation documented by microscopy at real exposed samples disagree with modelling.

Results published in [25] were calculated for stable state of alloy. There is no information about kinetics of transformation. Transformation kinetics is unfortunately most interesting for application of the structural modelling.

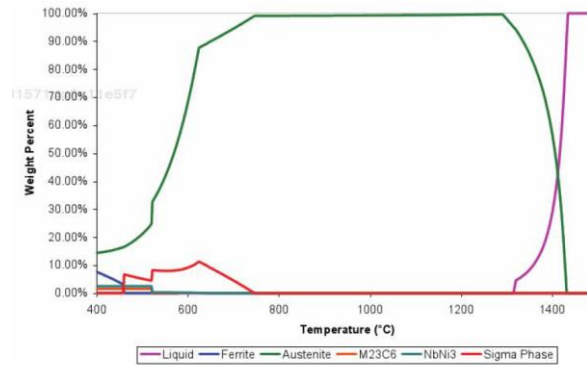


Fig. 48 Phase predicted in 347HFG stainless steel with Thermo-Calc software [25]

Thermodynamic calculations were used for precipitation modelling in the steel SUPER 304H. The Thermo-Calc with database TCFE6 and USER was used. Temperature dependant modelled coexist phases illustrates Fig. 49. Temperature dependence of sigma phase chemical composition is summarised in Fig. 50. The constitution diagrams in Fig. 51 for 800°C, in Fig. 52 for 700°C and in Fig. 53 for 600°C shows that steel SUPER 304H is out of the sigma phase precipitation range. This result contrary base information about sigma phase precipitation published in [10]. Steel SUPER 304H investigations for sigma phase precipitation are necessary.

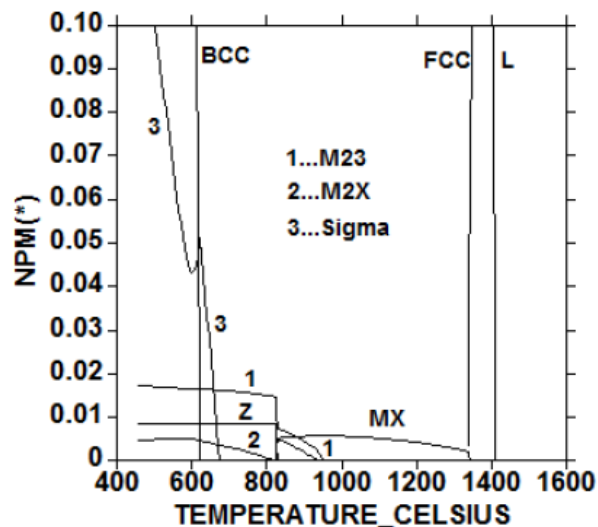


Fig. 49 Modelled coexist phases for chemical composition of steel SUPER 304H [32]

Published results (Fig. 49) seem like probably unreal. SUPER 304H steel is stable austenite and crystallised in FCC system. BCC system cannot occur for SUPER 304H steel. Modelled results must be strongly inflated by used database.

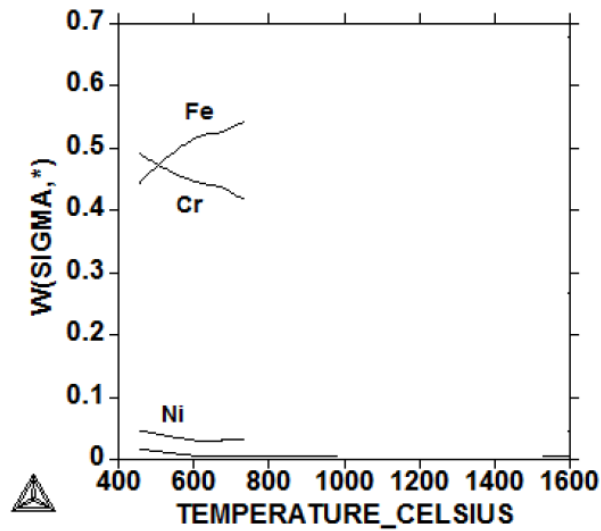


Fig. 50 Chemical composition of sigma phase is SEUPR 304H steel dependence on temperature [32]

Following images were calculated by using a modified database. But there are still areas with coexisting BCC matrix.

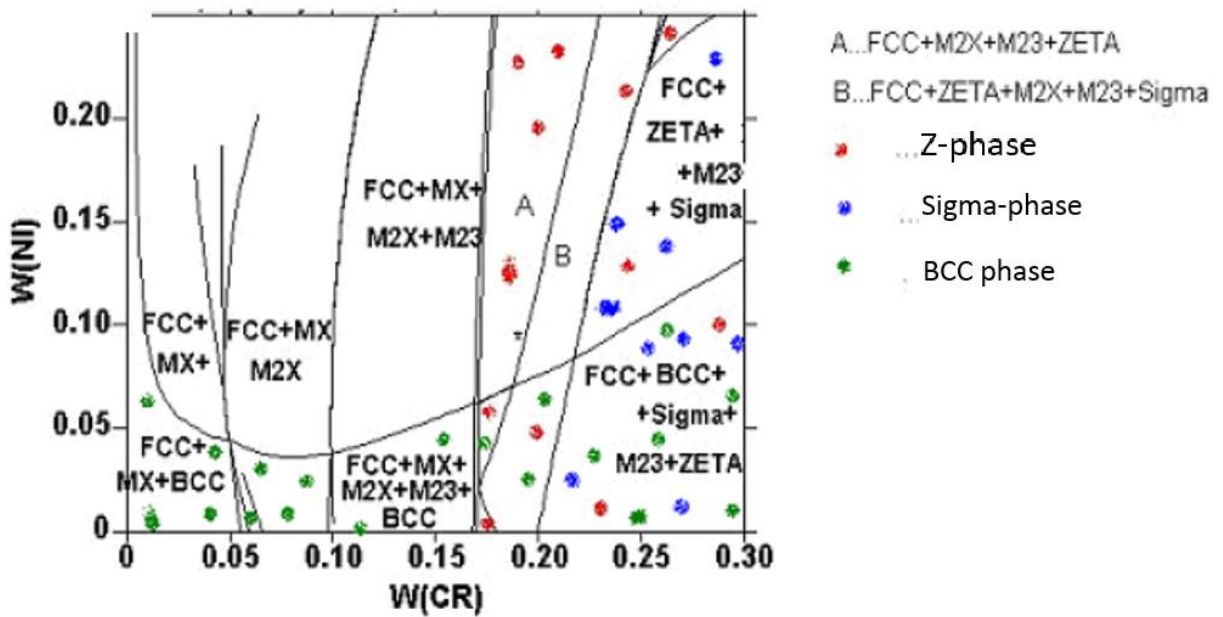


Fig. 51 Isothermal phase diagram of steel SUPER 304H at temperature 800°C [33]

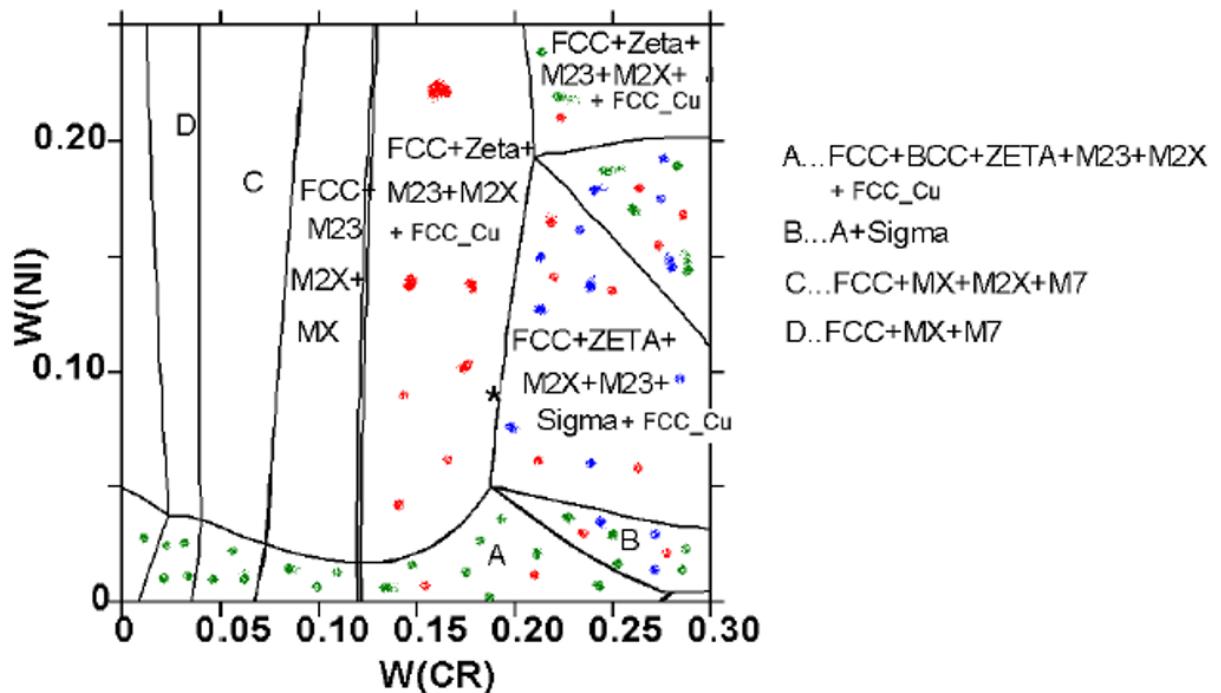


Fig. 52 Isothermal phase diagram of steel SUPER 304H at temperature 700°C [33]

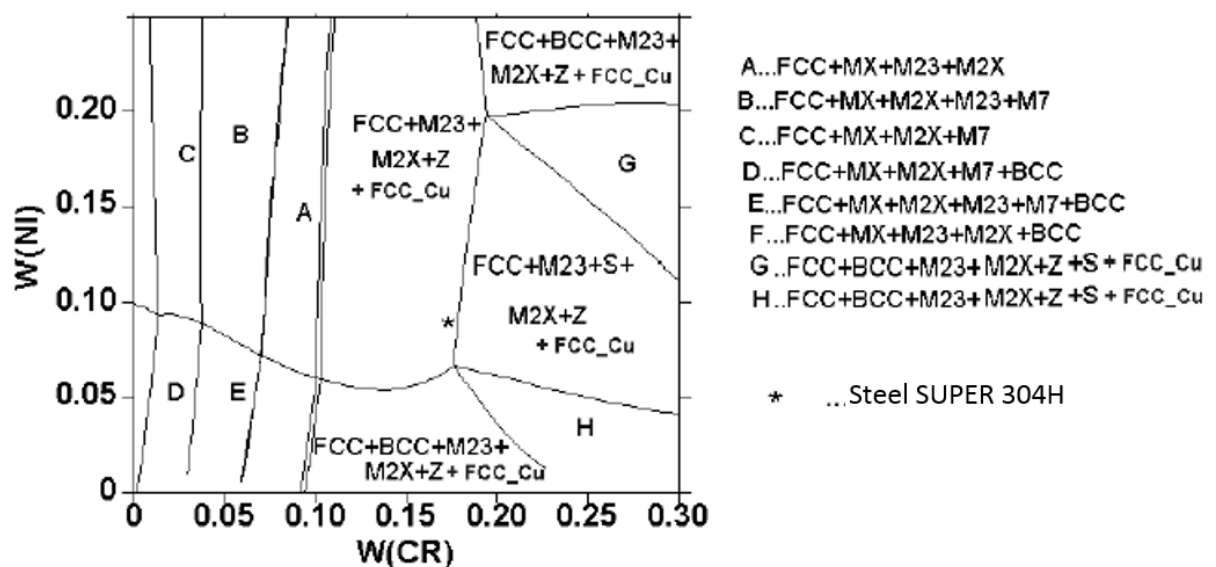


Fig. 53 Isothermal phase diagram of steel SUPER 304H at temperature 600°C [33]

### 2.3.3.1 The basis of commercially used modelling methods

#### Free enthalpy method

An analytical method, the greatest advantage of which is the simplicity the free energy of the systems can be calculated, with including the microstructures of several types of precipitates. In addition, when the system's free energy is evaluated, it is assumed that the method will predict partial evolutions of



current reactions as the method comprehensively compares each change of microstructure to a common scalar energy scale.

As an example of using of this method precipitation of sigma phase and  $M_{23}C_6$  carbide for 18/8 austenitic steel is shown in [34]. The system free energies of the microstructures in which precipitates ( $M_{23}C_6$  and sigma phase) formed in the austenitic matrix were estimated from the sum of the following quantities: chemical free energy  $G_0$  of the Fe–C–Cr–Ni quaternary steel, the elastic strain energies  $E_{str}$  resulting from difference in the lattice constants between the g matrix and the respective precipitation, and the interfacial energies  $E_{surf}$  between the matrix and the respective precipitation. The system free energy of the microstructure is given by the sum of these energies:

$$G_{system} = G_0 + E_{str} + E_{surf} \quad \text{Eq. (4)}$$

The relationship between the evolution of microstructures and the free energy change can be plotted for the above mentioned case, as shown in Fig. 54. This figure presents a schematic illustration of the changes in the free energy during precipitation in the austenitic matrix. The dashed curves labelled  $G_g$  and  $G_p$  show the composition dependence of the chemical free energy of the g matrix and the precipitates, respectively. If the concentration of precipitates formed in the austenitic matrix reaches  $c_p$  and the concentration of the g matrix in the steel is  $c_g$  with the average concentration being  $c_0$ , the free energy is generally assumed to decrease from the energy level of the supersaturated g solid solution  $G_s$  to the equilibrium energy level  $G_0$ . However, because precipitation invariably results in additional free energies such as the elastic strain energy and interfacial energy, the total free energy of the microstructure is not  $G_0$  but  $G_{system}$ . Consequently, the change in the free energy resulting from the precipitation is only  $(G_s - G_{system})$ , and the remaining energy  $(G_{system} - G_0)$  gradually decreases during the subsequent structural coarsening of the precipitates or the loss of coherence between the matrix and the precipitates. Therefore, an evaluation of  $G_{system}$  and the identification of the minimum energy path is expected to enable the prediction of  $M_{23}C_6$  and sigma phase in the precipitation in 18Cr–8Ni austenitic steel. [34]

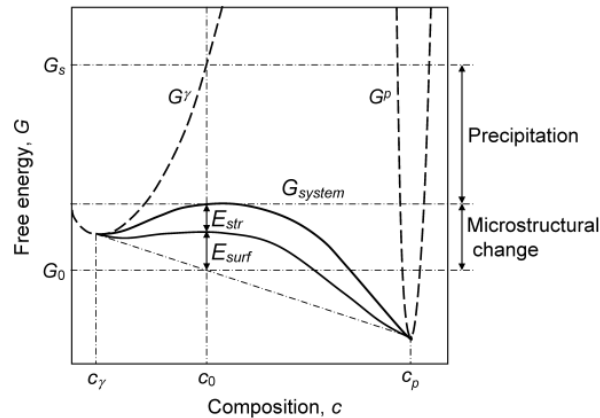


Fig. 54 A schematic illustration of the change in free energy during the precipitation of  $M_{23}C_6$  and  $s$  phase from the  $g$  matrix [34]

### The CALPHAD methodology

CALPHAD is originally an abbreviation for CALculation of PHase Diagrams, but was later expanded to refer to Computer Coupling of Phase Diagrams and Thermochemistry. [35]

In the CALPHAD method, one collects and assesses all available experimental and theoretical information available on phase equilibria and thermochemical properties in a system. The thermodynamic properties of each phase are then described through the Gibbs free energy, applying a mathematical model containing adjustable parameters. These parameters are evaluated by optimizing the fit of the model to all the assessed information, also involving coexisting phases. Following this it is possible to recalculate the phase diagram, as well as the thermodynamic properties of all the phases and the system as a whole. The philosophy of the CALPHAD method is to obtain a consistent description of the phase diagram and the thermodynamic properties so as to predict reliably the set of stable phases and their thermodynamic properties in regions without experimental information and for metastable states during simulations of phase transformations. [35]

A core ingredient of the CALPHAD method is the development of models to represent thermodynamic properties for various phases which permit prediction of properties of multicomponent systems from those of binary and ternary subsystems. This is accomplished by considering physical and chemical

properties of the system in the thermodynamic model, for example, account is taken for crystallography, type of bonding, order-disorder transitions and magnetic properties. [35]

## **3 The thesis goals**

As it was mentioned above both steels SUPER 304H and Tp 347HFG are structurally unstable under USC operation conditions. In general, there is just a little or no information about kinetics of the sigma phase precipitation in these types of steels. The structural changes strongly influence mechanical properties of the steel. It gives a possible field for study of the structural stability of this type of steels. Moreover, precipitation is thermally activated and driven by historically described physical laws which give possibility for modification of a small material group with similar chemical composition.

Set goals are:

- Describe sigma phase precipitation processes for steel SUPER 304H and perform their general mathematical description
- Model precipitation kinetics processes based on chemical composition and physical laws like modification of the steel Tp 347HFG
- Correlate model with measured particles after the long-term heat exposition for steel Tp 347HFG
- Find and describe the kinetic function of the sigma phase precipitation for the steel SUPER 304H

## 4 Methodology

Experimental part summarizes the used experimental methods applied for reaching the thesis goals. It is specialized just for methods description to get possibility of experiments repetition.

### 4.1 Used experimental materials

Most of the performed experiments were done at the material SUPER 304H because of its availability. Specification of steel is listed in [36]. Material was supplied by the Sumitomo Metals. Steel SUPER 304H was supplied in the form of the seamless tubes with outer diameter 38 mm, wall thickness 6,3 mm and a tube length of 5700 mm [36]. Heat treatment made by producer (Sumitomo) was solution annealing under conditions 1150°C / 2 min. / cold by water quenched [36]. Samples were separated into two groups Not annealed (NA) and Annealed (A). Solution annealing was done under condition 1130°C / 15 min. / water cooling.

The heat number of supplied steel is F124139. Its chemical composition is summarized in Tab. 11. Supplied steel is in accordance with prescribed values by the standard ASME Case 2328-1.

*Tab. 11 Chemical composition of supplied steel SUPER 304H [36]*

|                         | C    | Si   | Mn   | P     | S    | Cu   | Cr   | Ni   | Nb   | B     | N    | Al    |
|-------------------------|------|------|------|-------|------|------|------|------|------|-------|------|-------|
| Min. (ASME Case 2328-1) | 0,07 | -    | -    | -     | -    | 2,50 | 17,0 | 7,5  | 0,30 | 0,001 | 0,05 | 0,003 |
| Max. (ASME Case 2328-1) | 0,13 | 0,30 | 1,00 | 0,04  | 0,01 | 3,50 | 19,0 | 10,5 | 0,60 | 0,010 | 0,12 | 0,030 |
| Heat No. F124139        | 0,08 | 0,25 | 0,81 | 0,003 | 0    | 3,07 | 18,3 | 9,0  | 0,49 | 0,004 | 0,11 | 0,005 |

Mechanical properties according [36] tested for complete tubes are listed in Tab. 12. All measured mechanical properties are in prescribed range. Impact testing was performed at specimens with 2 mm V notch 10 x 2,5 mm. Average value is  $KV_{2,5} = 30J$ . Grain size of supplied steel according [36] is G 9,5.

Tab. 12 Mechanical properties of supplied steel SUPER 304H [36]

|                     | Room Temperature           |                          |                         |          | 600 °C                     |                          |                         |          |
|---------------------|----------------------------|--------------------------|-------------------------|----------|----------------------------|--------------------------|-------------------------|----------|
|                     | R <sub>p0,2</sub><br>[MPa] | R <sub>p1</sub><br>[MPa] | R <sub>m</sub><br>[MPa] | A<br>[%] | R <sub>p0,2</sub><br>[MPa] | R <sub>p1</sub><br>[MPa] | R <sub>m</sub><br>[MPa] | A<br>[%] |
| Min.                | 235                        | 270                      | 590                     | 35       | 140                        | 165                      | 405                     | -        |
| Max.                | -                          | -                        | 850                     | -        | -                          | -                        | 850                     | -        |
| Heat No.<br>F124139 | 326                        | 376                      | 624                     | 43       | 200                        | 239                      | 464                     | 37       |

Part of experiments at the beginning of the thesis was performed for steel HR3C because of its availability. Specific chemical composition of used steel HR3C is summarised by Tab. 13.

Tab. 13 Chemical composition of used steel HR3C [37]

|                 | C    | Si   | Mn   | P      | S     | Cr   | Ni   | Nb   | N    |
|-----------------|------|------|------|--------|-------|------|------|------|------|
| Min             | -    | -    | -    | -      | -     | 23,0 | 17,0 | 0,20 | 0,15 |
| Max             | 0,10 | 1,50 | 2,00 | 0,0030 | 0,003 | 27,0 | 23,0 | 0,60 | 0,35 |
| Heat<br>F122036 | 0,06 | 0,41 | 1,19 | 0,0016 | 0     | 24,9 | 19,9 | 0,44 | 0,26 |

## 4.2 The laboratory isothermally ageing

For reaching of the degraded state of the austenitic steels SUPER 304H and Tp 347HFG laboratory isothermal aging without special protective atmosphere was used. Example of the used laboratory furnaces is shown at Fig. 55 and Fig. 56. Used temperatures were 650, 675 and 700°C. Those temperatures were selected like slightly higher with comparison with operation parameters of USC power plant, because of the degradation processes acceleration. Time of isothermal ageing was up to  $2,45 \times 10^4$ .



Fig. 55 *Furnace used for isothermal aging*



Fig. 56 *The furnace cavity interior*

### 4.3 Preparation of the experimental samples

#### 4.3.1 Preparation

The samples were after isothermal ageing removed from furnace and kept naturally cooled down. Cutting into semi-finished products for microscopy and mechanical properties testing was made at metallographic laboratory cutter Struers by 1,5 mm width cut off wheel 40A25.

The semi-finished samples for mechanical testing specimens were passed to the workshops for machining into final shape.

The semi-finished samples for microscopy were mounted in case of optical microscopy into the Sturers Epofix, in case of electron microscopy into the conductive Struers PolyFast.

#### 4.3.2 Mechanical processing

For samples grinding metallographic  $\text{Al}_2\text{O}_3$  grind papers with roughness 180, 800, 1200 and 2500 were used. Polishing was divided into two following steps. First rough polishing by diamond paste D3 (3  $\mu\text{m}$ ) and then fine polishing by alumina oxide (0,1  $\mu\text{m}$ ).

### 4.3.3 Etching

Three types of etching were used:

- Selective etching for the sigma phase revealed – Electrolytic etching with 10% KOH in distilled water (3 V dc, 4 s)
- Uniform etching – mixture of HCl, CH<sub>3</sub>COOH, HNO<sub>3</sub> (ration 3:2:1) and 0,1 (ration value) of glycerol. Applied by swabbing
- Uniform etching – Glyceregia [38] – HCl, glycerol, HNO<sub>3</sub> (ration 3:2:1). Applied by swabbing

## 4.4 Description of the used experimental methods

Sub-chapter 4.4 provides a brief description of used experimental methods. Sub-chapter division is into two groups the microstructure changes and the mechanical properties testing.

### 4.4.1 The structural changes study methodology

Part of the thesis focused on the characterisation of structural changes is crucial for reaching the thesis goals. The sigma phase quantification is based on colour (selective) etching and optical microscopy. Before quantification of the sigma phase it was necessary to confirm this phase by more sophisticated methods. For the phase identification TEM, SEM, EBSD were used. Chemical analysis of the sigma phase and its near surrounding of austenitic matrix were measured by EDS method.

#### 4.4.1.1 Optical microscopy

The optical microscopy is based on observation in visible spectrum of light. Wave length of the visible part of the spectrum is from 350 to 750 nm. This combination gave maximal useful magnification 1500x. [39] The scheme of optical microscope is shown in Fig. 57.

Quantification of the sigma phase was made at the optical microscope Nikon eclipse MA200 (Fig. 58) in magnification 1000x. Image analysis was made



in the software NIS-Elements Ar by automatic binary image detection with followed operator refinement.

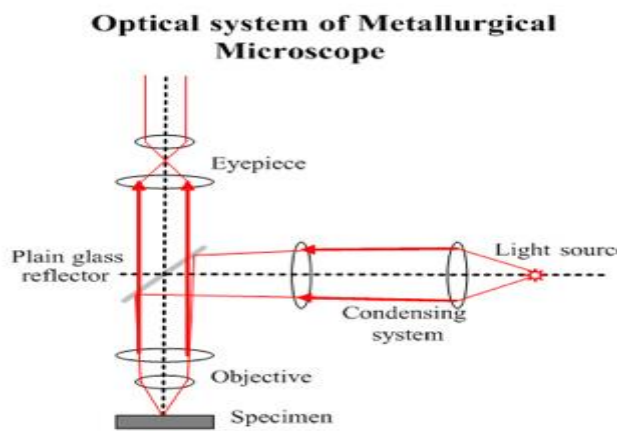


Fig. 57 *Optical system of metallurgical microscope [40]*



Fig. 58 *Nikon eclipse MA200 – Optical microscope*

#### 4.4.1.2 Scanning electron microscopy (SEM)

Observation by SEM is based on nearly the same principal like optical microscope, but source of signal are electrons. Wave length and then useful magnification depends on acceleration voltage. The electron spot can have less than nanometre in the diameter and rostering at the sample [41]. Resolution of SEM can be 10 nm [39]. For the sigma phase observation is SEM resolution satisfactory. Base scheme of SEM microscope is displayed in Fig. 59.

Used SEM microscope Jeol JSM-7600F is equipped with EDS detector and EBSD detector is displayed in Fig. 60. Used acceleration voltage was in range 10-20 KV (dependence on examine sample). Images were taken by LEI detector (secondary electrons) and LABE detector (back scattered electrons).

The secondary electrons provide information about structure and morphology of the observed sample. The back scattered electrons slightly reflect the chemical composition of an observed sample.

Observation was aimed to document the particles at the grain boundaries. Phase analysis inside grains was performed via EDS analysis. After mechanical properties testing SEM was used for observation of the fraction surfaces to provide information about morphology of a fracture.

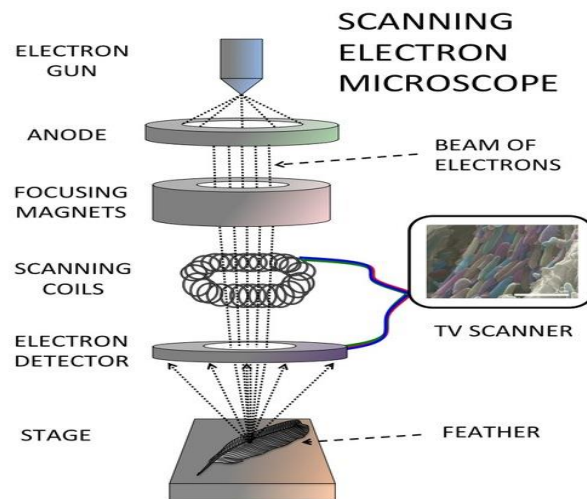


Fig. 59 Scheme of scanning electron microscope [42]



Fig. 60 SEM microscope Jeol JSM-7600F

#### 4.4.1.3 Transmission electron microscopy (TEM)

Transmission electron microscopy is based on the electron beam passage through the thin foil made from the sample, interacts with foil and provides information to the detector under a foil sample. [41] Scheme of the transmission electron microscope is shown in Fig. 61.

The samples observation was made at microscope JEOL JEM-2100F (Fig. 62). Microscope has point-to-point resolution 0.23 nm, it is equipped with X-Max80 Oxford Instruments EDS detector for X-ray microanalysis with analytical system Aztec, HAADF and BF detectors for STEM mode, 8Mpix camera by Gatan and software Digital Micrograph. [43]

TEM was used for precise particles identification and microchemical EDS analysis under higher magnification.

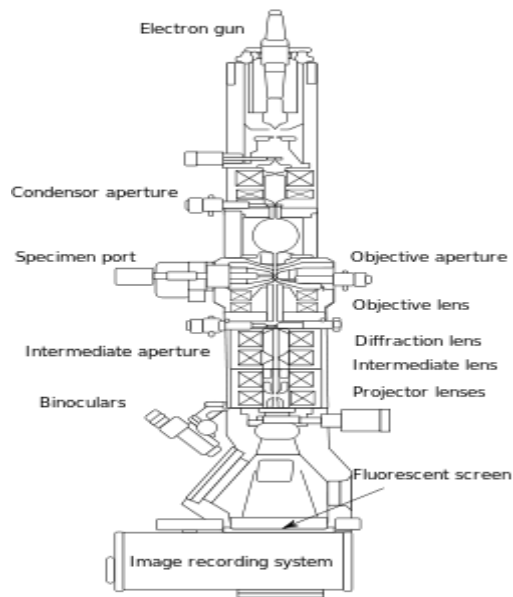


Fig. 61 *The scheme of transmission electron microscope [44]*



Fig. 62 *Transmission electron microscope JEOL JEM-2100F [43]*

#### 4.4.1.4 The energy dispersive spectroscopy (EDS)

This method is based on detection of the characteristic X-ray radiation generated from the examine sample by interaction with electron beam. Resolution is maximally about one nanometre. The accuracy of the measurement is on average 10% of measurement value (with usage of the etalons accuracy can be improved to 1%). [41]

SEM – EDS analysis was performed by the detector Oxford X-Max 50 mm<sup>2</sup> with operation software Inca. Chemical analysis provides information not just about constitution of the precipitates but also about surrounding area or chemical elements depleted zones. Last application of EDS analysis used in this paper was mapping of chemical composition.

#### 4.4.1.5 The electron backscattered diffraction (EBSD)

EBSD provides quantitative microstructural information about the crystallographic nature of metals, minerals, semiconductors, and ceramics - in fact most inorganic crystalline materials. [45]

EBSD operates by arranging a flat, highly polished (or as-deposited thin film) sample at a shallow angle, usually 20°, to the incident electron beam

(Fig. 63) (since the SEM stage is often used to tilt the plane of the sample to this shallow angle, the value of stage tilt is often referred to and is typically 70°). With an accelerating voltage of 10–30 kV, and incident beam currents of 1–50 nA, electron diffraction occurs from the incident beam point on the sample surface. With the beam stationary, an EBSD pattern (EBSDP) emanates spherically from this point.

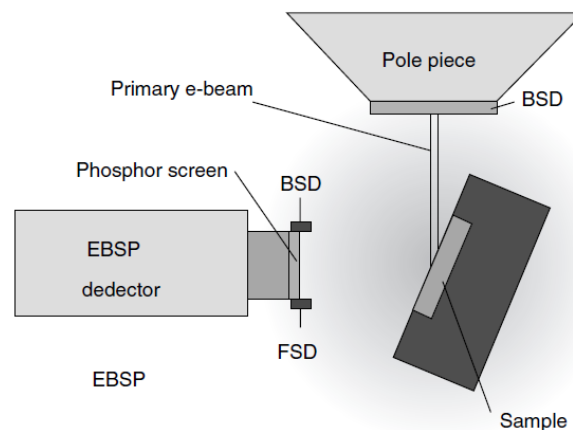


Fig. 63 Schematic arrangement of sample orientation in the SEM [45]

By application of this method the particles contain in thermal exposed samples was identified.

#### 4.4.2 Mechanical properties testing methods

Microstructural changes do not mean just precipitation of the particles inside of microstructure but also precipitation dependency changes of the mechanical properties like hardness, strength, stiffness etc. Sub-chapter 4.4.2 provides information about used testing methods for mechanical properties changes description.

##### 4.4.2.1 The tensile test

All tensile tests were performed under conditions specified by the norm [46]. It was used short test specimens with reduced diameter 5 mm and equal test length 25 mm. Heads of tensile test specimens were threaded. All tests were carried out with stable deformation velocity 0,5 mm/min. The scheme drawing of used sample type is shown in Fig. 64.

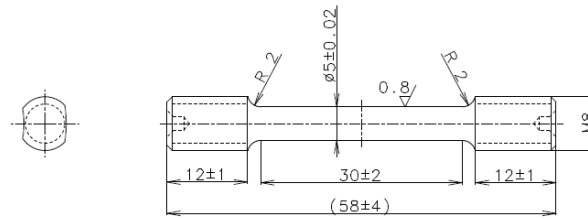


Fig. 64 The tensile test specimen drawing

#### 4.4.2.2 The Charpy pendulum impact test

The impact strength measurement was done by specifications in the norm [47]. The reduced impact samples with 2 mm V notch and 5 mm width were used. Energy of the used Charpy hammer was 300 J. The scheme drawing of the used sample type is shown in Fig. 65

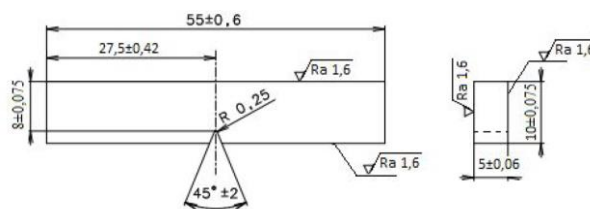


Fig. 65 The pendulum impact test specimen drawing

### 4.5 The precipitation and structural modelling

There are some possible approaches for quantification and description of the material degradation state and actual mechanical properties description. One of those approaches is presented in [48]. Presented method was developed for the steel 12022 and it compares microstructural changes and hardness measurement. Summarization of the methods is presented by table and plots Tab. 14, Fig. 66, Fig. 67 and Fig. 68. Methodology of degradation description for low alloyed ferritic-bainitic steels is well known. On the other hand, no results are published for austenitic creep resistant steels, which provided motivation for this thesis. Principle of the method published in [48] can be modified for austenitic steels.

Tab. 14 Characteristic of degradation phase of structure [48]

| Degree of degradation | Ferritic-pearlitic structure   | Ferritic-bainitic structure  |
|-----------------------|--|--|
| A                     | Pure ferritic grain + pearlite   | Pure ferritic grain + bainite  |
| B                     | Incipient spheroidisation of cementite lamellae in pearlitic grains and isolated precipitation of grain boundary ferrite     | Incipient precipitation of carbide on ferritic grain boundary, begin of coarsening of carbide in bainite                 |
| C                     | Significant spheroidisation of cementite in pearlite grains, ongoing precipitation of carbide at grain boundary ferrite      | Observable coarsening of carbide in bainite, finishing of precipitation ferrite, coarsening of carbide on grain boundary |
| D                     | Nearly complete spheroidisation of cementite, rough carbide on grain boundary, weak precipitation of carbide inside of grain | Rough carbide, deletion of difference between ferritic and bainitic grains   |
| E                     | Rough sphere carbide inside grain and on grain boundary, partial deletion of difference between ferrite and pearlite grain   | Rough globular carbide into grain and on grain boundary, ferrite-carbide morphology                                      |
| F                     | Rough carbide mainly on grain boundary, some carbide inside of grain   | Rough carbide mainly on grain boundary, some carbide inside of grain   |

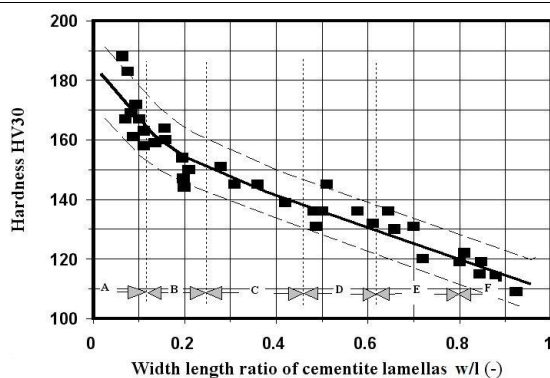


Fig. 66 The dependence of hardness on globularisation of cementite for ČSN steel 12 022 [48]

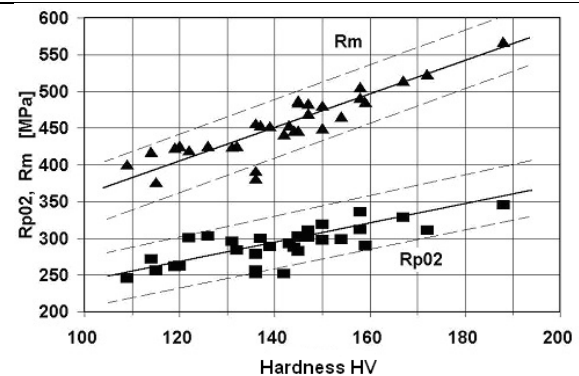


Fig. 67 The dependence of strength on hardness of ČSN steel 12 022 [48]

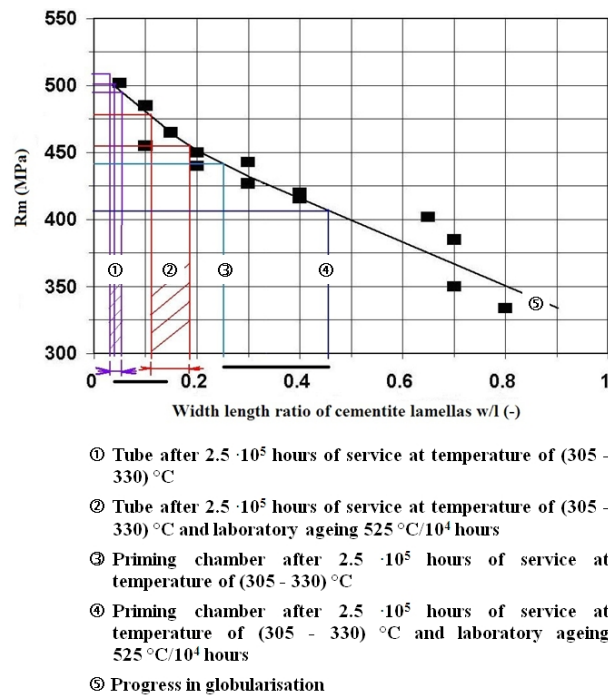


Fig. 68 The dependence of tensile strength on structural parameters [48]

The method presented in literature [48] is just descriptive and there is a problem with making of a prediction. This problem can be eliminated by usage of dynamic variable.

Model will be based on combination of the Fick laws, changes of free enthalpy of system and information about sigma phase. With additional information this model can be used for other predictions like residual lifetime calculation.

The input parameters for the model will be chemical composition of alloy, pressure and temperature,

The first part like length, diameter etc. measurement will be done by optical microscope/ colour etching. Electron microscopy and EDX analysis provides information for later researches. The matrix relations and disorientation in austenite/sigma will be subjected to investigation by EBSD. If it will be possible TEM will be used.

The prediction model gets together chemical composition of alloy, temperature and pressure of expose with Fick's laws of diffusion and changes of Gibbs free enthalpy.

Combination of the used equations leads to a dynamic computation model. The advantage of the dynamic model is possibility to stop the computation in any time. The possibility of any time computations ends gave better practical applicability of the model results.

All the information obtained by microscopy will be used for verification of the prepared prediction model.



## 5 Experimental part

Chapter 5 briefly summarizes obtained experimental results linked to publications where there were published.

### 5.1 The electron microscopy

#### 5.1.1 The sigma phase particles identification

Exact particles identification is crucial for reaching this thesis goal. The overview article about sigma phase ([10]) summarises a critical group of austenitic steels which is suitable for the sigma phase precipitation. This group contains SUPER 304H, Tp 347HFG and HR3C steels. HR3C is the only one from those steels with coarse grains. Particles identification for coarse grains steel is quite easier in comparison with fine grains type. That was the reason why to start with identification of the sigma phase for steel HR3C. Base material and welding joints of HR3C were used. Literature [49] shows precipitation processes in steel HR3C which belong to the from same category like SUPER 304H (heat resistant austenitic steel). Precipitation processes are additionally influenced by plastic deformation etc.

Precipitation accelerated by plastic deformation is shown in Fig. 69 and Fig. 70. After 15000 hours of thermal exposition precipitation is conclusive (Fig. 70) [49]. Fig. 69 and Fig. 70 present various types of precipitates. The thesis is based on the sigma phase description. That calls for precise particles description.

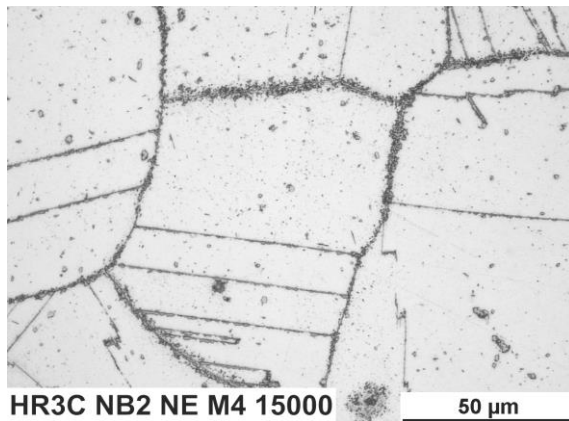


Fig. 69 Grain boundary in neutral wall of R60 bend without HT, aged 15000 hours/650°C [49]

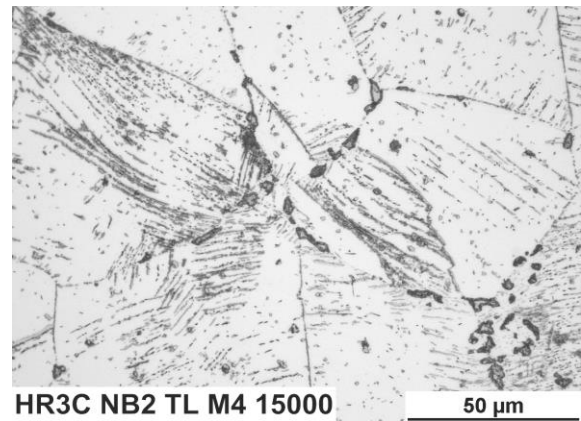


Fig. 70 Grain boundary in pressured wall of R60 bend without HT, aged 15000 hours/650°C [49]

Published results in [50] allocated steel Super 304H into critical group of steels which is suitable for the sigma phase precipitation. The investigation was focused on the influence of deformation degree on incidence of brittle sigma phase precipitation and its effect on the mechanical properties.

Fig. 71 and Fig. 72 show exposed SUPER 304H base material microstructure. Boiler exposition condition was within the temperature range of 650 - 680°C and time of exposition  $7.5 \cdot 10^3$  hours. On the grain boundaries and inside the grains it is possible to document precipitation of various types of particles. The particles identification was focused on sigma phase occurrence which preferably precipitates on grain boundaries. [50]

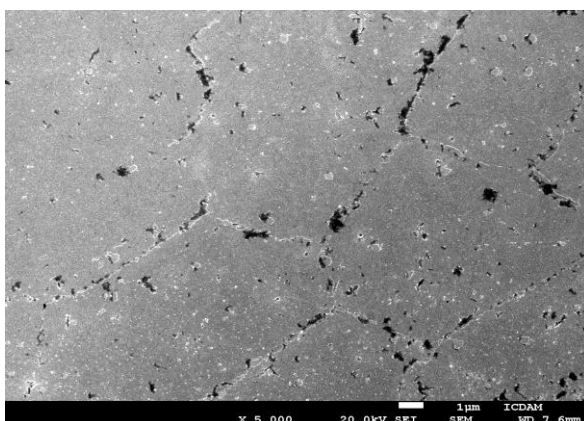


Fig. 71 SEM microstructure of parent material after exposition in boiler conditions [50]

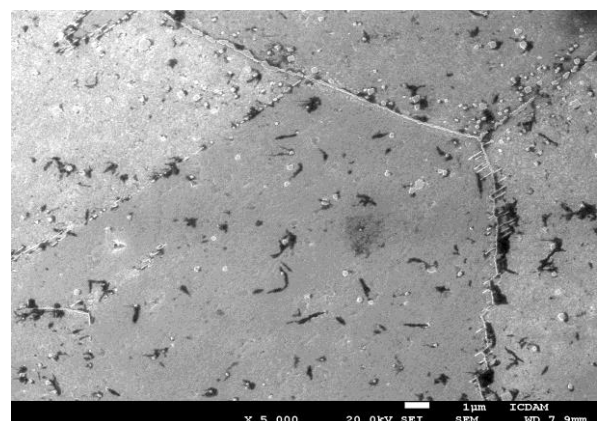


Fig. 72 SEM annealed microstructure of parent material after exposition in boiler conditions [50]

For the particles identification combination of various methods was used. Scanning electron microscope (SEM) provided with EDS detector was used for the base material chemical composition measurement. [50]

Investigated particles in microstructure are summarised in Fig. 73. Corresponding EDS spectra are summarise in Fig. 74.

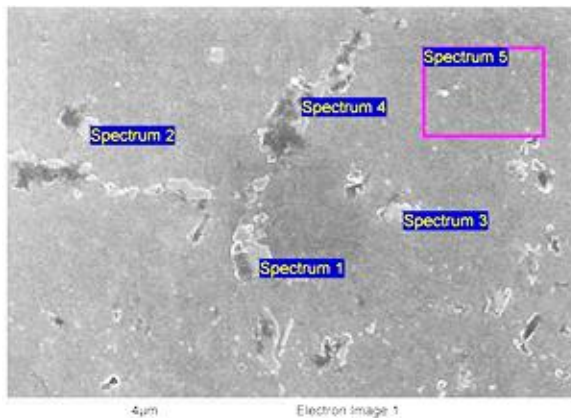


Fig. 73 Analysed particles in microstructure [50]

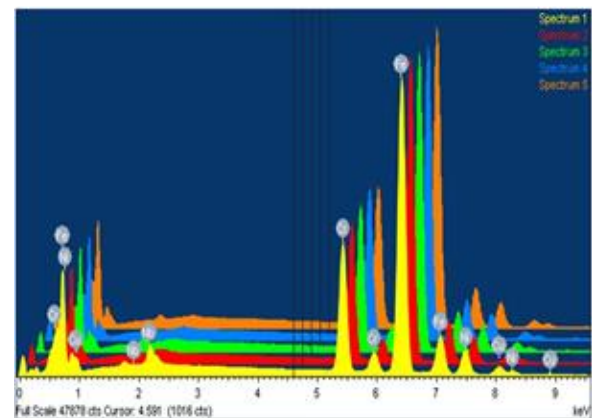


Fig. 74 The EDS spectra measured for difference particle (Fig. 73) [50]

Chemical composition of measured particles is shown in the Tab. 15. The differences of chemical composition are negligible. Chemical composition of particles is approximately same like the base material. As shown in Fig. 74 there are no significant differences in measured EDS spectra. Any particles occurred in base material cannot be characterised like the sigma phase, which have composition approximately 50 % Cr and 50 % Fe. [50] Small difference between sigma phase and base material chemical composition was caused by the etching method. During etching sigma phase was firstly etching and then base material. This caused removal of the sigma phase.

Tab. 15 Measured chemical composition (Fig. 73) [50]

| Spectrum   | Cr [%] | Fe [%] | Ni [%] | Cu [%] | Nb [%] | Mo [%] |
|------------|--------|--------|--------|--------|--------|--------|
| Spectrum 1 | 18.28  | 65.63  | 8.72   | 3.43   | 3.60   | 0.34   |
| Spectrum 2 | 19.15  | 67.65  | 8.96   | 3.02   | 0.78   | 0.44   |
| Spectrum 3 | 20.27  | 66.60  | 8.96   | 3.49   | 0.30   | 0.39   |
| Spectrum 4 | 21.18  | 66.24  | 8.91   | 3.28   |        | 0.39   |
| Spectrum 5 | 19.82  | 67.60  | 8.96   | 2.99   | 0.23   | 0.40   |

Results from precipitation investigation of SUPER 304H samples after longer time of laboratory exposition (20 000 hours) was published in [51]. Precipitated sigma phase is marked at the base of chromium detection in Fig. 75. Position of precipitation on the grain boundaries triple points agrees with chapter 2.1.5.

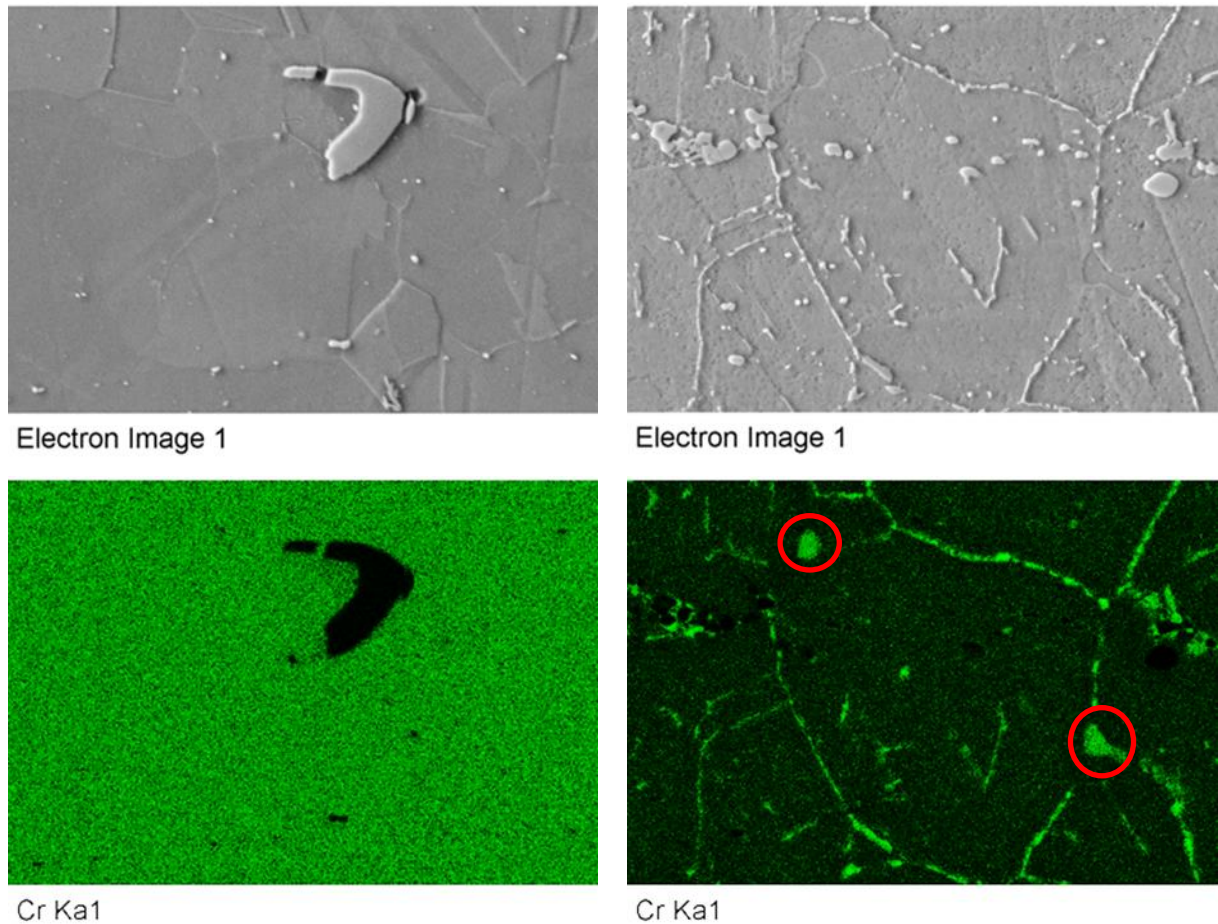


Fig. 75 *Microstructure and Cr map of base material (left) and aged by 20000 hours (right)*  
[51]

The same mechanism was documented for welding joints of steel SUPER 304H. Fig. 76 shows microstructure of SUPER 304H initial state in the crown layer of HAZ. Analysis of microstructure of unaged crown layer showed that the mean grain size area in the crown layer in HAZ was about  $193 \mu\text{m}^2$  and the  $\sigma$ -phase was not detected for initial state. Long-term isothermal ageing caused no significant coarsening of austenitic grains (Tab. 16), however led to the formation of brittle  $\sigma$ -phase (Fig. 77). A detailed investigation of the microstructure showed that  $\sigma$ -phase was predominantly situated at triple points and also along boundaries of austenitic grains. In the structure of aged based

material approximately 2.3 % of  $\sigma$ -phase was present. Slightly higher values of the  $\sigma$ -phase concentration and mean grain size were derived in HAZ of crown layer (Tab. 16). In this area  $\sigma$ -phase was also predominantly formed at triple points and grain boundaries (Fig. 78). The largest changes in microstructure were observed in central and root layers of HAZ (Fig. 79). Results demonstrate that these areas contain significantly larger grains and reduced portion of  $\sigma$ -phase in comparison with based material and crown layer after long-term isothermal ageing (Tab. 16). [52] White particles are niobium carbonitrides.

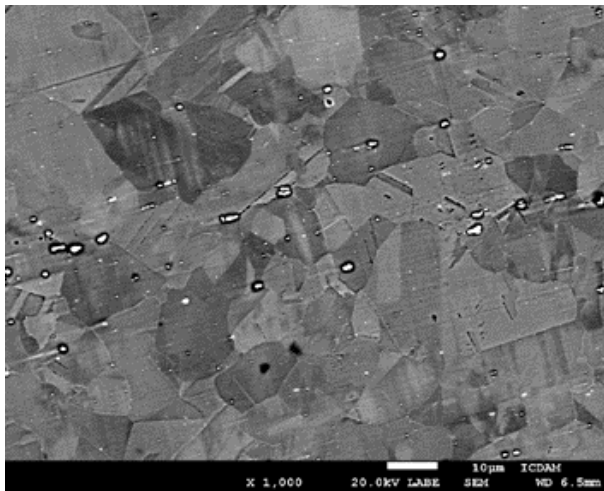


Fig. 76 Microstructure of as-received state in crown layer [52]

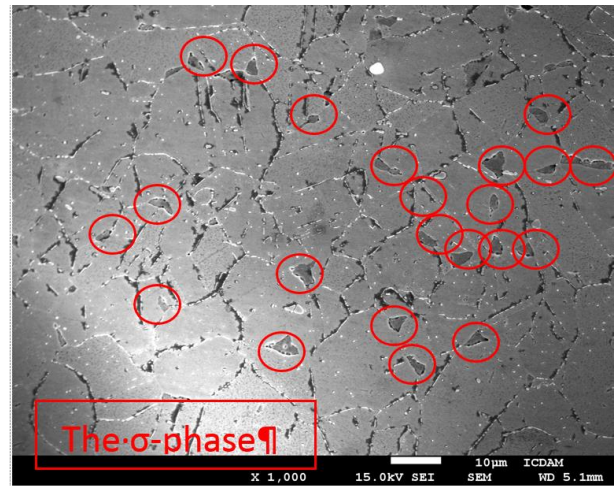


Fig. 77 Formation of  $\sigma$  phase after aging  $2 \times 10^4$  h [52]

Tab. 16 Microstructure characteristics in base material and welding joints zones [52]

| Zone              |                      | Objects | Portion of area | Grain size |                     |
|-------------------|----------------------|---------|-----------------|------------|---------------------|
|                   |                      | [-]     | [%]             | [G]        | [ $\mu\text{m}^2$ ] |
| As-received state |                      | 0       | 0               | 9          | 267                 |
| Aged              | Base material        | 54      | 2.265           | 9          | 234                 |
|                   | Outer diameter layer | 67      | 2.734           | 9.5        | 118                 |
|                   | Middle layer         | 25      | 1.002           | 6.5        | 1830                |
|                   | Inner diameter layer | 13      | 0.489           | 5          | 3924                |

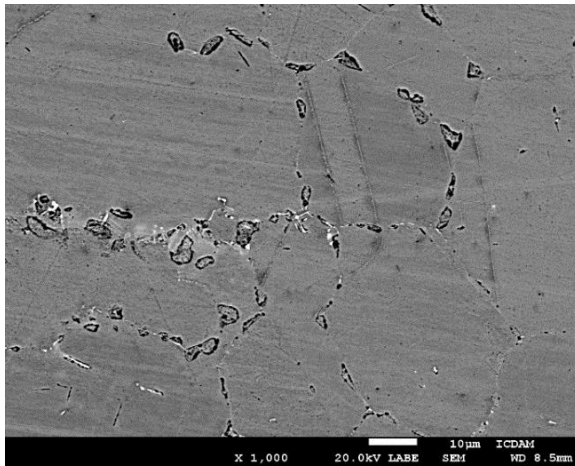


Fig. 78 *Distribution of  $\sigma$ -phase in the crown layer [52]*

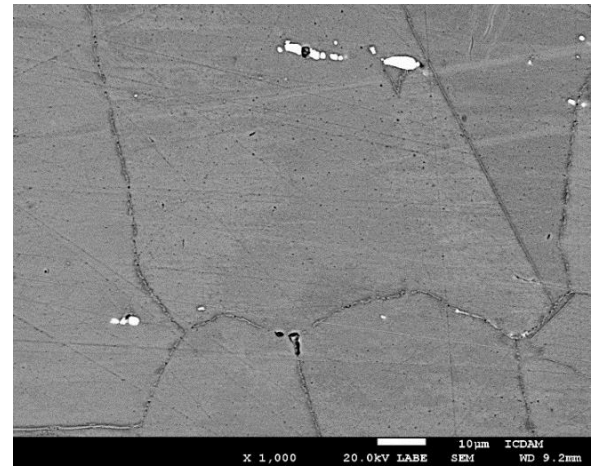


Fig. 79 *Distribution of  $\sigma$ -phase in the root layer [52]*

The cross-section of  $\sigma$ -phase obtained by FIB technique used for TEM-foils preparation enabled more detailed investigation of  $\sigma$ -phase situated on the boundaries. Fig. 80 shows the distribution of Cr (green color), Nb (dark blue) and Cu (magenta) around the grain boundaries. It can be seen that colonies of relatively fine  $\sigma$ -phases (mean size  $\sim 300$  nm) were formed along the grain boundaries which are covered by large Cr and Nb carbides. It was also observed that Cu particles (denoted B) are located very often at the interphase of boundaries between  $\sigma$ -phase and matrix (Fig. 81). In the  $\sigma$ -phase interior (denoted A) Nb carbides (denoted C), Cu particles (denoted B) sitting on the  $\sigma$ -phase edges were observed (Fig. 80, Fig. 81). [52]

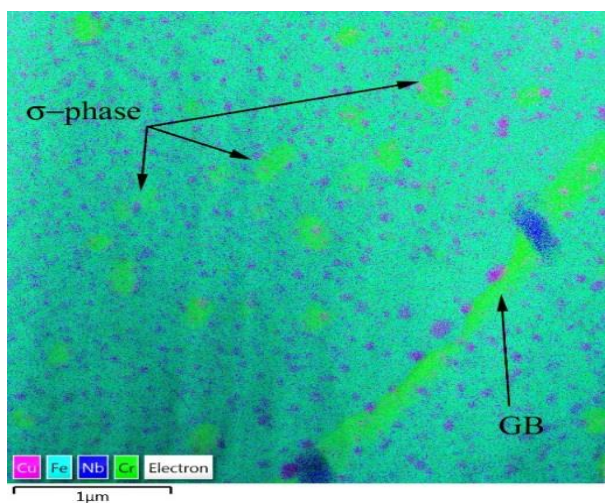


Fig. 80 *Distribution of elements around austenitic grain boundary [52]*

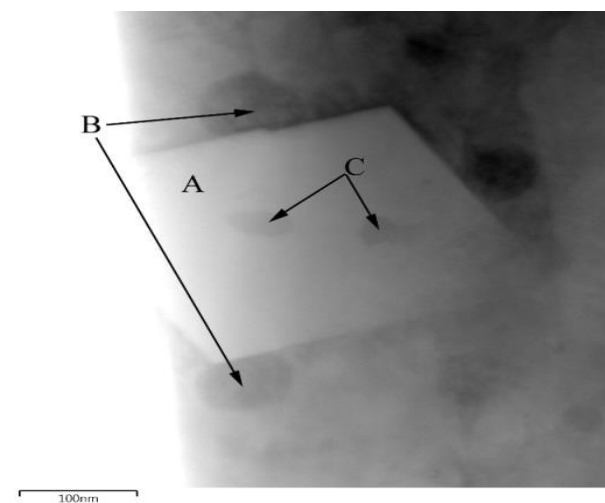


Fig. 81 *TEM image of  $\sigma$ -phase cross-section [52]*

Based on the published results detailed SEM and TEM analyses were performed. Results of chemical composition mapping are summarized in Fig. 82 and Fig. 83. The aim of these analyses is to validate sigma phase in microstructure at the base of phase's chemical compositions.

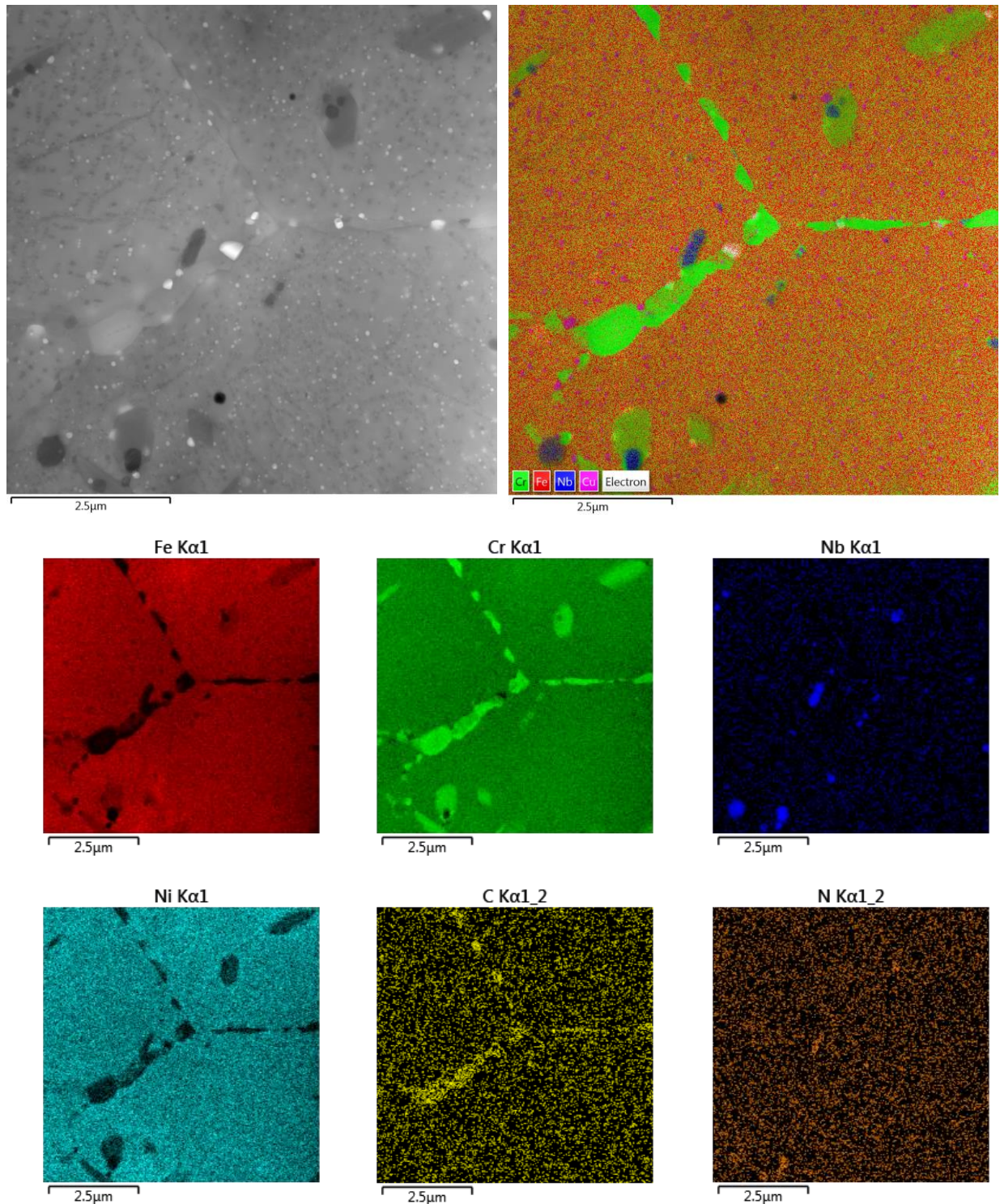


Fig. 82 SEM analyses around grain boundaries

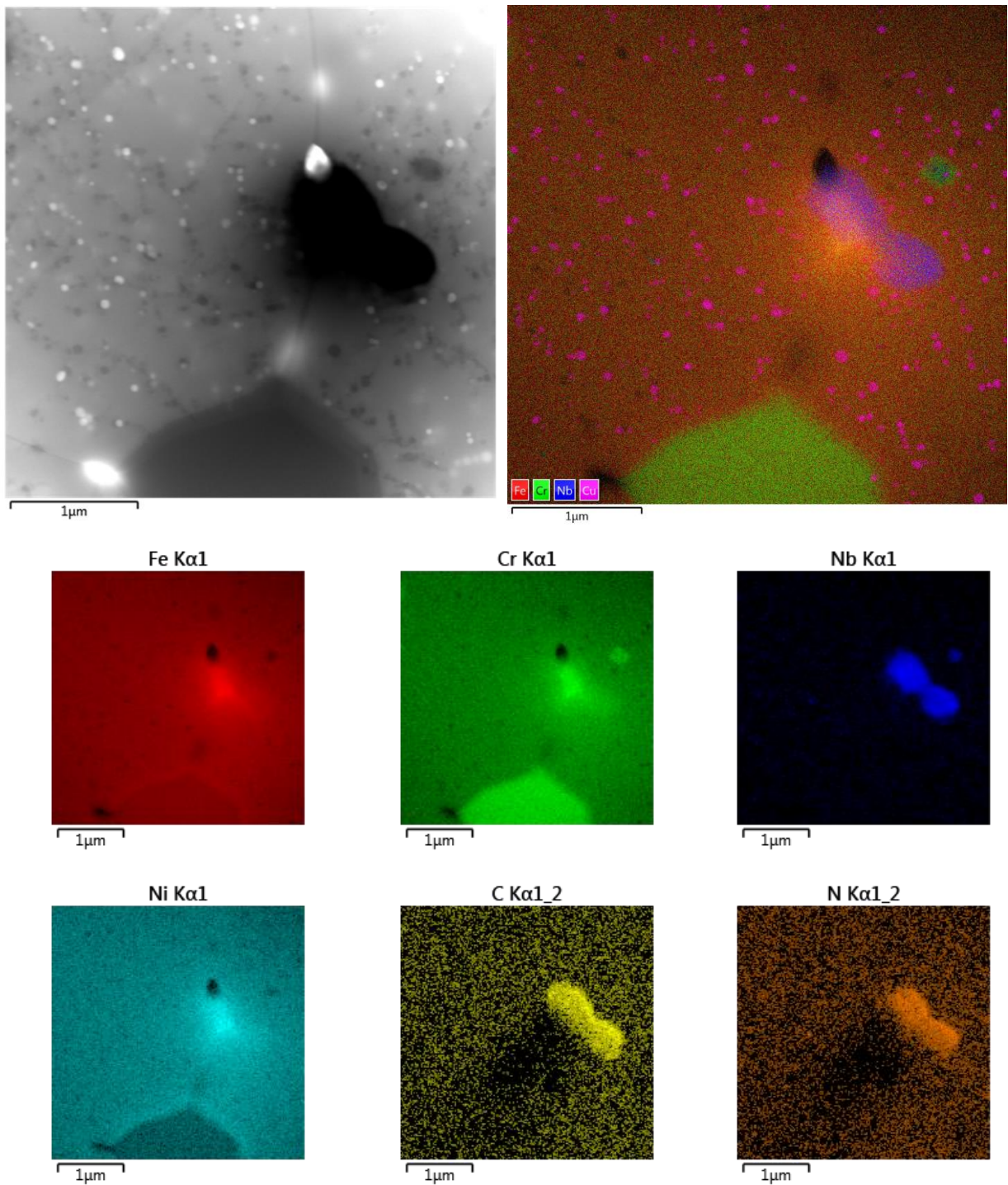


Fig. 83 *TEM analysis of particles*

According to the chemical composition results obtained by SEM and TEM chemical composition corresponds with base data published in [10].

Phase identification shown in Fig. 85 was based on the morphology and chemical composition of the particles. Chemical composition of marked sigma phase is summarized in Tab. 17. Fig. 84 summarises the sigma phase lattice



parameters and chemical composition variation. For absolute accuracy identification it is necessary to perform atomic diffraction of the phase or to use the EBSD method.

| Alloy                 | Lattice parameter (Å)                          | Composition of phase (wt%) |       |       |       |     | Formula            |
|-----------------------|--|----------------------------|-------|-------|-------|-----|--------------------|
|                       |  | Fe                         | Cr    | Ni    | Mo    | Si  |                    |
| Fe-Cr                 | $a_0 = 8.799, c_0 = 4.544$                     |                            |       |       |       |     | Fe-Cr              |
| Fe-Mo                 | $a_0 = 9.188, c_0 = 4.812$                     |                            |       |       |       |     | Fe-Mo              |
| 17Cr-11Ni-2Mo-0.4Ti   | —  |                            | 30    | 4.3   | 9     | 0.8 | $(FeNi)_x(CrMo)_y$ |
| 17Cr-11Ni-0.9Mo-0.5Ti | —  |                            | 33    | 4.5   | 5.4   | 0.7 |                    |
| Type 316              | $a_0 = 8.28 \sim 8.38, c_0 = 4.597 \sim 4.599$ | 55                         | 29    | 5     | 11    | —   |                    |
| Type 316L             | $a_0 = 9.21, c_0 = 4.78$                       |                            |       |       |       |     |                    |
| 20Cr-25-34Ni-6.5-8Mo  | $a_0 = 8.87, c_0 = 4.61$                       | 35/37                      | 17/26 | 15/21 | 21/28 | —   |                    |
| 25Cr-20Ni             | —  | 40                         | 46    | 9.4   | —     | 3   |                    |

Fig. 84 Lattice parameters and chemical composition of the sigma phase [10]

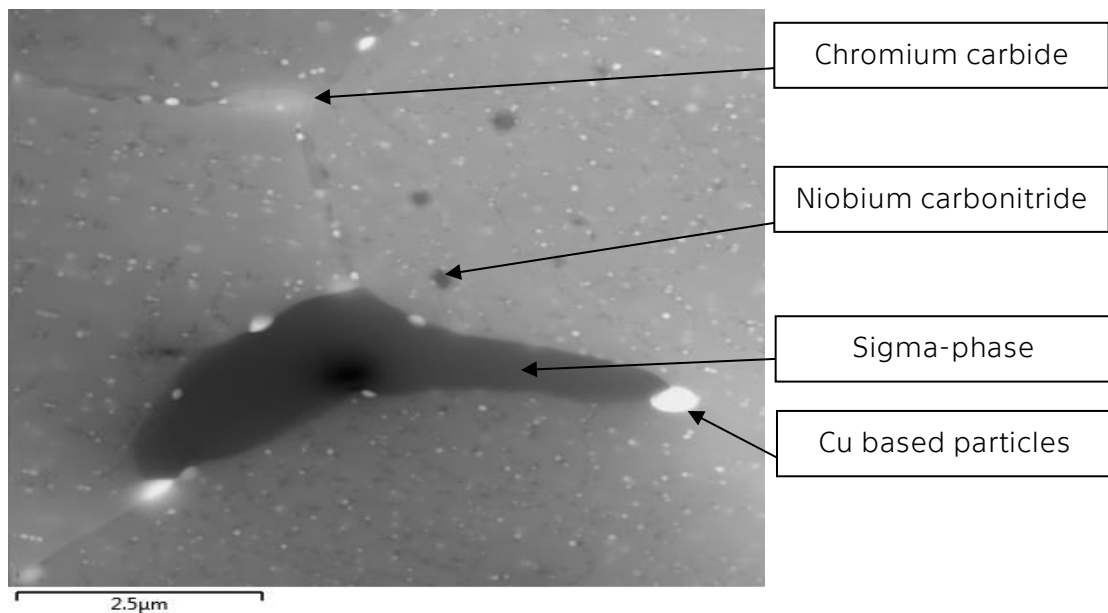


Fig. 85 Identification of particles and sigma-phase – State after 15 000 hours of ageing [53]

Tab. 17 Chemical composition of sigma-phase – State after 15 000 hours of ageing [53]

| Point analysis of chemical composition of sigma-phase (w.%) |      |
|---|------|
| Fe  | 53,1 |
| Cr  | 40,8 |
| Ni  | 3,2  |
| Mo  | 2,2  |
| Si  | 0,8  |

The kikutchi lines obtained from transmission diffraction (Fig. 86a) were compared with a theoretical model for sigma-phase. Conformity with the theoretical model is shown in Fig. 86b. [53]

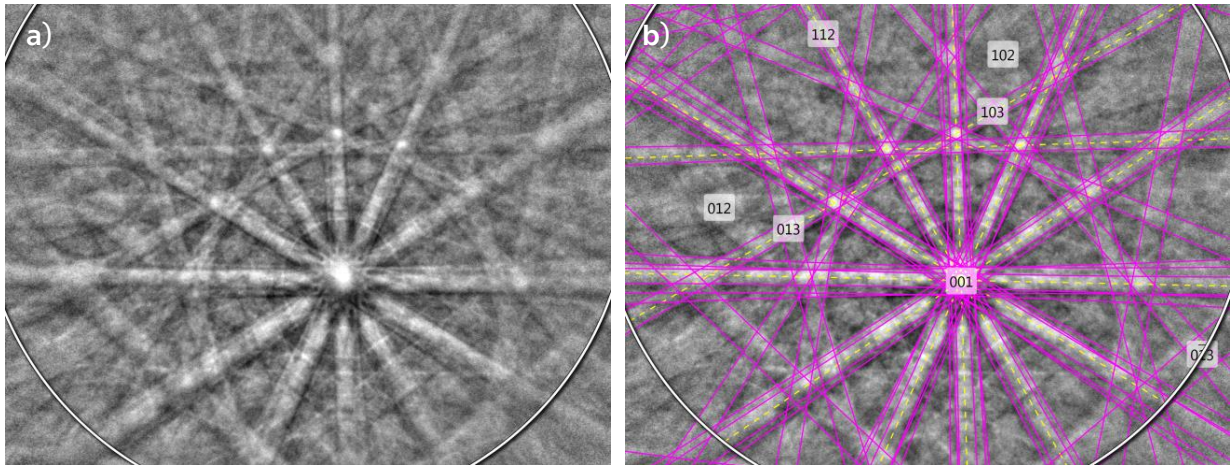


Fig. 86 Kikuchi lines obtained in the analysis of sigma phase in the steel Super 304H a) measured lines b) conformity with the theoretical model [53]

EBSM phase map is shown in Fig. 87. Identification of phases:

- Red - Austenitic matrix
- Green – Chromium carbide
- Light blue – Sigma-phase

Phase map confirms that the sigma-phase precipitates on the grain boundaries, respectively starts precipitation inside the grains.

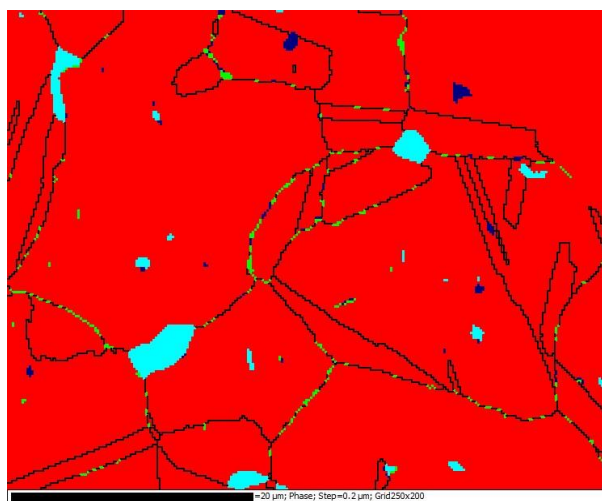


Fig. 87 EBSM phase map analysis [53]

### 5.1.2 The sigma phase precipitation morphology

After 15 000 hours of isothermal ageing (675°C) significant changes in microstructure occur. As it shown in Fig. 88 there are several types of precipitates. On the grain boundaries the chromium carbides and niobium carbonitrides precipitated. The niobium carbonitrides of the dimension up to 3  $\mu\text{m}$  precipitated inside the grains. The last group of precipitates can be identified like sigma-phase with maximal dimension of about 6,5  $\mu\text{m}$  [53].

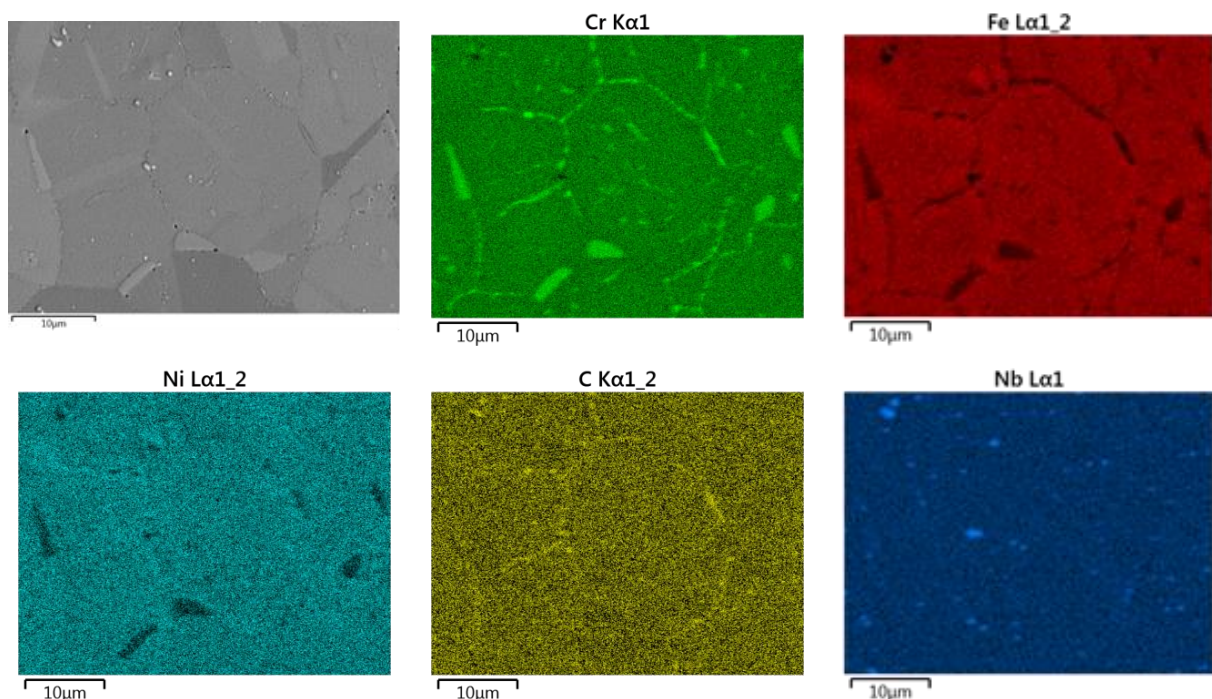


Fig. 88 Maps of chemical composition SEM/EDS – State after 15 000 of ageing [53]

For identification of sigma-phase particles transmission electron microscopy was used. Fig. 89 shows chemical composition maps made by EDS detector on thin foil. There (Fig. 89) are three elliptic particles which can be classified like the sigma-phase. The length of these particles is around 2,5  $\mu\text{m}$  [53].

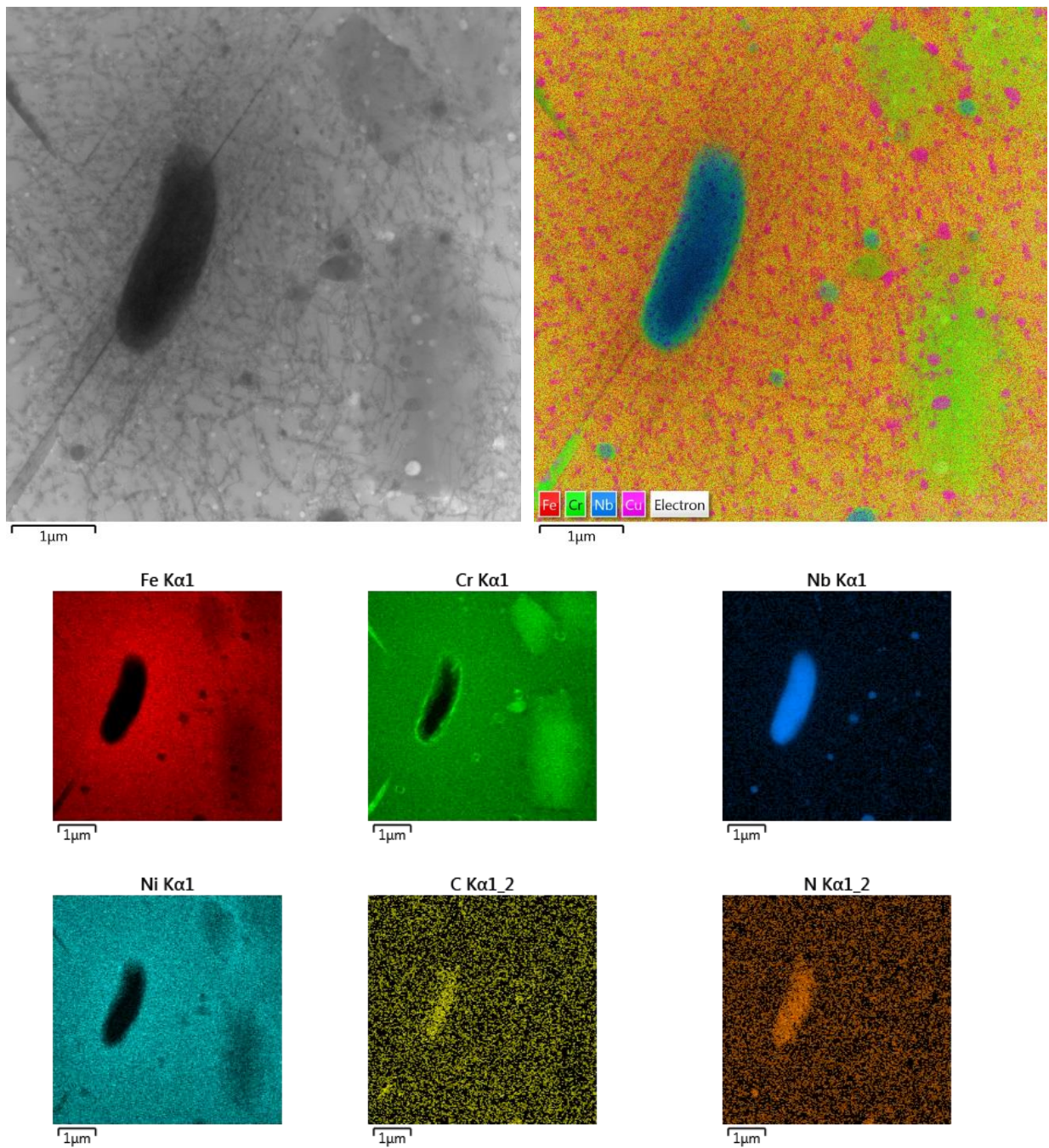


Fig. 89 Maps of chemical composition TEM/EDS - State after 15 000 of ageing [53]

A change between states after 15 000 and 20 000 hours of ageing consists in an increase of the sigma phase size. Sigma-phase of the dimension about 10  $\mu\text{m}$  (Fig. 90) can lead to significant decreasing of the impact strength [53].

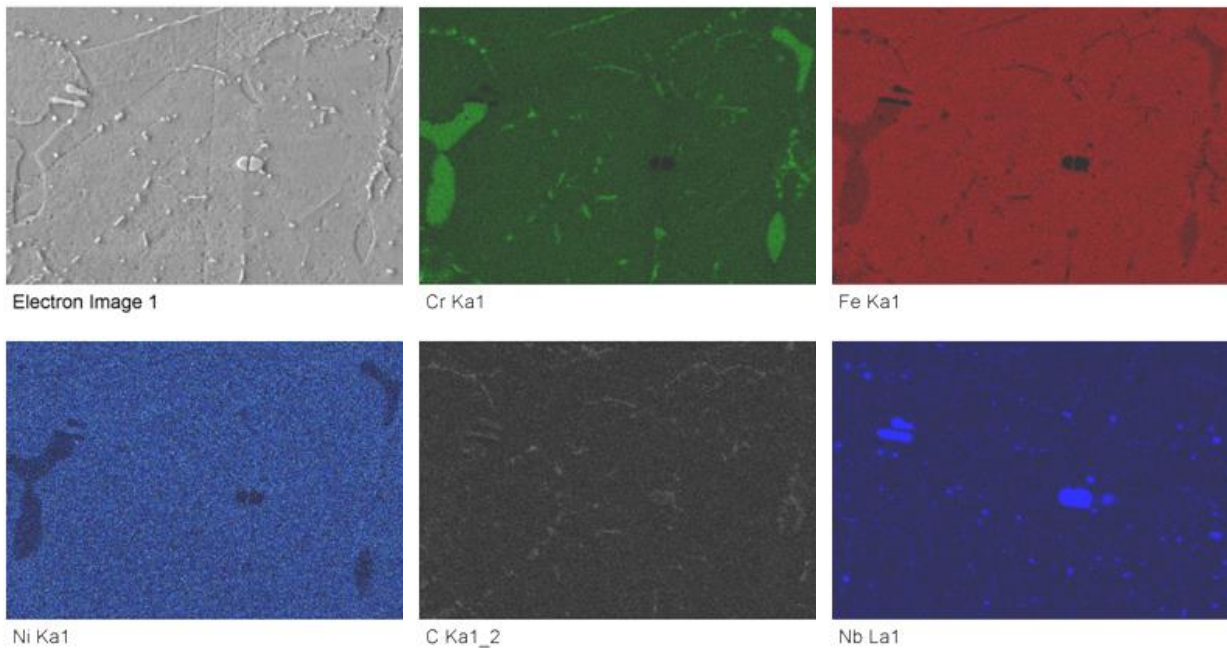


Fig. 90 Maps of chemical composition SEM/EDS – State after 20 000 of ageing [53]

In general precipitation of the sigma phase starts on the grain boundaries especially at the triple grain boundaries intersection.

In case of welding joints the situation is quite different. Difference in grain size across welding joint layers is caused by absorbed heat energy during the welding process. It means that the root layer was exposed longer to higher temperatures than the last crown layer because it was repetitively heated by additional welding passes. Coarsening of grains in root layer led to the significant reduction of  $\sigma$ -phase formation. This result indicates that sigma phase is predominantly formed at triple points and grain boundaries due to the higher Cr content and defect concentration. It was proposed that sigma phase is formed from  $M_{23}C_6$  by carbon elimination. It was also observed that sigma phase formation occurred independently of  $M_{23}C_6$ . In alloys without  $M_{23}C_6$  carbides precipitation will be slower [52].

### 5.1.3 The correlation between the electron and the optical microscopy

It is possible to say that the amount of Sigma-phase in microstructure leads to decreasing of the impact strength. A possible approach for quantification of sigma-phase in quite lower magnification would be using of

light-microscopy/color etching (LM). Comparison of the microstructure from LM and the microstructure from SEM is shown in Fig. 91 and Fig. 92. White particles in Fig. 91 are sigma-phases. These white particles have sufficient contrast in comparison with matrix. Thus, the image analysis for quantification of the amount of the sigma-phase will be possible to use. [53]

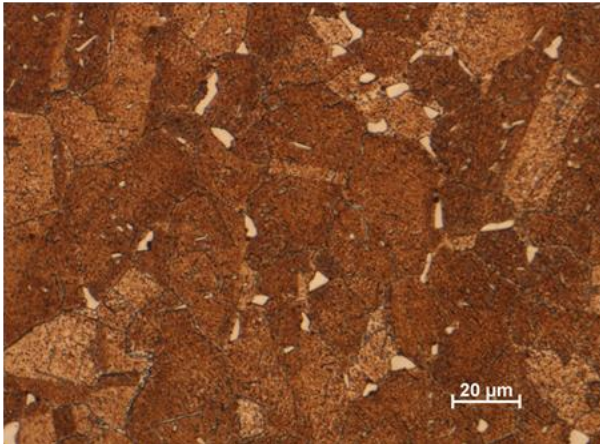


Fig. 91 Microstructure after color etching (sigma-phase white) [53]

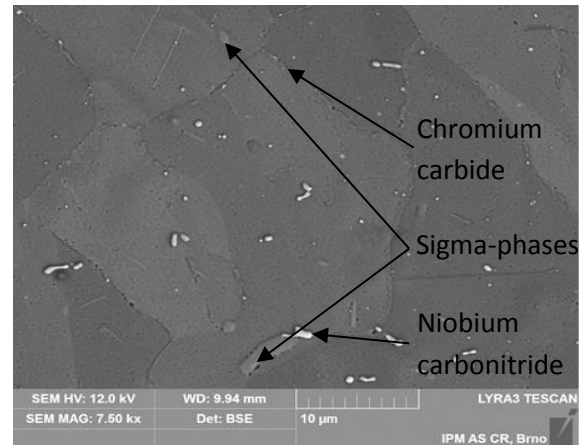


Fig. 92 Microstructure with marked phases for comparison with Fig. 91 [53]

To meet this thesis goals quantification of the sigma phase is crucial. Subchapter 5.1.1 confirms the sigma phase in SUPER 304H steel. The correlation sample is used for direct comparison between an electron and optical microscope.

The chemical composition of the sigma phase and SUPER 304H steel matrix measured on the correlation sample is presented by Fig. 93, chemical composition results by Tab. 18. In Tab. 18 chromium and iron content are highlighted. Ratio of chromium and iron for Spectrum 1 confirms the sigma phase.

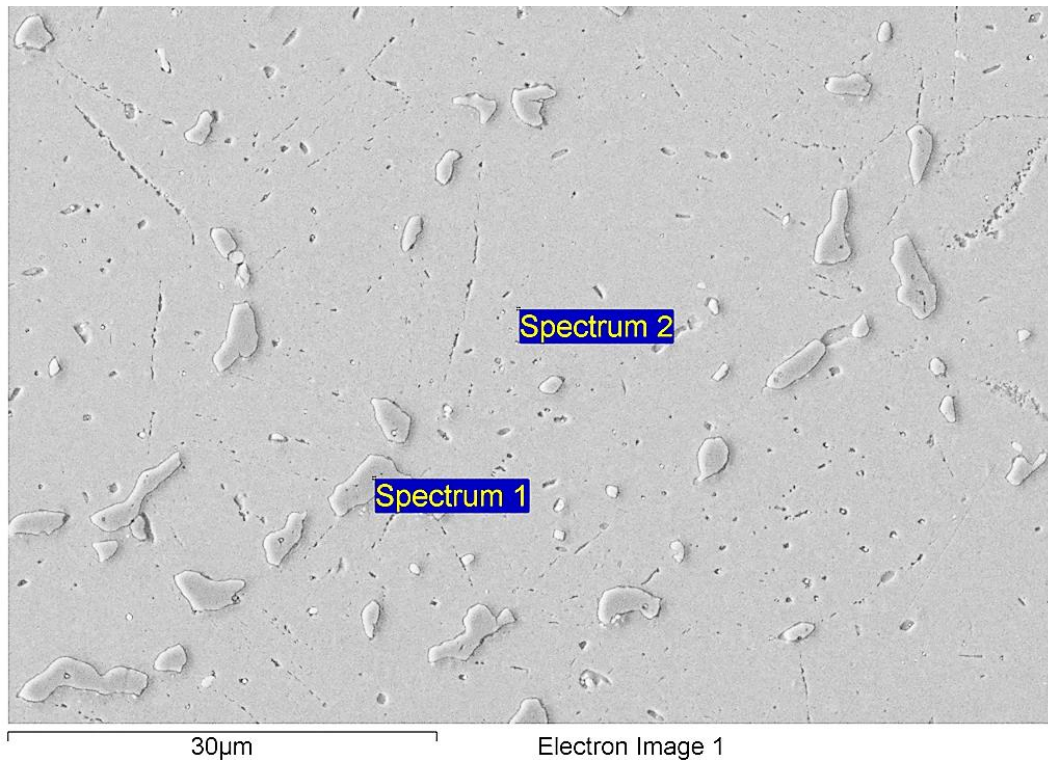


Fig. 93 EDS point analysis for correlation sample

Tab. 18 Chemical measurement results for Fig. 93

| Spectrum   | Si   | P    | Ca   | Cr    | Fe    | Ni   | Cu   | Nb   | Mo   | W    |
|------------|------|------|------|-------|-------|------|------|------|------|------|
| Spectrum 1 | 0.97 | 0.46 | 0.35 | 36.29 | 56.27 | 3.33 |      |      | 1.98 | 0.35 |
| Spectrum 2 | 0.37 |      |      | 18.84 | 66.95 | 8.80 | 4.54 | 0.15 | 0.35 |      |

The following image (Fig. 94) shows direct comparison between the electron microscope image, measured chromium and iron maps and the optical microscope image. The blue circles added to Fig. 94 connect one of the sigma phases visualised by different methods.

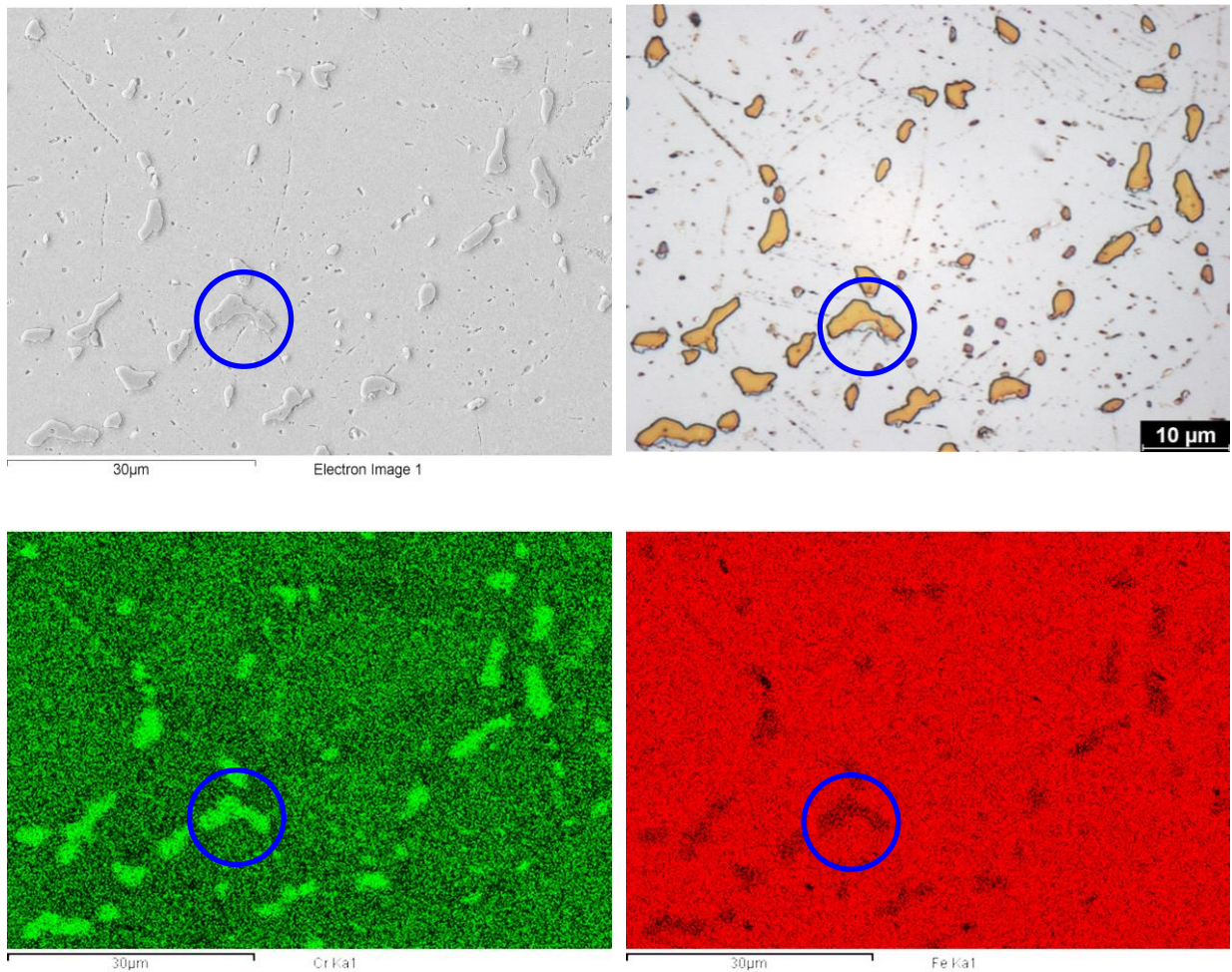


Fig. 94 *Comparative image for sigma phase verification for optical microscopy*

Results documented by Fig. 94 give possibility to use optical microscopy for the sigma phase quantification.

## 5.2 The optical microscopy

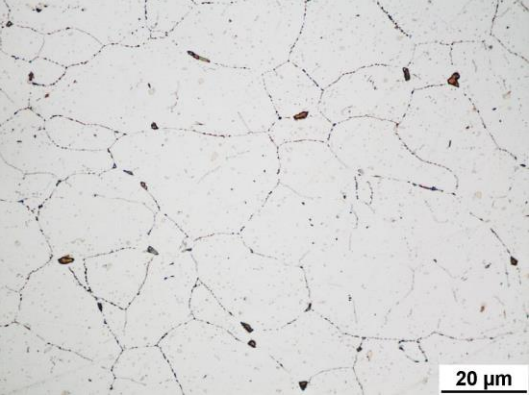
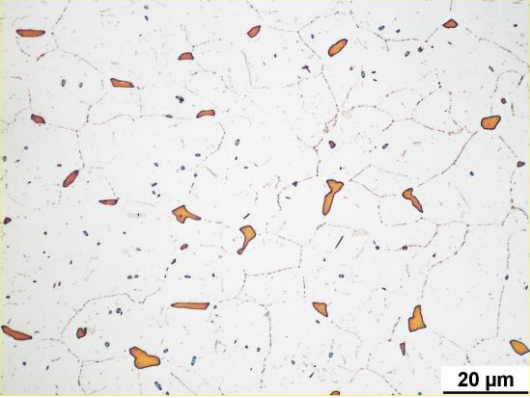
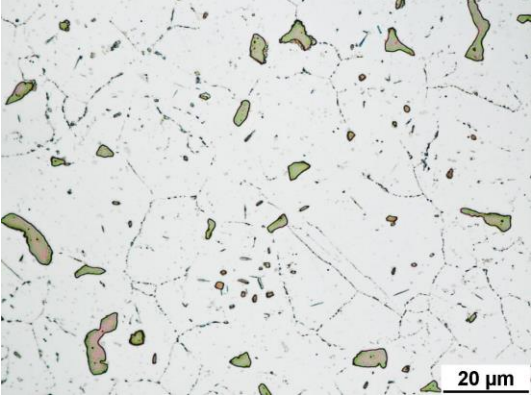
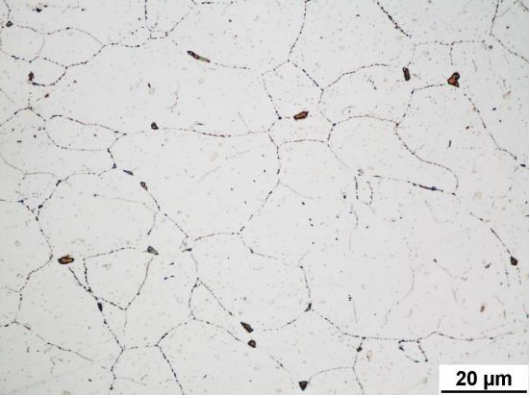
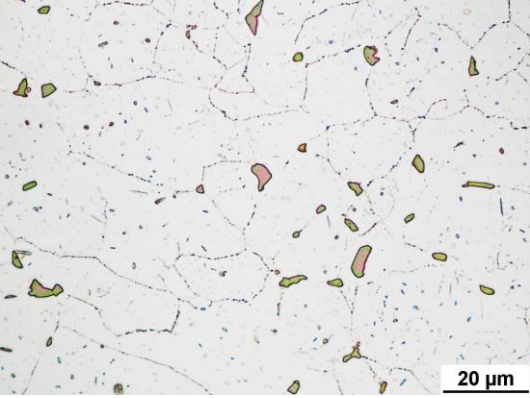
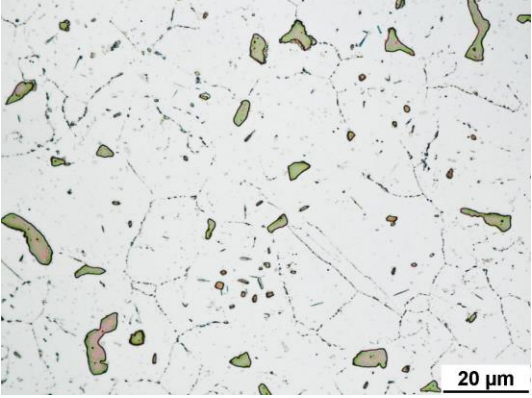
The optical microscopy is used for the sigma phase precipitation description and its quantification. Subchapters deal with precipitation morphology and then with quantitative description of the sigma phase precipitation.

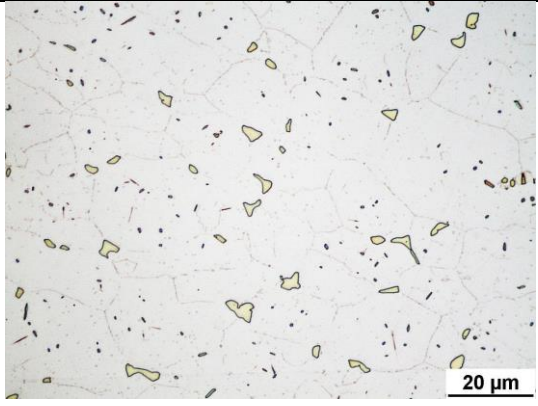
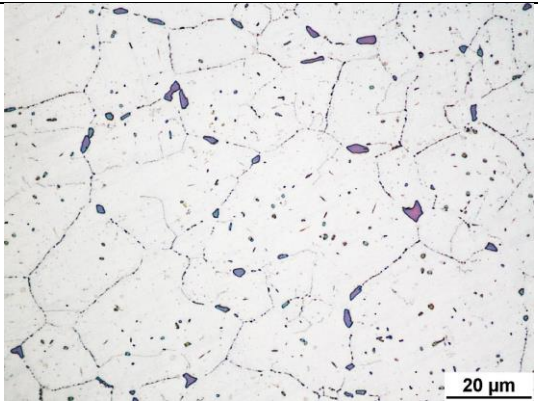
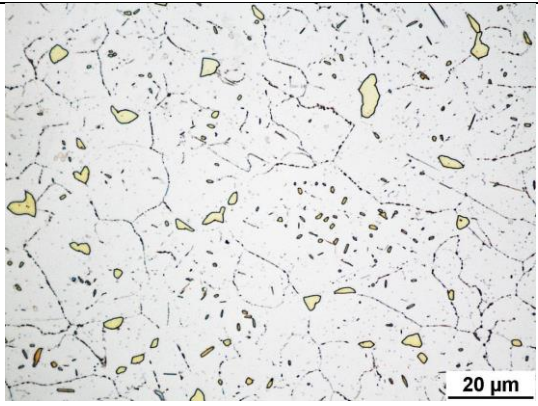
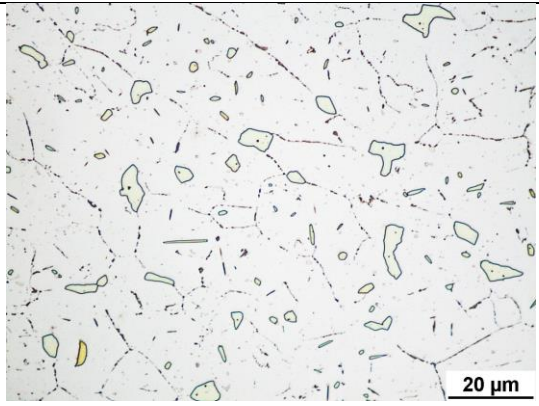


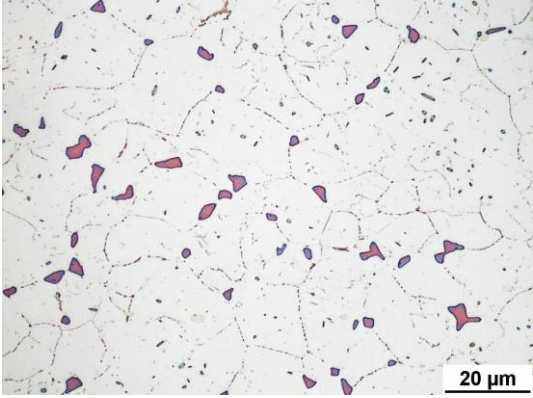
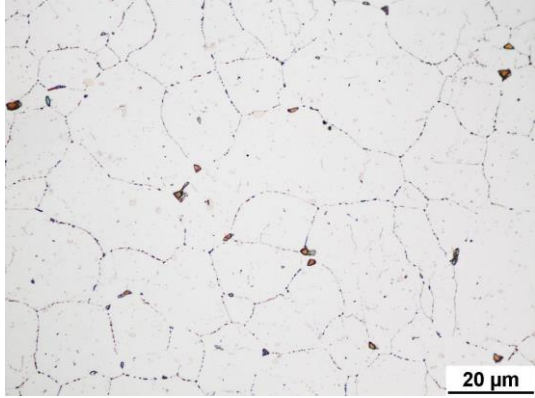
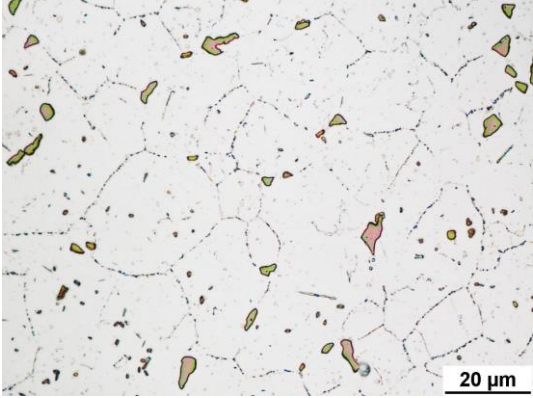
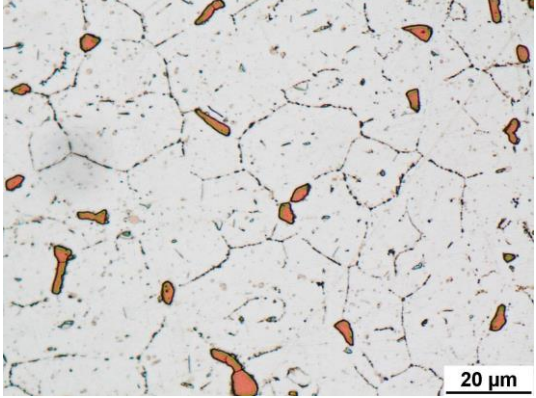
### **5.2.1 Evolving of the sigma phase morphology during aging for steel SUPER 304H**

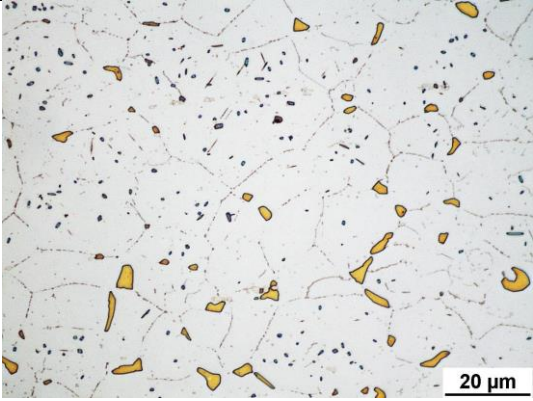
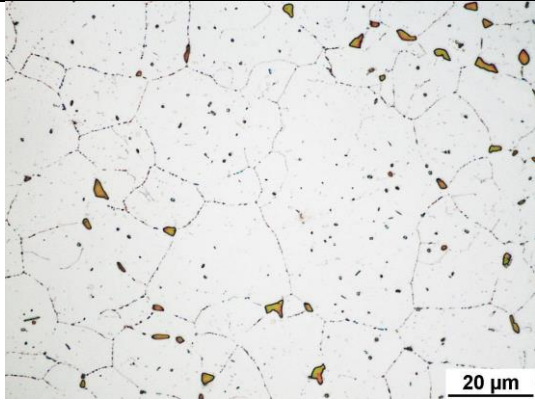
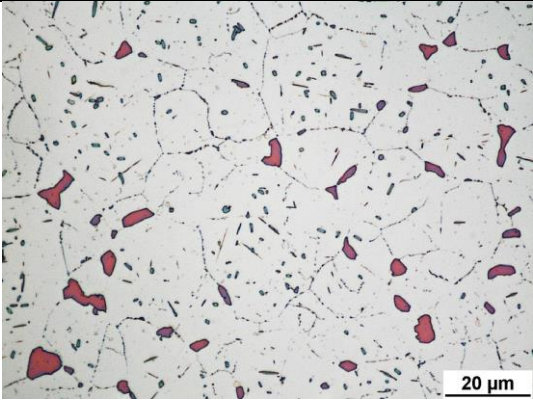
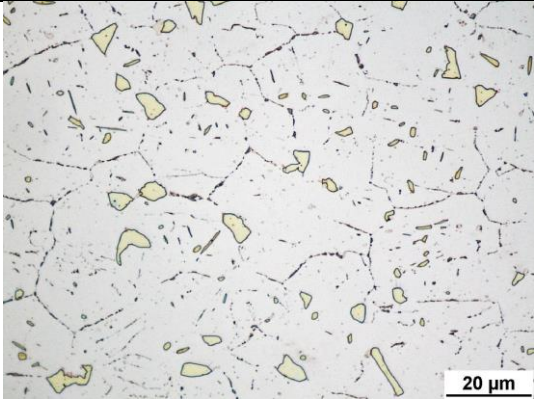
Not annealed (NA) state samples are summarised by figures from Fig. 95 to Fig. 102 . Annealed (A) state samples are summarised by figures from Fig. 103 to Fig. 110.

For each of sample figures are added LMP value. Higher LMP value means higher degradation state.

| Temperature<br>Aging time | 650 °C  | 675 °C   | 700 °C  |
|---------------------------|---|--|---|
| 12000 hours               |   |  <p data-bbox="1032 847 1384 879">Fig. 95 <i>LMP 23589 NA (3)</i></p>    |   |
| 15000 hours               |  <p data-bbox="472 1347 824 1378">Fig. 96 <i>LMP 23057 NA (1)</i></p> |  <p data-bbox="1032 1347 1384 1378">Fig. 97 <i>LMP 23681 NA (4)</i></p> |  <p data-bbox="1594 1347 1946 1378">Fig. 98 <i>LMP 24305 NA (7)</i></p> |

| Temperature<br>Aging time | 650 °C   | 675 °C  | 700 °C   |
|---------------------------|--|---|--|
| 20000 hours               | X  |  <p data-bbox="1028 842 1384 879">Fig. 99 <i>LMP 23800 NA (5)</i></p>     | X  |
| 24500 hours               |  <p data-bbox="470 1345 826 1382">Fig. 100 <i>LMP 23253 NA (2)</i></p> |  <p data-bbox="1028 1345 1384 1382">Fig. 101 <i>LMP 23883 NA (6)</i></p> |  <p data-bbox="1592 1345 1948 1382">Fig. 102 <i>LMP 24513 NA (8)</i></p> |

| Temperature<br>Aging<br>time | 650 °C  | 675 °C   | 700 °C  |
|------------------------------|---|--|---|
| 12000 hours                  | X   |  <p data-bbox="1043 810 1375 842">Fig. 103 <i>LMP 23589 A (3)</i></p>    | X   |
| 15000 hours                  |  <p data-bbox="483 1308 819 1340">Fig. 104 <i>LMP 23057 A (1)</i></p> |  <p data-bbox="1043 1308 1375 1340">Fig. 105 <i>LMP 23681 A (4)</i></p> |  <p data-bbox="1599 1308 1935 1340">Fig. 106 <i>LMP 24305 A (7)</i></p> |

| Temperature<br>Aging<br>time | 650 °C  | 675 °C   | 700 °C  |
|------------------------------|---|--|---|
| 20000 hours                  | X   |  <p data-bbox="1043 810 1375 842">Fig. 107 <i>LMP 23800 A (5)</i></p>    | X   |
| 24500 hours                  |  <p data-bbox="483 1308 815 1340">Fig. 108 <i>LMP 23253 A (2)</i></p> |  <p data-bbox="1043 1308 1375 1340">Fig. 109 <i>LMP 23883 A (6)</i></p> |  <p data-bbox="1599 1308 1930 1340">Fig. 110 <i>LMP 24513 A (8)</i></p> |

## 5.2.2 Evolving of the precipitation kinetics

Use of the sigma phase quantified fraction area is the most precision possibility for description of the sigma phase precipitation kinetics. This method considered all types of the sigma phase precipitates during its precipitation and further growth of processes. This descriptive model considered all of the three sigma phase precipitation types (Type 1 - Triple grain boundary intersection, Type 2 – Grain boundary and Type 3 – Inner-grain precipitates).

Plot summarising measured sigma phase fraction area is shown in Fig. 111. Precipitation curves are plotted separately for state NA and A. For a common description of time and temperature LMP parameter is use.

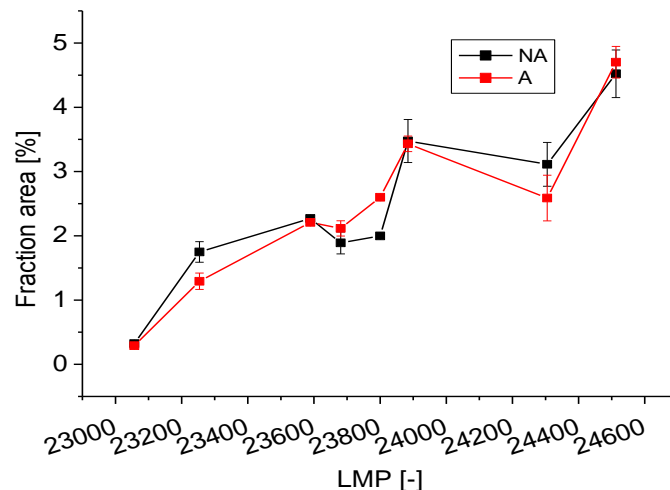


Fig. 111 Evolving of the sigma phase fraction area to LMP

Separately plotted sigma phase portion area for state NA is shown in Fig. 112. Exponential growth of dependence is marked into graphs by green lines. Mathematical description of exponential growth for state NA which describes precipitation of the sigma phase summarised Eq. (5). The precipitation rate equation obtained like the time derivation of the sigma portion area presents Eq. (6). The same system was used for A state samples. The sigma phase fraction area growth summarise graph Fig. 113 and mathematical description Eq. (7). Precipitation rate in state A describe equation Eq. (8). Used range of LMP covers the whole planned lifetime of power plant.

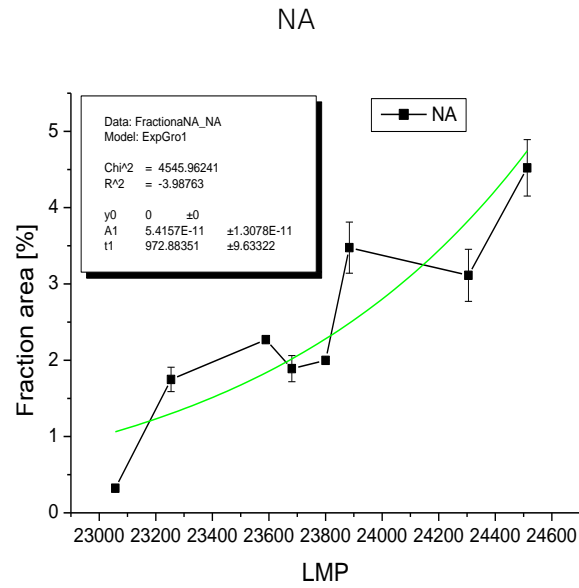


Fig. 112 Evolving of the sigma phase fraction area to LMP for NA state

$$\text{Fraction area} = 5,42 * 10^{-11} * e^{(LMP/972,88)} \quad \text{Eq. (5)}$$

$$\text{Precipitation rate} = 5,57 * 10^{-14} * e^{(LMP/972,88)} \quad \text{Eq. (6)}$$

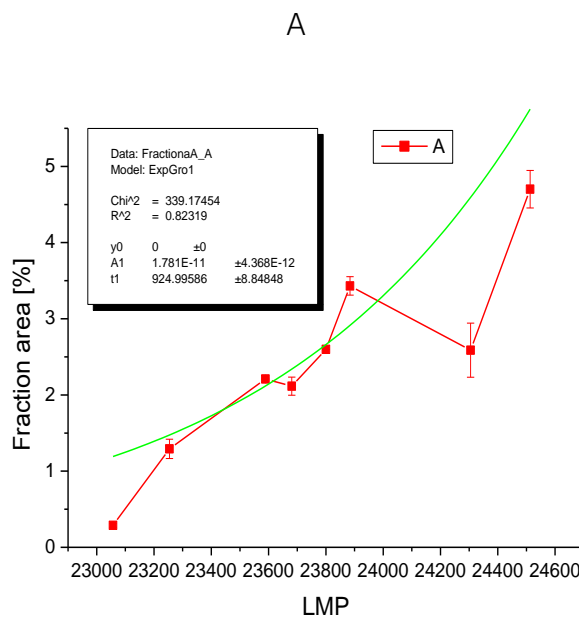


Fig. 113 Evolving of the sigma phase fraction area to LMP for A state

$$\text{Fraction area} = 1,78 * 10^{-11} * e^{(LMP/925)} \quad \text{Eq. (7)}$$

$$\text{Precipitation rate} = 1,93 * 10^{-14} * e^{(LMP/925)} \quad \text{Eq. (8)}$$

## 5.3 The mechanical properties testing

### 5.3.1 Tensile testing

Short testing specimens with 5 mm diameter were used for tensile testing at the room temperature. The loading speed was 0.5 mm/s. Experimental material was isothermally aged at 675 °C for 20 000 hours. Results are summarized in Tab. 19 where abbreviations BM, E-NA, E-A mean base material, exposed – not annealed, exposed - annealed. Achieved values of yield strength  $R_{p0.2}$ , tensile strength  $R_m$  and elongation  $A$  meet the requirements listed in standards. It can be mentioned that tensile strength of exposed states (E-NA and E-A) has significantly increased compared with as-received state for both steels. [54]

Tab. 19 Results of tensile testing of SUPER 304H and HR3C steels [54]

| Steel    | SUPER 304H       |             |           | HR3C             |             |           |
|----------|------------------|-------------|-----------|------------------|-------------|-----------|
|          | $R_{p0.2}$ [MPa] | $R_m$ [MPa] | A [%]     | $R_{p0.2}$ [MPa] | $R_m$ [MPa] | A [%]     |
| Standard | min. 235         | 590-850     | min. 35.0 | min. 295         | 655-900     | min. 30.0 |
| BM       | 395              | 657         | 54.5      | 369              | 769         | 55.9      |
| E-NA     | 355              | 740         | 45.0      | 504              | 813         | 18.9      |
| E-A      | 357              | 727         | 45.8      | 439              | 839         | 14.3      |

### 5.3.2 V notch pendulum testing

Because of probable sigma-phase assisted embrittlement of exposed steels, the impact strength measurements with reduced width (5 mm) of the specimens with V notch were carried out. Experimental material was isothermally aged at 675 °C for 20 000 hours. Results are summarized in Tab. 20 where abbreviations BM, E-NA, E-A mean as written above. As can be seen, applied dissolving annealing and/or isothermal ageing (E-NA and E-A states) have strong deteriorating influence on absorbed energy KV 300/5, especially for HR3C steel. Difference between fracture surfaces of HR3C base material (Fig. 116) and exposed material (Fig. 117) is significant. The base material fracture surface can be assumed to be ductile. However, for exposed material, only several areas



of the fracture surface were ductile. The rest of the surface showed brittle fracture. [54] Similar situation can be observed for steel SUPER 304H. Base material fracture surface (Fig. 114) is ductile with no marks of brittle fracture. Fracture surface after exposition (Fig. 115) is mostly brittle. This change is caused by the sigma phase precipitation in both case SUPER 304H and HR3C.

Tab. 20 Results of impact testing of SUPER 304 and HR3C steels [54]

| Steel | SUPER 304H   |                                   | HR3C         |                                   |
|-------|--------------|-----------------------------------|--------------|-----------------------------------|
| State | KV 300/5 [J] | The sigma phase area fraction [%] | KV 300/5 [J] | The sigma phase area fraction [%] |
| BM    | 44.7 ± 1.0   | 0.0                               | 164.5 ± 3.2  | 0.0                               |
| E-NA  | 11.4 ± 0.4   | 2.6                               | 3.2 ± 0.1    | 1.9                               |
| E-A   | 11.5 ± 0.3   | 2.8                               | 2.7 ± 0.2    | 2.2                               |

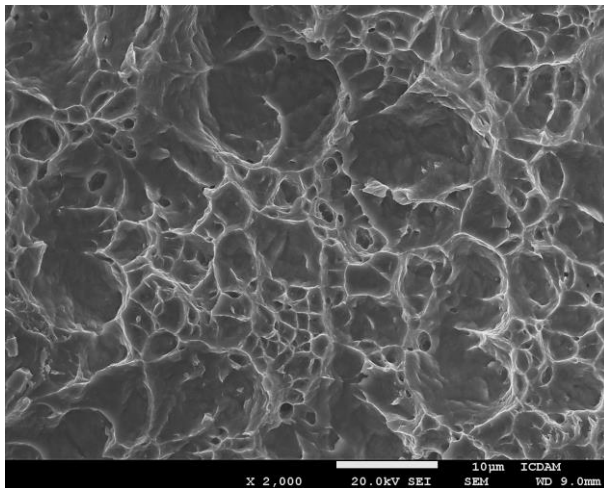


Fig. 114 Ductile fracture surface of as-received SUPER 304H steel

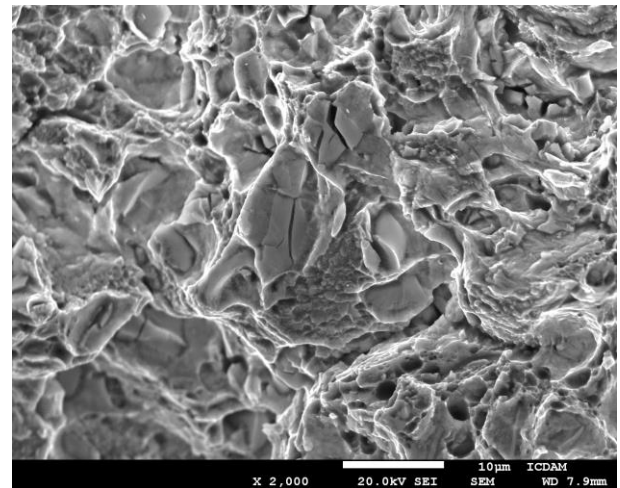


Fig. 115 Brittle fracture surface of exposed SUPER 304H steel in E-NA state

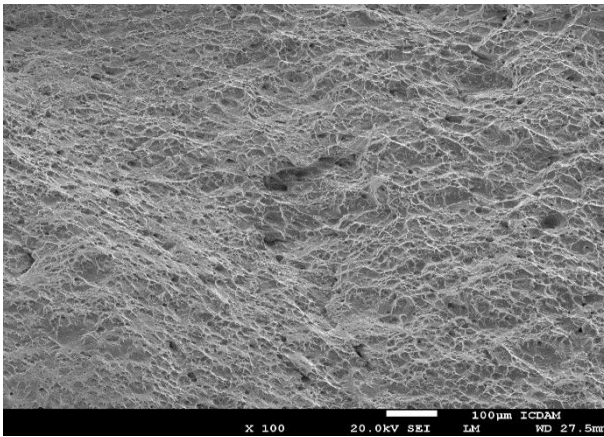


Fig. 116 Ductile fracture surface of as-received HR3C steel [54]

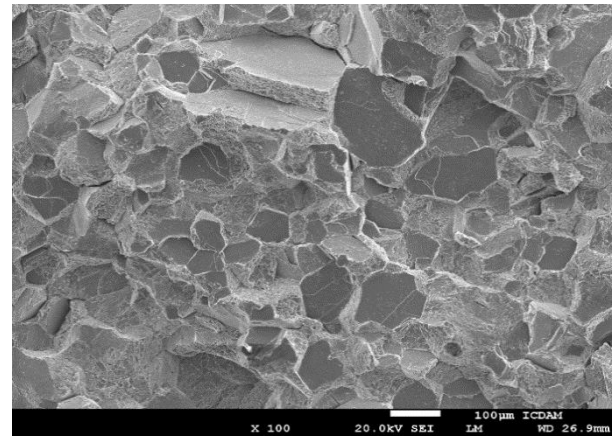


Fig. 117 Brittle fracture surface of exposed HR3C steel in E-NA state [54]

Phase analysis, higher magnification, TEM diffraction patterns, and EDX analysis were used to identify secondary phases located on the fracture surfaces, as illustrated in Fig. 118 and Fig. 119. The analyses of those particles are implemented into the figures. The measured chemical composition is in accordance with nominal sigma phase chemical composition. As-received materials do not contain any sigma phase, but in case of the exposed samples, the area fractions of sigma phase are 1.9 % (E-NA), 2.2 % (E-A) for HR3C steel and 2.6 % (E-NA), 2.8 % (E-A) for SUPER 304H steel, respectively. Except sigma phase, chromium carbides were observed in all samples. [54]

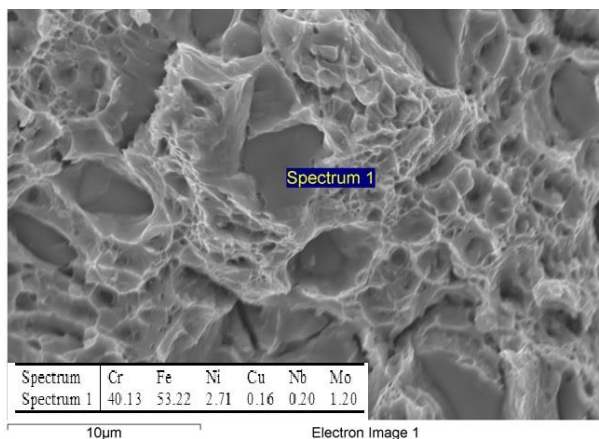


Fig. 118 Sigma phase with its chemical composition (Spectrum 1) on fracture surface of SUPER 304H steel [54]

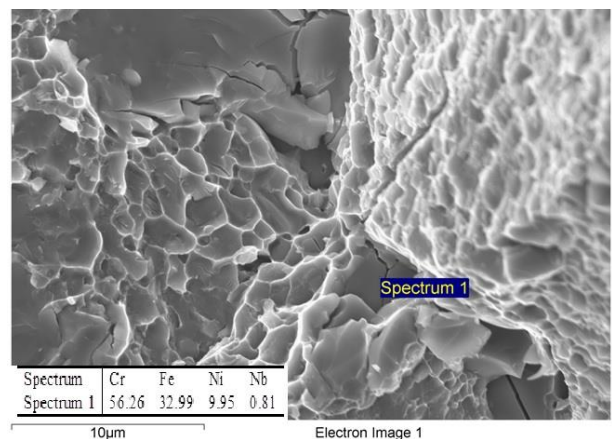


Fig. 119 Sigma phase with its chemical composition (Spectrum 1) on fracture surface of HR3C steel [54]

Steel SUPER 304H is alloyed with ~3 % Cu. Addition of copper may lead to increase of creep properties of steel. Recently it was suggested that Cu particles

can not only increase mechanical properties but may also pin the motion of  $\sigma$ -phase/austenite interfaces. [52]

The impact strength of homogenous welding joints decreases from  $109.4 \pm 0.4 \text{ J/cm}^2$  measured in as-received base material to value about  $28.2 \pm 0.6 \text{ J/cm}^2$  determined in aged state (20000 hours/675°C). It can be suggested that higher contents of  $\sigma$ -phase in the crown layer and significantly larger grain size in root and central layers probably cause further reduction of impact strength. Recently, it was reported that significant decrease in impact energy may be expected already after short-time annealing (for about  $10^3 \text{ h}$ ) at 650 and 700°C. [52]

On the basis of microstructure results it can be suggested that a drop of impact strength after long-term ageing is significantly influenced by  $\sigma$ -phase formation. This suggestion could be supported by analysis of fracture surfaces obtained from impact strength tests. The aged state exhibited the mixture of transgranular ductile fracture of matrix and intragranular fracture along  $\sigma$ -phase (Fig. 120). [52]

SUPER 304H matrix keeps ductile behaviour during exposition. Brittleness of steel is caused by the sigma phase precipitation.

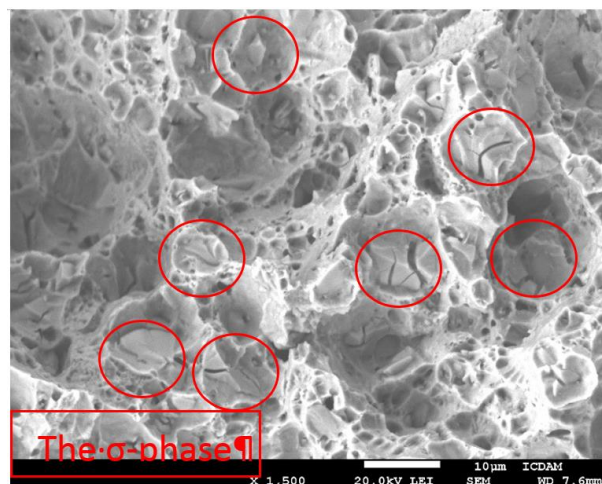


Fig. 120 Fracture surface of as-received state after long-term ageing [52]

## 6 Experimental results discussion

This chapter summarizes briefly conclusions reached by the thesis. Practical applicability of the thesis results is discussed in the last part.

### 6.1 The sigma phase verification and extension for optical microscopy quantification

First and the most crucial step is to identify particles precipitated in steel microstructure. Steels SUPER 304H and TP 347HFG are highly susceptible for the sigma phase precipitation according literature sources [10],[12],[13]. Main attention was given to the sigma phase identification in steel SUPER 304H and later to its quantification.

The sigma phase identification was based on combination of four methods. Measurement of chemical composition via SEM EDS detector, TEM microscope include STEM mode for taking pictures and chemical composition measurement, correlation of Kikuchi lines and EBSD method were used. Measured results are summarised in the subchapter 5.1.1. All of the previous named methods confirm precipitation of the sigma phases in microstructure of steel SUPER 304H.

Identification of the sigma phase was done by various types of electron microscopes. Next part of phase investigation is quantification of the phase. Usage of electron microscopes especially TEM is enormously time consuming. Suitable method for quantification can be classical optical microscopy in combination with colour etching. This method is suitable for large number of samples which are necessary for the sigma phase quantification. Another advantage of optical microscopy and colour etching is short sample processing time.

Application of optical microscopy and colour etching require verification between electron and optical microscope. The verification is summarised in the subchapter 5.1.3. Fig. 94 compared image made by electron microscope to image from optical microscopy with EDS method measured chemical maps.

The verification confirms possibility of usage of the optical microscope and colour etching (Fig. 94).

## **6.2 The sigma phase precipitation morphology**

Process of the sigma phase precipitation is documented by Fig. 95 - Fig. 102 for NA state and by Fig. 103 - Fig. 110 for A state. Each of used characteristic images was randomly chosen from about two hundred of images made for definite combination of exposed time and temperature.

No sigma phase precipitation was documented for original state (without any exposition). This result means that the sigma phase precipitation is induced by heat exposition of experimental material. Used combination of exposed temperatures and times covered through LMP whole power plant lifetime.

The sigma phase precipitation begins at triple points. During continuous thermal exposition precipitation continuous at triple point and also starts along boundaries of austenitic grains.

Particles get coarser with longer heat exposure. Dominant direction of coarsening is along austenitic matrix grain boundaries. Particles precipitated at the triple points get into the shape of a triangle. Others precipitating on the grain boundaries are elongating in direction of grain boundary. Coarsening perpendicular to grain boundary is slower.

Last part of the precipitation process is precipitation of the sigma phase inside the austenitic grains. Precipitation starts like spheroid particles which continuously elongated into the final elliptic shape.

In general, it is possible to state that precipitation of the sigma phase is a continuous process which decreases free enthalpy of system and it is possible to quantify and model it.

The difference between precipitation morphology of state NA and A is negligible. It seems that the state after annealing (A) consists of the rougher particles in comparison with the state NA. This result suggested that solution annealing performed after technology operations like welding or bending

accelerate degradation of steel SUPER 304H. Quantitative particles documentation was made by using the optical analysis. Those data are used for description of the precipitation curves.

### **6.3 The precipitation kinetics curves**

Description of the sigma phase precipitation was based on quantification of the sigma phase in various states of degradation conditions. LMP parameter was used for possibility of combination of the degradation description. Used raw data were obtained from quantification of about 2150 images of SUPER 304H steel microstructure. That gave very broad datasheet which is definitely representative for those processes.

No sigma phase precipitation was documented for initial state (before laboratory long heat exposition). Summarisation of measured data is shown in Fig. 111. Results displayed by Fig. 111 confirm that there is no significant difference in precipitate quantification between states without annealing (NA) and annealed after some technological operation (A). The sigma phase precipitation has nearly the same precipitation behaviour in both cases.

The sigma phase precipitation and its growth are driven by diffusion processes [10]. Obtained results are in accordance with this fact. Description of the precipitation process is like all nature processes exponentially. Equations (Eq. (5), Eq. (6)) which describe the sigma phase precipitation confirm that long term precipitation of the sigma phase is not involved by the pre-exposition solution annealing.

Equations Eq. (7) and Eq. (8) describe precipitation rate for both states of solution annealing. Results that are clear from precipitation rate description prove that precipitation processes still accelerate. This acceleration is caused by relatively long incubation time of precipitation and quite fast coarsening of particles precipitated at the triple points. The triple points sigma phase coarsening is clearly visible from comparison of for example Fig. 108 and Fig. 110.

The sigma phase is highly brittle intermetallic particle [10]. If we consider triple points precipitation and those particles accelerate coarsening it will strongly influence mechanical properties. Precipitates will affect crack propagation and probably formation of the creep cavity. Describe precipitates and identify their position is necessary for decaying about those problems.

#### **6.4 Influence of the precipitation to the mechanical properties**

The sigma phase is classified like brittle intermetallic particle. Precipitation of the sigma phase can be classified like precipitation hardening. It is consistent with measured results from tensile testing. Exposed material shows an increase in the ultimate strength. On the other hand, there is a drop in the yield strength and elongation documented. Results from tensile testing support a degradation theory of the steel SUPER 304H.

Pendulum testing of exposed samples from the steel SUPER 304H declined from the original value of 109,4 J to 28,2 J after 20 000 hours of exposition at 675°C. That is a drop by approximately 75%. The drop by 75% is significant and there must be a reason for such a change. The sigma phase was documented by electron microscope on the fracture surfaces of experimental samples.

Results about decreasing of mechanical properties support the need for this thesis because there is no information about precipitation processes for the steel SUPER 304H.

#### **6.5 The modelling and achieved results comparison**

The sigma phase precipitation modelling for the steel Tp 347HFG is based on similarity with the steel SUPER 304H. The similarity means near base chemical composition, similarity in high fine grain size and stable austenitic microstructure. Those assumptions provide possibility to apply modification through physical laws which describe chemical components diffusion for the sigma phase precipitation modelling. Slight difference in chemical composition will cause difference of the sigma phase precipitation rate.

The sigma phase precipitation process is dependent on the time and concentration of chromium, iron and nickel. Description of the chemical elements transition in solid is provided by Fick laws. Mathematical equation of the second Fick law (Eq. (9) [55]) describes time and distance dependence of difunding chemical element.

$$\frac{\partial c_k}{\partial \tau} = D_{kl} \frac{\partial^2 c_k}{\partial z^2} \quad \text{Eq. (9)}$$

$C_k$  means chemical element concentration,  $\tau$  – time,  $D_{kl}$  diffusion coefficient and  $z$  describes distance in case of 1D diffusion.

According to the literature [56] [57] [58] it deals with mathematical analysis and fundamental book of applied mathematics [59] can be Eq. (9) categorised like Parabolic shape second grade partial differential equation with constant coefficient.

Solution of Eq. (9) gives function which describes time and position relation of chemical composition. This function or functions for more difunding elements can be in advance used for modification of the sigma phase precipitation rate described in subchapter 5.2.2. Fundamental solution of Eq. (9) provides function Eq. (10) [59].

$$c_k = f(z, \tau) \quad \text{Eq. (10)}$$

Base diffusion equation Eq. (9) is the same type like heat transfer type equations. Four possible methods for calculus fundamental solution equation are summarising for heat transfer by [56] - [59].

All of the methods are strongly dependant on boundary conditions and a fundamental system. Furrier transformation [59] of original equation (Eq. (9)) can be in this case unstable. The most suitable solving methods seem to be through application of error function. The error function method is described in [39] and [58].

If we consider 1D model with semi-infinite boundaries there is a fundamental solution system of Eq. (9) for diffusion saturation summarized by Eq. (11) and for diffuse depletion by Eq. (12). The semi-infinite boundaries mean



that the sigma phase grew from infinite base material region. This region provides enough of the source elements like chromium for the sigma phase growth. This type of descriptive modification can be used for precipitation processes description in the small surrounding area.

$$\frac{c - c_0}{c_1 - c_0} = 1 - \operatorname{erf} \left[ \frac{x}{2(D\tau)^{1/2}} \right] \quad \text{Eq. (11)}$$

$$\frac{c - c_1}{c_0 - c_1} = \operatorname{erf} \left[ \frac{x}{2(D\tau)^{1/2}} \right] \quad \text{Eq. (12)}$$

Equation Eq. (11) describes chromium transport process and Eq. (12) describes opposite processes (depletion) for iron and nickel. Transformation of those equations can be used for the element concentration description. Time derivation will provide chemical element diffusion velocity. Chromium, iron and nickel diffusion velocity drive the sigma phase precipitation. The difference between results for the SUPER 304H and Tp 347HFG can be used for modification of the SUPER 304H sigma phase precipitation rate function.

For solution of equation Eq. (11) and Eq. (12) it is necessary to define diffusivity for each of the three elements (chromium, iron, nickel). Diffusivity calculation function is summarized by Eq. (13) [39].

$$D = D_0 \exp \left( -\frac{Q_d}{RT} \right) \quad \text{Eq. (13)}$$

Activation energies  $Q_d$  and diffusion coefficients  $D_0$  published by [60] for austenitic steel matrix is summarized in Tab. 21.

Tab. 21 Diffusivity calculation coefficients [60]

| In Fe <sub>v</sub> | D <sub>0</sub> [cm <sup>2</sup> s <sup>-1</sup> ] | Q <sub>d</sub> [kJmol <sup>-1</sup> ] |
|--------------------|---|---------------------------------------|
| Cr                 | 10,8  | 291,8                                 |
| Ni                 | 0,77  | 280,5                                 |
| Fe                 | 4,085   | 311,1                                 |

Eq. (11) and Eq. (12) respect diffusion direction of chemical elements. General solution of both equations is the same Eq. (14).

$$c = (c_0 - c_1) \operatorname{erf} \left[ \frac{x}{2(D\tau)^{1/2}} \right] + c_1 \quad \text{Eq. (14)}$$

The error function  $\operatorname{erf} [ ]$  can be approximate by four grade exponential function Eq. (15). Approximation error is  $5 \cdot 10^{-4}$ . [39]

$$\operatorname{erf}(z) \doteq 1 - \left( 1 + 0,196854 \cdot \sqrt{2} \cdot z + 0,115194 \cdot 2 \cdot z^2 + 0,000344 \cdot 2 \cdot \sqrt{2} \cdot z^3 + 0,019527 \cdot 4 \cdot z^4 \right)^{-4} \quad \text{Eq. (15)}$$

Coefficients represent time (especially LMP) dependant chemical elements movement which influencing the sigma phase precipitation was calculated by numerical solution of Eq. (14) and Eq. (15). Calculated coefficient for steel SUPER 304H are summarised in Tab. 22 and for steel Tp 347HFG in Tab. 23.

Tab. 22 Calculated coefficient for steel SUPER 304H

| SUPER 304H       |       |             |          |          |
|------------------|-------|-------------|----------|----------|
| Temperature/time | LMP   | Coefficient |          |          |
| [K/Hours]        | -     | Cr          | Ni       | Fe       |
| 923,15/10000     | 22894 | -8,33E-10   | 4,18E-09 | 3,38E-10 |
| 948,15/10000     | 23514 | -1,38E-09   | 6,77E-09 | 5,77E-10 |
| 973,15/10000     | 24134 | -2,21E-09   | 1,07E-08 | 9,57E-10 |

Tab. 23 Calculated coefficient for steel Tp 347HFG

| Tp 347HFG        |       |             |          |          |
|------------------|-------|-------------|----------|----------|
| Temperature/time | LMP   | Coefficient |          |          |
| [K/Hours]        | -     | Cr          | Ni       | Fe       |
| 923,15/10000     | 22802 | -8,39E-10   | 3,23E-09 | 3,17E-10 |
| 948,15/10000     | 23419 | -1,38E-09   | 5,23E-09 | 5,40E-10 |
| 973,15/10000     | 24037 | -2,23E-09   | 8,27E-09 | 8,97E-10 |

Calculated coefficients represent influence of chemical composition and C constant (for LMP parameter calculation). Precipitation rate curve (Fig. 112) can be modified by those coefficients for Tp 347HFG application.

Transformation methodology is based on removal influence of the SUPER 304H chemical composition to precipitation rate and then adding influence of Tp 347HFG chemical composition. Representation of the two step modification is summarised by coefficient ratio listed in Tab. 24.

*Tab. 24* Calculated specific coefficients ration

| SUPER304H/Tp 347HFG coefficient |         |         |         |         |
|---------------------------------|---------|---------|---------|---------|
| Temperature/time                | Element |         |         |         |
| [K/Hours]                       | Cr      | Ni      | Fe      | Average |
| 923,15/10000                    | 1,00675 | 0,77374 | 0,93710 | 0,90586 |
| 948,15/10000                    | 1,00611 | 0,77326 | 0,93652 | 0,90530 |
| 973,15/10000                    | 1,00669 | 0,77370 | 0,93708 | 0,90582 |

### **6.5.1 Tp 347HFG precipitation rate transformation verification**

Verification was based on comparison between the recalculated fraction area for Tp 347HFG and the measured fraction area on the Tp 347HFG samples after isothermal aging of 700°C for 10 000 hours.

The measured fraction area is summarised in Tab. 25. The value for comparison is on average 0,0282 (equal with 2,82%).

Tab. 25 Measured sigma phase fraction area for Tp 347HFG

|                  |               |
|------------------|---------------|
| Tp 347HFG        |               |
| Time/Temperature |               |
| 973,15/10000     |               |
| [K/Hours]        |               |
| Sample           | Fraction area |
| 1                | 0,023         |
| 2                | 0,027         |
| 3                | 0,027         |
| 4                | 0,032         |
| 5                | 0,032         |
| Average          | 0,0282        |
| Deviation        | 0,00343       |

The SUPER 304H fraction area is 3,24% calculated according Fig. 121 and Eq. (16) for combination of exposition 700°C for 10 000 hours.

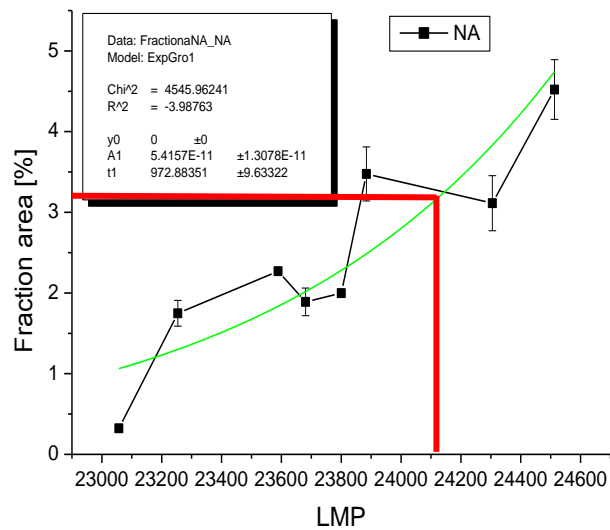


Fig. 121 Evolving of the sigma phase fraction area to LMP for SUPER 304H NA state

$$Fraction\ area = 5,42 * 10^{-11} * e^{(LMP/972,88)} \quad Eq. (16)$$

The correlated fraction area for steel Tp 347HFG by average value of coefficients is listed in Tab. 24 summarises in Tab. 26.

Tab. 26 Calculated and measured results comparison

| SUPER 304H | Tp 347HFG  | Tp 347HFG |
|------------|------------|-----------|
| Calculated | Calculated | Measured  |
| 3,24       | 2,94       | 2,82      |

Verification was done by comparison of Tp 347HFG measured and calculated values. Difference between calculated and measured values is 4,08 %. That confirms applicability of coefficient modification methodology.

## 6.6 The practical application of the thesis results

If we consider that the descriptive model is based on combination of physical laws and experimentally obtained results for specific group of materials, there can be three possibilities for practical results application.

### 6.6.1 The degradation prediction

The power plant operation conditions are not stable. There are many unstable states like heat fluxes during operation. Another non-stable state occurs during the power plant starts up and cooling down. Those operation conditions instabilities cause hardly predictable influence on degradation of the superheaters.

The precipitation model can be used inverse. It means that input will be distribution and size of particles and output temperature of exposition. Inverse model type in combination with the creep data of the steel can give information about remaining lifetime.

### 6.6.2 The state of degradation

Under the operation condition (heat and pressure long-term exposition) austenitic creep resistant steels change mechanical properties. The steels microstructure changes cause degradation. Many factors like grain coarsening, precipitation of particles and cavity formation act a role in the degradation process.

Previously we said that under the operation conditions degradation progress occurs. The question is, how fast the degradation process will be.

The model based on physically confirmed equation and information obtained from examination of real exposed material can give the answer to the question „How fast?“.

Respectively the model can give information about precipitation process. State of precipitation can be compared with the mechanical properties changes.

### **6.6.3 Information for future production of the next steels generation**

In general designing of the new special alloys is based on historical knowledge and theoretical based information. It leads to designing of special alloys with superior properties, which are tested just in short time examinations. Commercial distribution of the new material starts just after confirmation of materials requirement by short time tests.

The main problem is that short time testing can't predict changes of the material properties caused by medium-term or long-term exposition. Microstructural changes, precipitation or decrease of hardening effects can occur. Those changes may cause just small changes in case of mechanical or technology properties. In worse case changes will be more relevant.

One of the possible applications of modelling of the precipitation processes can be during testing period of a new material. Structural stability or changes in the microstructure can be predicted by modelling. Precipitation has definitely influence on creep resistance and mechanical properties. Precipitation model will be useful for prediction of changes caused by heat expose.

Results obtained by this thesis are that copper alloying leads to probably slower sigma phase precipitation rate by pinning interface between the austenitic matrix and the sigma phase. This result provides with combination of theoretical information in subchapter 2.1.4 possible way through chemical composition modification.

## 7 Summary

### 7.1 Meet the thesis goal

- Describe sigma phase precipitation processes for steel SUPER 304H and perform their general mathematical description

The precipitation processes were described through the sigma phase fraction area. Mathematical description of the sigma phase precipitation was made by exponential growth function.

- Model precipitation kinetics processes based on chemical composition and physical laws like modification of the steel Tp 347HFG

The sigma phase modelling was based on measured values for SUPER 304H and modification coefficients. Modification coefficients were calculated according Fick laws and Larson-Miller construction. Through application of modification coefficients (which describe chemical composition and LMP differences) sigma phase fraction area for steel Tp 347HFG was calculated.

- Correlate model with measured particles after the long-term heat exposition for steel Tp 347HFG

Correlation was performed for available degraded samples of Tp 3247HFG after exposition 700°C for 10 000 hours. Difference between calculated values (based on coefficient modification) and real measured sigma phase fraction area was 4,08 %. This difference confirms applicability of coefficient modification methodology.

- Find and describe the kinetic function of the sigma phase precipitation for the steel SUPER 304H

The sigma phase kinetic function was described like time derivation of the fraction area exponential growth function.

## 7.2 The main conclusion description

This thesis confirms high structural instability of the steel SUPER 304H and a similarity with the steel TP 347HFG. The sigma phase kinetics description was performed by exponential growth type equations.

Description of the fraction area was based on the sigma phase measurements in various degraded states of the steel SUPER 304H summarised by LMP parameter. This approach is based on examination of various degradation time and temperature combinations. Accelerated precipitation processes are obtained by this set of expositions.

Time derivation of the sigma phase fraction area function gave the sigma phase kinetics description. This function can be used for degradation state description during operation.

At the bases of this function modification for steel Tp 347HFG based on differences in chemical composition and LMP constant was performed. This result confirms possibility for extending of those results for creep resistant complex alloyed steels group 18/9.

## 7.3 The practical application recommendation

Practical application of materials investigated by the thesis is for supercritical and ultra-supercritical coal power plants. Austenitic creep resistant steels group 18/9 sigmatisation under operation conditions (application for reheaters, superheaters and heat exchanging surfaces) is nowadays problem.

Precipitation of the sigma phases leads to a serious embrittlement (example: Tab. 20). The microstructural changes and embrittlement phenomena mean for power plants operators:

- The need to find out description of the critical crack dimensions for unstable propagation
- The need to prepare welding procedure specifications for repair welds in combination new x old (exposed and embrittle) material



## 7.4 Proposal of further experimental work on the problem

The precipitation mechanism was identified and described. Quantification of the sigma phase was based on changes of the sigma phase fraction area. Used methodology considered sigma phase precipitation in microstructure at all. There are two types of the sigma phase precipitate: massive particles at triple points and grain boundaries, and needle-shaped particles inside grains. Done quantification contains both data fraction area measurement and specific description of each measured particle. In fact, there is a datasheet containing measured information for more than 210 000 particles.

According to the results described by chapter 5.3 and 6.4 the sigma phase strongly affects mechanical properties and crack propagation. The sigma phase datasheet provides strong base for making correlation between the precipitated particles and influence on the mechanical properties.

Moreover, the datasheet provides base data for possible investigation for the sigma phase base austenitic material interface. The interface is crucial for creep cavity formation and propagation.

TEM observation confirms location of Cu rich areas at the interface between sigma phase and austenitic matrix. These Cu areas block or slow down the sigma phase precipitation. Investigation of the various copper content influences may provide benefit information for chemical composition optimization for future alloys.

Embrittlement is a negative repercussion of the sigma phase precipitation. Future experimental work can deal with removal of this bad influence. The sigma phase dissolves over temperature of 800°C. High temperature annealing can cause removal of precipitated sigma phase. First results from this investigation will be presented by the author at 27<sup>th</sup> International Conference on Metallurgy and Materials at the end of May.

---

## 8 Bibliography

### 8.1 Thesis bibliography

- [1] Roční zpráva o provozu ES ČR 2016. *Energetický regulační úřad* [online]. 2016 [cit. 2018-04-05]. Dostupné z:  
  
[https://www.eru.cz/documents/10540/462820/Rocni\\_zprava\\_provoz\\_ES\\_2016.pdf/800e5a09-a58a-4a73-913f-abc30cda42a5](https://www.eru.cz/documents/10540/462820/Rocni_zprava_provoz_ES_2016.pdf/800e5a09-a58a-4a73-913f-abc30cda42a5)
- [2] FUKUDA, Masafumi, Eiji SAITO, Yoshinori TANAKA, Takeo TAKAHASHI, Shinji NAKAMURA, Jun IWASAKI, Sninichi TAKANO a Sakae IZUMI. Advanced USC technology development in Japan. In: *Advances in materials technology for fossil power plants: proceedings from the sixth International Conference, August 31-September 3, 2010, Santa Fe, New Mexico, USA*. Materials Park, Ohio: ASM International, c2011, p 325-341, ISBN 978-1-61503-724-7.
- [3] POLACH, Vladislav. Parní kotle. In: *Katedra energetických strojů a zařízení - O projektu* [online]. Plzeň: ZČU, 2012 [cit. 2017-08-14]. Dostupné z:  
[http://kke.zcu.cz/export/sites/kke/about/projekty/enazp/projekty/01\\_Stavba-a-provoz-stroju\\_1-3/1\\_IUT/005\\_Parn-kotle---Polach---P0.pdf](http://kke.zcu.cz/export/sites/kke/about/projekty/enazp/projekty/01_Stavba-a-provoz-stroju_1-3/1_IUT/005_Parn-kotle---Polach---P0.pdf)
- [4] BLUM, Rudolph a Jorgen BUGGE. The european perspective and advancemente for advanced USC power plants. In: *Advances in materials technology for fossil power plants: proceedings from the sixth International Conference, August 31-September 3, 2010, Santa Fe, New Mexico, USA*. Materials Park, Ohio: ASM International, c2011, p 1-10, ISBN 978-1-61503-724-7.
- [5] PHILLIPS, Jeffrey a John WHEELDON. Economic analyss of asvanced ultra-supercritical pulverizes coal power plants: A cost-effective CO2 emission reduction option?. In: *Advances in materials technology for fossil power plants: proceedings from the sixth International Conference, August 31-September 3, 2010, Santa Fe, New Mexico, USA*. Materials Park, Ohio: ASM International, c2011, p 53-64, ISBN 978-1-61503-724-7.

- [6] VISWANATHAN, R., J.F. HENREY, J. TONZOSH, G. STANKO, J. SHINGLEDECKER, B. VITALIS a R PURGERT. *U.S. Program on Materials Technology for Ultra-Supercritical Coal Power Plant*. *Journal of Materials Engineering and Performance*. 2005, (14): 281-292.
- [7] ABE, Fujito, Torsten-Ulf KERN a R VISWANATHAN. *Creep-resistant steels*. England: Woodhead Publishing Limited and CRC Press LLC, 2008. ISBN 978-1-84569-178-3.
- [8] SUN, Rui, Zhazhong CUI a Ye TAO. PROGRESS OF CHINA 700°C USC DEVELOPMENT PROGRAM. In: *Advances in Materials Technology for Fossil Power Plants Proceedings from the Seventh International Conference October 22–25, 2013 Waikoloa, Hawaii, USA*. Hawaii: ASM International, 2014, s. 1-8. ISBN 978-1627080606.
- [9] VISWANATHAN, Vis, Robert PURGERT a Patricia RAWLES. Coal - fired power materials. *Advanced materials and processes*. 2008, (August 2008): 47-49.
- [10] HSIEH, Chih-Chun a Weite WU. Overview of Intermetallic Sigma ( $\sigma$ ) Phase Precipitation in Stainless Steels. *ISRN Metallurgy*. 2012, (vol. 2012): 16s.
- [11] HORVÁTH, Jakub. Vliv velkých plastických deformací na vlastnosti žárovevných ocelí HR3C a SUPER 304H. Praha, 2014. Diplomová práce. České vysoké učení technické v Praze.
- [12] HORVÁTH, Ladislav, Irena ANDRŠOVÁ, Božena PODHORNÁ a Jakub HORVÁTH. Zpráva UJP 1584: Program MPO TIP „Materiálové řešení průmyslových zařízení pracujících s ultrapřehřátou parou“ Zpráva o průběhu řešení za rok 2014. Praha, 2014.
- [13] HORVÁTH, Ladislav, Irena ANDRŠOVÁ a Jakub HORVÁTH. Zpráva UJP 1639: Program TA ČR ALFA Zpráva o průběhu řešení za rok 2014 *Technologie ohybů trubek pro přestupní plochy přehříváků a mezipřehříváků progresivních konstrukcí kotlů (IV)*. Praha, 2014.

- [14] SMALLMAN, R. E. a A. H. W. NGAN. *Physical metallurgy and advanced materials*. 7th ed. / . Boston: Butterworth Heinemann, 2007. ISBN 978-0-7506-6906-1.
- [15] VISWANATHAN, Ramaswamy. *Damage mechanisms and life assessment of high-temperature components*. Metals Park, Ohio: ASM International, c1989. ISBN 0871703580.
- [16] *Žárupevné oceli a slitiny*. 1. vyd. V Žilině: ZUSI, 2002, 389 s. ISBN 80-968605-6-9.
- [17] ALANEME, K.K., S.M. HONG, I. SEN, E. FLEURY a U. RAMAMUTRY. Effect of copper addition on the fracture and fatigue crack growth behaviour of solution heat-treated SUS 304H austenitic steel. *Materials Science and Engineering A*. 2010, (527): 4600-4604.
- [18] *Handbook of Materials Selection: Chapter 3 Stainless steels*. Rochester Michigan: John Wiley a Sons, 2002. ISBN 978-0-471-35924-1.
- [19] KUBOŇ, Zdeněk a Lenka PEKAŘOVÁ. Materiálové řešení průmyslových zařízení pracujících s ultrapřehřátou parou: Závěrečná zpráva projektu FR-TI3/458. Ostrava, 2014.
- [20] VdTÜV-Werkstoffblatt 550. Warmfester Walz- und Schmiedestahl X10CrNiCuNb18-9-3 (1.4907). Německo: VdTÜV, 2008
- [21] PRABHA, B., P. SUNDARAMOORTHY, S. SURESH, S. MANIMOZHI a B. RAVISHANKAR. Studies on stress corrosion cracking of super 304H austenitic stainless steel. *Journals of material engineering and performance*. 2009, (18): 1294-1299.
- [22] PASTERNAK, Jerzy a Janusz DOBROZANSKI. Properties of Weld Joints on Superheater Coils Made from New Generation High Alloy Martensitic Steel Connected to Austenitic Creep-Resisting Steels and Supper Alloy Grades, for Supercritical Parameters. *Advanced Materials Research*. 2011, (Vol 278): 466-471.

- [23] *Datasheet: DMV 304 HCu*. 1. Germany: Salzgitter Mannesmann Stainless Tubes, 2008.
- [24] ZIELIŃSKI, A. Structure and properties of Super 304H steel for pressure elements of boilers with ultra-supercritical parameters. *Journal of achievements in materials and manufacturing engineering*. 2012, 2(55): 403-409.
- [25] WEST, D., J. HULANCE, R.L. HIGGINSON a G. WILCOX. Sigma phase precipitation in 347HFG stainless steel for supercritical power plant operation. In: *Advances in materials technology for fossil power plants: proceedings from the sixth International Conference, August 31-September 3, 2010, Santa Fe, New Mexico, USA*. Materials Park, Ohio: ASM International, c2011, p 972-985, ISBN 978-1-61503-724-7
- [26] *Datasheet: DMV 347 HFG*. 1. Germany: Salzgitter Mannesmann Stainless Tubes, 2008.
- [27] JANOVEC, Jiří, Jiří CEJP a Josef STEIDL. *Perspektivní materiály*. Vyd. 3., přeprac. V Praze: České vysoké učení technické, 2008. ISBN 978-80-01-04167-3.
- [28] ZHU, F., R.G. FAULKNER, R.L. HIGGINSON, S. SPINDLER, A. BAKER a C.D. HAMM. Prediction of microstructural evolution in austenitic stainless steels for extended life power plant application. In: *Advances in materials technology for fossil power plants: proceedings from the sixth International Conference, August 31-September 3, 2010, Santa Fe, New Mexico, USA*. Materials Park, Ohio: ASM International, c2011, p 949-961, ISBN 978-1-61503-724-7
- [29] ABOU-ELAZM, A. Saad, I. EI MAHALLAWI, R. ABDEL-KARIM a R. RASHAD. Failure investigation of secondary super-heater tubes in power boiler. *Engineering Failure Analysis*. 2009, (16): 433-448.

- [30] WARREN, A.D., R.L. HARNIMAN, Z. GUO, C.M. YOUNES, P.E.J. FLEWITT a T.B. SCOTT. Quantification of sigma-phase evolution in thermally aged 2205 duplex stainless steel. *J Mater Sci.* 2016, 2016(51), 694-707. DOI: 10.1007/s10853-015-9131-9
- [31] SIEURIN, Henrik a Rolf SANDSTRÖM. Sigma phase precipitation in duplex stainless steel 2205. *Materials science and engineering A.* 2007, 2007(444), 271-276.
- [32] SOPOUŠEK, Jiří. *Vybrané aspekty termodynamické stability a kinetiky karbonitridu Nb v oceli SUPER 304H.* Brno, 2013.
- [33] SOPOUŠEK, Jiří. *Termodynamická stabilita fází v oceli SUPER 304H.* Brno, 2013.
- [34] TODA, Yoshiaki a Fujio ABE. Prediction of Precipitation Sequences within Grains in 18Cr–8Ni Austenitic Steel by Using System Free Energy Method. *ISIJ International.* 2009, 3(49), 439-445.
- [35] The CALPHAD methodology. *Thermocalc* [online]. Sweden: Thermocalc software, 2017 [cit. 2017-08-22]. Dostupné z: <http://www.thermocalc.com/products-services/databases/the-calphad-methodology/>
- [36] Inspection certificate: Super 304H – heat F124139. 1. Japan: Sumitomo metals, 2011.
- [37] Inspection certificate: HR3C - heat F122036. 1. Japan: Sumitomo metals, 2011
- [38] *Buehler Sum-Met the science behind materials preparation; a guide to materials preparation and analysis.* Lake Bluff, IL: Buehler, 2004. p. 76. ISBN 0975289802.
- [39] PTÁČEK, Luděk. *Nauka o materiálu I. 2., opr. a rozš. vyd.* Brno: Akademické nakladatelství CERM, c2003. ISBN 8072042831.

- [40] Optical Microscopy. *Spectrographic* [online]. The Siding: Spectro, 2017 [cit. 2017-08-15]. Dostupné z: <http://www.spectrographic.co.uk/support/trouble-shooting/>
- [41] KARLÍK, Miroslav. *Úvod do transmisní elektronové mikroskopie*. Praha: České vysoké učení technické v Praze, 2011. ISBN 9788001047293.
- [42] Electron Microscopy for Biological Sciences. *Diamond* [online]. England: Diamond, 2018 [cit. 2017-08-16]. Dostupné z: <http://www.diamond.ac.uk/industry/Industry-News/Latest-News/Synchrotron-Industry-News-eBIC.html>
- [43] Facilities: Transmission electron microscope JEOL JEM-2100F. *Institute of physics of materials Academy of science of the Czech Republic* [online]. Brno: IPM, 2018 [cit. 2017-08-16]. Dostupné z: <http://www.ipm.cz/vybaveni-transmisni-elektronovy-mikroskop-jeol-jem-2100f.html>
- [44] Transmission electron microscopy. In: *Wikipedia: the free encyclopedia* [online]. San Francisco (CA): Wikimedia Foundation, 2001- [cit. 2017-08-16]. Dostupné z: [https://en.wikipedia.org/wiki/Transmission\\_electron\\_microscopy](https://en.wikipedia.org/wiki/Transmission_electron_microscopy)
- [45] ZHOU, Weili. a Zhong Lin. WANG. *Scanning microscopy for nanotechnology: techniques and applications*. New York: Springer, 2007. p. 42-75 ISBN 9780387333250.
- [46] ČSN EN ISO 6892-1: *Metallic materials - Tensile testing - Part 1: Method of test at room temperature*. 1. Prague: ÚNMZ, 2007.
- [47] ČSN EN ISO 148-1: *Metallic materials - Charpy pendulum impact test - Part 1: Test method*. 1. Prague: ÚNMZ, 2007.
- [48] HORVÁTH, Ladislav, Jindřich DOUDA, Jakub HORVÁTH a Marie SVOBODOVÁ. Degradation of Czechoslovak creep resistant steels after 50 years of service. *Materials engineering/materiálové inžinierstvo*. Žilina: Faculty of mechanical engineering university of Žilina, 2014, 2(21), 80-87. ISSN 13350803.

- [49] HORVÁTH, Jakub, Jiří JANOVEC a Marie SVOBODOVÁ. Impact of plastic deformation on thermal induced structural changes in HR3C steel. In: *Zvyšování životnosti komponent energetických zařízení v elektrárnách: Sborník z 9. konference. Plzeň: ZČU, 2014, s. 153-158. ISBN 978802614063.*
- [50] HERMANOVÁ, Šárka, Ladislav KANDER a Jakub HORVÁTH. The Effect of Cold Bending Process and Degradation at Boiler Conditions on the Properties of New Austenitic Creep Resistant Steel SUPER 304H for Boiler Super-heaters Tubes. *Materials Science Forum*. 2017, (891), 230-234. ISSN 0255-5476.
- [51] HERMANOVÁ, Šárka, Radomír ČINČILA, Jakub HORVÁTH a Jiří JANOVEC. INFLUENCE OF COLD BENDING OF STRUCTURAL STABILITY OF USC OUTLET SUPERHEATER MADE FROM AUSTENITIC CREEP RESISTANT STEELS In: *Zvyšování životnosti komponent energetických zařízení v elektrárnách: Sborník z 10. konference. Plzeň: Západočeská univerzita v Plzni, 2015, s. 89-92. ISBN 978-80-261-0522-0.*
- [52] HORVÁTH, Jakub, Petr KRÁL a Jiří JANOVEC. The Effect of Sigma-Phase Formation on Long-Term Durability of Welding Joints in SUPER 304H Steels. *Acta Physica Polonica A*. Warsaw, 2016, 130(4), 960-962. ISSN 0587-4246.
- [53] HORVÁTH, Jakub, Petr KRÁL, Jiří JANOVEC a Václav SKLENIČKA. THE EFFECT OF SIGMA-PHASE FORMATION ON LONG-TERM DURABILITY OF SUPER 304H STEEL. *METAL 2015: 24TH INTERNATIONAL CONFERENCE ON METALLURGY AND MATERIALS*. Brno, CZECH REPUBLIC: Tanger, 2015, s. 505-510. ISBN 978-80-87294-62-8.
- [54] HORVÁTH, Jakub, Michal JUNEK a Jiří JANOVEC. The Changes in Mechanical Properties of Austenitic Creep Resistant Steels SUPER 304H and HR3C Caused by Medium-term Isothermal Ageing. *Solid State Phenomena*. 2017, 258, 639-642. ISSN 1012-0394.
- [55] MÍKA, Vladimír. Kinetika sdílení hmoty. In: *VSČT: Ústav chemického inženýrství* [online]. Praha: VSČT, 2006 [cit. 2018-02-13]. Dostupné z: <https://vscht.cz/uchi/ped/chi/chi.ii.text.k22.kinetika.sdileni.hmoty.pdf>



- [56] ROKYTA, Mirko. *Parciální diferenciální rovnice I: Klasická teorie* [online]. Verze textu ze dne 14.ledna 2011. Praha: Univerzita Karlova, 2011 [cit. 2018-02-13]. Dostupné z:  
<https://www.karlin.mff.cuni.cz/~rokyta/vyuka/1011/zs/Pdr1/texopis/PDR1-20110114.pdf>
- [57] JANOVSÁ, Drahoslava. Matematika pro chemické inženýry: Prciální diferenciální rovnice. In: *VSČT: Ústav matematiky, fakulta chemicko-inženýrská* [online]. Praha: VSČT, 2016 [cit. 2018-02-13]. Dostupné z:  
[https://old.vscht.cz/mat/MCHI/13\\_prednaska\\_2015.pdf](https://old.vscht.cz/mat/MCHI/13_prednaska_2015.pdf)
- [58] DRÁPALA, Jaromír. Pěstování krystalů Czochralského metodou (Hurle, Cochrayne): DIFUZNÍ PROCESY V PEVNÝCH LÁTKÁCH SE ZAMĚŘENÍM NA RŮST A LEGOVÁNÍ KRYSTALŮ. In: *The Czechoslovak Association for Crystal Growth (CSACG)* [online]. Ostrava: Institute of Physics Academy of Sciences of the Czech Republic, 2017 [cit. 2018-02-14]. Dostupné z:  
[http://csacg.fzu.cz/func/viewpdf.php?file=2004\\_37Drapala.pdf](http://csacg.fzu.cz/func/viewpdf.php?file=2004_37Drapala.pdf)
- [59] REKTORYS, Karel. *Přehled užití matematiky*. Praha: Státní nakladatelství technické literatury (SNTL), 1963.
- [60] BRANDES, Eric A., G. B. BROOK a Colin J. SMITHELLS. *Smithells metals reference book*. 7th ed / edited by E.A. Brandes and G.B. Brook. Boston: Butterworth-Heinemann, 1998. ISBN 0750636246.

## 8.2 Authors publications

The author's publications since 2014 to 2018 are summarised by this chapter.

### 8.2.1 Impact and WoS publications

- (1) HORVÁTH, Jakub, Petr KRÁL a Jiří JANOVEC. The Effect of Sigma-Phase Formation on Long-Term Durability of Welding Joints in SUPER 304H Steels. *Acta Physica Polonica A*. Warsaw, 2016, 130(4), 960-962. ISSN 0587-4246. [52]
- (2) HORVÁTH, Jakub, Michal JUNEK a Jiří JANOVEC. The Changes in Mechanical Properties of Austenitic Creep Resistant Steels SUPER 304H and HR3C Caused by Medium-term Isothermal Ageing. *Solid State Phenomena*. 2017, 258, 639-642. ISSN 1012-0394. [54]
- (3) JUNEK, Michal, Marie SVOBODOVÁ, Jiří JANOVEC a Jakub HORVÁTH. Mechanical Properties and Microstructures of Narrow Gap Orbital Welded P91 Steel. *Solid State Phenomena*. 2017, 258, 635-638. ISSN 1012-0394.
- (4) HORVÁTH, Jakub, Petr KRÁL, Jiří JANOVEC a Václav SKLENIČKA. THE EFFECT OF SIGMA-PHASE FORMATION ON LONG-TERM DURABILITY OF SUPER 304H STEEL. *METAL 2015: 24TH INTERNATIONAL CONFERENCE ON METALLURGY AND MATERIALS*. Brno, CZECH REPUBLIC: Tanger, 2015, s. 505-510. ISBN 978-80-87294-62-8. [53]
- (5) HERMANOVÁ, Šárka, Ladislav KANDER a Jakub HORVÁTH. The Effect of Cold Bending Process and Degradation at Boiler Conditions on the Properties of New Austenitic Creep Resistant Steel SUPER 304H for Boiler Super-heaters Tubes. *Materials Science Forum*. 2017, (891), 230-234. ISSN 0255-5476. [50]
- (6) HORVÁTH, Jakub. The influence of high temperature overheating to microstructure of degraded steel SUPER 304H. *METAL 2018: 27TH INTERNATIONAL CONFERENCE ON METALLURGY AND MATERIALS*. Brno, CZECH REPUBLIC: Tanger, 2018 (Under review)

### 8.2.2 Indexed and other publications

- (7) HORVÁTH, Jakub a Jiří JANOVEC. MODELING AND VERIFICATION OF THE CLADDING TUBE BEND. *INTERNATIONAL JOURNAL OF ENGINEERING SCIENCES & RESEARCH TECHNOLOGY*. 2015, 4(10), 491-495. ISSN 2277-9655.
- (8) HORVÁTH, Ladislav, Jindřich DOUDA, Jakub HORVÁTH a Marie SVOBODOVÁ. Degradation of Czechoslovak creep resistant steels after 50 years of service. *Materials engineering/materiálové inženýrstvo*. Žilina: Faculty of mechanical engineering university of Žilina, 2014, 2(21), 80-87. ISSN 13350803.
- (9) HORVÁTH, Jakub, Jiří JANOVEC a Marie SVOBODOVÁ. Impact of plastic deformation on thermal induced structural changes in HR3C steel. In: *Zvyšování životnosti komponent energetických zařízení v elektrárnách: Sborník z 9. konference*. Plzeň: ZČU, 2014, s. 153-158. ISBN 978802614063. [49]
- (10) HORVÁTH, Jakub, Petr KRÁL, Jiří JANOVEC a Václav SKLENIČKA. THE EFFECT OF SIGMA-PHASE FORMATION ON LONG-TERM DURABILITY OF SUPER 304H STEEL. In: *Metal 2015: 24th International conference on Metallurgy and materials*. Ostrava: Tanger, 2015, s. 57-58. ISBN 978-80-87294-58-1.
- (11) HORVÁTH, Jakub. 2015. FAILURE ANALYSIS OF PAPER MACHINE SHAFT. *Powder metallurgy progress*. Košice, 15(SS): 175-180. ISSN 1339-4533.
- (12) HERMANOVÁ, Šárka, Radomír ČINČILA, Jakub HORVÁTH a Jiří JANOVEC. INFLUENCE OF COLD BENDING OF STRUCTURAL STABILITY OF USC OUTLET SUPERHEATER MADE FROM AUSTENITIC CREEP RESISTANT STEELS In: *Zvyšování životnosti komponent energetických zařízení v elektrárnách: Sborník z 10. konference*. Plzeň: Západočeská univerzita v Plzni, 2015, s. 89-92. ISBN 978-80-261-0522-0. [51]

- (13) HORVÁTH, Jakub, Jiří JANOVEC a Michal JUNEK. Influence of the Diffusion Effect Caused by Welding Heat Input Lead to the Changes of Mechanical Properties Which Entering into the FEM Model of Cladding Tube Bending. *International Journal of Materials Science and Applications*. 2015, 4(6), 403-408. ISSN 2327-2635.
- (14) HORVÁTH, Jakub, Petr KRÁL, Jiří JANOVEC a Václav SKLENIČKA. The Effect of Microstructure Changes of Steel SUPER 304H during Laboratory Thermal Exposition. in: *Functionalized Nanostructures Towards Engineered Macrostructures*. 1. Jindřichův hradec: Epika, 2015, s. 131-141. ISBN 978-80-88113-20-1.
- (15) HORVÁTH, Jakub, Ladislav HORVÁTH a Josef ČMAKAL. PROPERTIES OF THE HIGH EXPOSED CLADDING TUBE BEND. In: *Zvyšování životnosti komponent energetických zařízení v elektrárnách: Sborník z 11. konference*. 1. Plzeň: Západočeská univerzita v Plzni, 2016, s. 123-126. ISBN 978-80-261-0644-9.
- (16) JANOVEC, Jiří a Jakub HORVÁTH. Použití plátovaných trubek pro tlaková zařízení. In: *Tlak 2016*. Líbeznice: Medim, 2016, s. 55-62. ISBN 978-80-87140-41-3.
- (17) HORVÁTH, Jakub, Michal JUNEK a Jiří JANOVEC. The Changes in Mechanical Properties of Austenitic Creep Resistant Steels SUPER 304H and HR3C Caused by Medium-term Isothermal Ageing. In: *Materials structure a micromechanics of fracture: Abstrat booklet*. Brno: VUTIUM, 2016, s. 216. ISBN 978-80-214-5357-9.
- (18) JUNEK, Michal, Marie SVOBODOVÁ, Jiří JANOVEC a Jakub HORVÁTH. Mechanical Properties and Microstructures of Narrow Gap Orbital Welded P91 Steel. In: *Materials structure a micromechanics of fracture: Abstrat booklet*. Brno: VUTIUM, 2016, s. 215. ISBN 978-80-214-5357-9.

- (19) HORVÁTH, Jakub, Jiří JANOVEC a Ladislav HORVÁTH. *VLIV LABORATORNÍ TEPLONÍ EXPOZICE NA ZPŮSOB MECHANICKÉHO PORUŠOVÁNÍ AUSTENITICKÉ OCELE HR3C*. Sborník příspěvků z 12. konference "Zvyšování životnosti komponent energetických zařízení v elektrárnách": Plzeň: Západočeská universita, 2017, 151-154. ISBN 978-80-261-0741-5.
- (20) HORVÁTH, Ladislav, Jakub HORVÁTH a Jiří JANOVEC. *POUŽITÍ PLÁTOVANÝCH TRUBEK NA KRITICKÁ MÍSTA KOTLŮ PRO ENERGETIKU*. Sborník příspěvků z 12. konference "Zvyšování životnosti komponent energetických zařízení v elektrárnách": Plzeň: Západočeská universita, 2017, 103-106. ISBN 978-80-261-0741-5.
- (21) JANOVEC, Jiří, Jakub HORVÁTH a Michal JUNEK. *ZVYŠOVÁNÍ ŽIVOTNOSTI KOMPONENT UHELNÝCH ELEKTRÁREN A SPALOVEN UŽITÍM NiCr TERMÁLNÍCH METALICKÝCH NÁSTŘIKŮ*. Sborník příspěvků z 12. konference "Zvyšování životnosti komponent energetických zařízení v elektrárnách": Plzeň: Západočeská universita, 2017, 97-102. ISBN 978-80-261-0741-5.

## 9 Lists

### 9.1 List of the abbreviations and variables

|                                 |                                    |                                |
|---------------------------------|------------------------------------|--------------------------------|
| A                               | Annealed                           | Heat treatment                 |
| A                               | Elongation                         | Mechanical property            |
| Å                               | Angstrom                           | Measurement unit               |
| A-USC                           | Advanced ultra supercritical       | Type of the working parameters |
| B                               | Boron                              | Chemical element               |
| BCC                             | Body cubic centre                  | Lattice type                   |
| BF                              | Bright field                       | Microscopy display             |
| BM                              | Base material                      |                                |
| C                               | Carbon                             | Chemical element               |
| $C_p$                           | Precipitate concentration          |                                |
| $C_0$                           | Initial concentration              |                                |
|                                 |                                    |                                |
| Co                              | Cobalt                             | Chemical element               |
| Cu                              | Copper                             | Chemical element               |
| CCGT                            | Combined cycle gas turbine         |                                |
| CH <sub>3</sub> COOH            | Acetic acid                        | Acid                           |
| Cr                              | Chromium                           | Chemical element               |
| Cr <sub>23</sub> C <sub>6</sub> | Chromium carbide                   | Chemical compound              |
| D                               | Diffusivity                        |                                |
| $D_0$                           | Diffusion coeficient               |                                |
| DMV                             | Mannesmann seamless tubes marking  |                                |
| E                               | Young module of elasticity         | Mechanical property            |
| E-A                             | Exposed annealed material          |                                |
| E-NA                            | Exposed nonannealed material       |                                |
| EBS                             | Electron backscattered diffraction | Experimental method            |
| EDS                             | Energy disperse spectrometry       | Experimental method            |

|                  |                                      |                     |
|------------------|--------------------------------------|---------------------|
| EPRI             | Electric Power Research<br>Institute |                     |
| Etc.             | et cetera                            | Shortcut            |
| FCC              | Face cubic centre                    | Lattice type        |
| FCT              | Face centre tetragonat               | Lattice type        |
| FIB              | Focused ion beam                     | Experimental method |
| GB               | Grain boundary                       |                     |
| Gg               | Matrix enthalpy                      |                     |
| Gp               | Precipitate enthalpy                 |                     |
| Gs               | Solid solution enthalpy              |                     |
| GWh              | Giga watt hours                      | Measurement unit    |
| HAZ              | Heat affected zone                   |                     |
| HCl              | Hydrochloric acid                    | Acid                |
| h                | Hour                                 | Measurement unit    |
| hr               | Hour                                 | Measurement unit    |
| HT               | Heat treatment                       |                     |
| IEA              | International energy<br>agency       |                     |
| LM               | Light microscopy                     | Diagnostic method   |
| LMP              | Larson-Miller parameter              | Parameter           |
| mils/yr          | Mils per year                        | Measurement unit    |
| mm/yr            | Millimeters per year                 | Measurement unit    |
| Mn               | Manganese                            | Chemical element    |
| Mo               | Molybdenum                           | Chemical element    |
| MPa              | Megapascal                           | Measurement unit    |
| MW               | Mega watt                            | Measurement unit    |
| N                | Nitrogen                             | Chemical element    |
| NA               | Not annealed                         | Heat treatment      |
| Nb               | Niobium                              | Chemical element    |
| NbC              | Niobium carbide                      | Chemical compound   |
| NHO <sub>3</sub> | Nitric acid                          | Acid                |
| Ni               | Nickel                               | Chemical element    |
| Qd               | Activation energy                    | Measurement unit    |
| R                | Gas constant                         |                     |

|                   |                                  |                                |
|-------------------|----------------------------------|--------------------------------|
| RH                | Reheater                         | Heat exchanging surface        |
| R <sub>e</sub>    | Yield strength                   | Mechanical property            |
| R <sub>m</sub>    | Ultimate strength                | Mechanical property            |
| R <sub>p0,2</sub> | Yield strength 0,2%              | Mechanical property            |
| R <sub>p1</sub>   | Yield strength 1%                | Mechanical property            |
| R <sub>T</sub>    | Room temperature                 | About 20°C                     |
| SEM               | Scanning electron microscopy     | Experimental method            |
| SH                | Superheater                      | Heat exchanging surface        |
| STEM              | Scanning transmission microscopy | Experimental method            |
| T                 | Absolute temperature             | Measurement unit               |
| Ta                | Tantalum                         | Chemical element               |
| TEM               | Transmission electron microscopy | Experimental method            |
| Ti                | Titanium                         | Chemical element               |
| TWh               | Tera watt hour                   | Measurement unit               |
| USC               | Ultra supercritical              | Type of the working parameters |
| U.T.S.            | Ultimate strength                | Mechanical property            |
| V                 | Vanadium                         | Chemical element               |
| W                 | Tungsten                         | Chemical element               |
| Wt.%              | Weight %                         | Measurement unit               |
| X                 | Diffusion distance               | 1D distance                    |
| Y.S.              | Yield strength                   | Mechanical property            |
| Zr                | Zirconium                        | Chemical element               |
| °C                | Degree of celsius                | Measurement unit               |



## 9.2 List of the tables

|         |   |    |
|---------|---|----|
| Tab. 1  | Chemical composition in mass % according ASME Case 2328-1 [23].....                   | 24 |
| Tab. 2  | Mechanical properties according ASME Code Case 2328-1 [23] .....                      | 24 |
| Tab. 3  | Creep rupture strength of steel SUPER 304H [24].....                                  | 25 |
| Tab. 4  | Creep rupture strength of steel SUPER 304H by [23] .....                              | 26 |
| Tab. 5  | Tp 347HFG chemical composition in Wt. % [25] .....                                    | 26 |
| Tab. 6  | Chemical composition in mass % according ASME SA-213/SA-213M [26].....                | 27 |
| Tab. 7  | Mechanical properties according ASME SA-213/SA-213M [26].....                         | 27 |
| Tab. 8  | The creep values of steel Tp 347HFG by [26].....                                      | 27 |
| Tab. 9  | Mechanical properties of SUPER 304H by copper content [17].....                       | 33 |
| Tab. 10 | SUS 304H mechanical properties after short them aging [29] .....                      | 34 |
| Tab. 11 | Chemical composition of supplied steel SUPER 304H [36] .....                          | 48 |
| Tab. 12 | Mechanical properties of supplied steel SUPER 304H [36] .....                         | 49 |
| Tab. 13 | Chemical composition of used steel HR3C [37] .....                                    | 49 |
| Tab. 14 | Characteristic of degradation phase of structure [48] .....                           | 57 |
| Tab. 15 | Measured chemical composition (Fig. 73) [50] .....                                    | 62 |
| Tab. 16 | Microstructure characteristics in base material and welding joints zones [52]64       |    |
| Tab. 17 | Chemical composition of sigma-phase – State after 15 000 hours of ageing<br>[53]..... | 68 |
| Tab. 18 | Chemical measurement results for Fig. 93.....   | 74 |
| Tab. 19 | Results of tensile testing of SUPER 304H and HR3C steels [54] .....                   | 83 |
| Tab. 20 | Results of impact testing of SUPER 304 and HR3C steels [54].....                      | 84 |
| Tab. 21 | Diffusivity calculation coefficients [60].....  | 92 |
| Tab. 22 | Calculated coefficient for steel SUPER 304H .....                                     | 93 |
| Tab. 23 | Calculated coefficient for steel Tp 347HFG .....                                      | 93 |
| Tab. 24 | Calculated specific coefficients ration.....  | 94 |
| Tab. 25 | Measured sigma phase fraction area for Tp 347HFG.....                                 | 95 |
| Tab. 26 | Calculated and measured results comparison .....                                      | 96 |

### 9.3 List of the figures

|         |   |    |
|---------|---|----|
| Fig. 1  | The electricity production development in the Czech Republic since year 2007 to 2016 [1].....   | 4  |
| Fig. 2  | The constitution of energy production by source in the Czech Republic in year 2016 [1] .....  | 4  |
| Fig. 3  | Annual power generation in Japan [2] .....  | 5  |
| Fig. 4  | IEA predictions for the development pf power production divided on primary fuels [4].....   | 5  |
| Fig. 5  | Four case study parameters set up for the 500MW power plant [2].....  | 6  |
| Fig. 6  | Estimate thermal efficiency for parameters listed in Fig. 5 [2].....  | 6  |
| Fig. 7  | Design parameters for the power plants examined in EPRI's 2008 study [5].....   | 7  |
| Fig. 8  | Key economic results from A-USC study – Assumes no cost penalty for CO <sub>2</sub> emission [5] .....                                    | 7  |
| Fig. 9  | The scheme of steam working parameters development in USA [6] .....   | 9  |
| Fig. 10 | Heat rate of steam power plants in Germany as a function of steam parameters since the year 1900 [7] .....                                | 9  |
| Fig. 11 | Steam parameter evolution of -Chinese fossil power plants [8].....  | 9  |
| Fig. 12 | Trends in steam condition in Japan [2].....   | 9  |
| Fig. 13 | Schematic illustration of creep curve changes with increasing stress and temperature [15] .....   | 12 |
| Fig. 14 | Historical improvement in creep rupture strength of boiler steels [7] .....   | 14 |
| Fig. 15 | Bill of Materials for various components of USC and A-USC coal-fired power plant boiler steam condition[9].....                           | 15 |
| Fig. 16 | General concept of alloy design for austenitic heat-resistant steels [7] .....  | 15 |
| Fig. 17 | Effect of Nb on creep rupture strength of 18Cr–8Ni steels [7] .....   | 17 |
| Fig. 18 | Effect of (Ti + Nb)/C ratio on creep rupture strength of 18Cr10NiNbTi steel [7]17   |    |
| Fig. 19 | Effect of Cu on creep rupture strength of 18Cr–8Ni steels [7].....  | 18 |
| Fig. 20 | The sigma phase lattice parameters depending on the chemical composition [10].....  | 19 |
| Fig. 21 | The sigma phase precipitation time – temperature dependence for system 19/9 [10].....   | 19 |
| Fig. 22 | The sigma phase precipitation scheme [10] .....   | 20 |
| Fig. 23 | Progress of the sigma phase precipitation in steel AISI 316L [10].....  | 21 |
| Fig. 24 | The sigma phase precipitation curves for various modification of austenitic steels [16] .....   | 21 |
| Fig. 25 | The influence of Si, Cr, Mn, Ni and C content to sigma phase precipitation (annealing 1250°C and exposition 1000 hours/ 850°C) [16] ..... | 22 |
| Fig. 26 | Time to rupture – temperature diagram for tension of 150 MPa [24] .....   | 25 |
| Fig. 27 | Time to rupture – temperature diagram for tension of 180 MPa [24] .....   | 25 |
| Fig. 28 | Development progress of austenitic boiler steels [7] .....  | 28 |
| Fig. 29 | Nominal chemical composition of austenitic steels for boilers [7].....  | 28 |

|         |   |    |
|---------|---|----|
| Fig. 30 | The chemical composition comparison [23][26].....   | 29 |
| Fig. 31 | Double binary diagram Fe-Cr and Fe-Ni [27] .....  | 29 |
| Fig. 32 | The initial state of steel SUPER 304H [24].....   | 31 |
| Fig. 33 | Microstructure of steel SUPER 304H after 3000 hours of ageing at 700°C [24]   | 31 |
| Fig. 34 | EBSD orientation map and phase map of type 316H [28] .....  | 31 |
| Fig. 35 | Fraction surface of type 316H steel with black pointed sigma phase [28] .....   | 32 |
| Fig. 36 | Sigma phase in 347HFG after a) 5 000 hours and b) 10 000 hours of aged 750°C [25].....  | 32 |
| Fig. 37 | Area fraction of the sigma phase in 347 HFG stainless steel [25] .....  | 33 |
| Fig. 38 | Yield and ultimate strengths for exposed material. Exposition parameters 650°C, exposition time 1000 and 3000 hours [24] .....        | 35 |
| Fig. 39 | Yield and ultimate strengths for exposed material. Exposition parameters 700°C, exposition time 1000 and 3000 hours [24] .....        | 35 |
| Fig. 40 | Elongation of exposed material. Exposition parameters 650°C, exposition time 1000 and 3000 hours [24] .....                           | 35 |
| Fig. 41 | Elongation of exposed material. Exposition parameters 700°C, exposition time 1000 and 3000 hours [24] .....                           | 35 |
| Fig. 42 | The impact strength of initial and exposed steel [24].....  | 36 |
| Fig. 43 | Schematic representation of constant stress lines for Larson-Miller parameter [15].....   | 37 |
| Fig. 44 | Schematic representation of constant stress lines for Orr-Sherby-Dorn parameter [15].....   | 38 |
| Fig. 45 | Schematic representation of constant stress lines for Manson-Haferd parameter [15].....   | 38 |
| Fig. 46 | The sigma phase precipitation scheme in stainless duplex steel[30].....   | 39 |
| Fig. 47 | Results of modelling for steel type 316H[28] .....  | 40 |
| Fig. 48 | Phase predicted in 347HFG stainless steel with Thermo-Calc software [25]....  | 41 |
| Fig. 49 | Modelled coexist phases for chemical composition of steel SUPER 304H [32]   | 41 |
| Fig. 50 | Chemical composition of sigma phase is SEUPR 304H steel dependence on temperature [32] .....  | 42 |
| Fig. 51 | Isothermal phase diagram of steel SUPER 304H at temperature 800°C [33]....  | 42 |
| Fig. 52 | Isothermal phase diagram of steel SUPER 304H at temperature 700°C [33]....  | 43 |
| Fig. 53 | Isothermal phase diagram of steel SUPER 304H at temperature 600°C [33]....  | 43 |
| Fig. 54 | A schematic illustration of the change in free energy during the precipitation of $M_{23}C_6$ and s phase from the g matrix [34]..... | 45 |
| Fig. 55 | Furnace used for isothermal aging.....  | 50 |
| Fig. 56 | The furnace cavity interior .....   | 50 |
| Fig. 57 | Optical system of metallurgical microscope [40] .....   | 52 |
| Fig. 58 | Nikon eclipse MA200 – Optical microscope .....  | 52 |
| Fig. 59 | Scheme of scanning electron microscope [42].....  | 53 |
| Fig. 60 | SEM microscope Jeol JSM-7600F .....   | 53 |

|         |   |    |
|---------|---|----|
| Fig. 61 | The scheme of transmission electron microscope [44].....  | 54 |
| Fig. 62 | Transmission electron microscope JEOL JEM-2100F [43].....   | 54 |
| Fig. 63 | Schematic arrangement of sample orientation in the SEM [45].....  | 55 |
| Fig. 64 | The tensile test specimen drawing.....  | 56 |
| Fig. 65 | The pendulum impact test specimen drawing.....  | 56 |
| Fig. 66 | The dependence of hardness on globularisation of cementite for ČSN steel 12 022 [48].....   | 57 |
| Fig. 67 | The dependence of strength on hardness of ČSN steel 12 022 [48].....  | 57 |
| Fig. 68 | The dependence of tensile strength on structural parameters [48].....   | 58 |
| Fig. 69 | Grain boundary in neutral wall of R60 bend without HT, aged 15000 hours/650°C [49] .....  | 61 |
| Fig. 70 | Grain boundary in pressured wall of R60 bend without HT, aged 15000 hours/650°C [49] .....  | 61 |
| Fig. 71 | SEM microstructure of parent material after exposition in boiler conditions [50].....   | 61 |
| Fig. 72 | SEM annealed microstructure of parent material after exposition in boiler conditions [50].....  | 61 |
| Fig. 73 | Analysed particles in microstructure [50].....  | 62 |
| Fig. 74 | The EDS spectra measured for difference particle (Fig. 73) [50] .....   | 62 |
| Fig. 75 | Microstructure and Cr map of base material (left) and aged by 20000 hours (right) [51].....   | 63 |
| Fig. 76 | Microstructure of as-received state in crown layer [52] .....   | 64 |
| Fig. 77 | Formation of $\sigma$ phase after aging $2 \times 10^4$ h [52] .....  | 64 |
| Fig. 78 | Distribution of $\sigma$ -phase in the crown layer [52].....  | 65 |
| Fig. 79 | Distribution of $\sigma$ -phase in the root layer [52].....   | 65 |
| Fig. 80 | Distribution of elements around austenitic grain boundary [52] .....  | 65 |
| Fig. 81 | TEM image of $\sigma$ -phase cross-section [52].....  | 65 |
| Fig. 82 | SEM analyses around grain boundaries.....   | 66 |
| Fig. 83 | TEM analysis of particles.....  | 67 |
| Fig. 84 | Lattice parameters and chemical composition of the sigma phase [10].....  | 68 |
| Fig. 85 | Identification of particles and sigma-phase – State after 15 000 hours of ageing [53].....  | 68 |
| Fig. 86 | Kikutchi lines obtained in the analysis of sigma phase in the steel Super 304H a) measured lines b) conformity with the theoretical model [53]..... | 69 |
| Fig. 87 | EBSD phase map analysis [53].....   | 69 |
| Fig. 88 | Maps of chemical composition SEM/EDS – State after 15 000 of ageing [53]..  | 70 |
| Fig. 89 | Maps of chemical composition TEM/EDS - State after 15 000 of ageing [53] ...  | 71 |
| Fig. 90 | Maps of chemical composition SEM/EDS – State after 20 000 of ageing [53]..  | 72 |
| Fig. 91 | Microstructure after color etching (sigma-phase white) [53].....  | 73 |
| Fig. 92 | Microstructure with marked phases for comparison with Fig. 91 [53].....   | 73 |
| Fig. 93 | EDS point analysis for correlation sample .....   | 74 |

---

|          |   |    |
|----------|---|----|
| Fig. 94  | Comparative image for sigma phase verification for optical microscopy .....                                 | 75 |
| Fig. 95  | LMP 23589 NA (3) .....  | 77 |
| Fig. 96  | LMP 23057 NA (1) .....  | 77 |
| Fig. 97  | LMP 23681 NA (4) .....  | 77 |
| Fig. 98  | LMP 24305 NA (7) .....  | 77 |
| Fig. 99  | LMP 23800 NA (5) .....  | 78 |
| Fig. 100 | LMP 23253 NA (2) .....  | 78 |
| Fig. 101 | LMP 23883 NA (6) .....  | 78 |
| Fig. 102 | LMP 24513 NA (8) .....  | 78 |
| Fig. 103 | LMP 23589 A (3) .....   | 79 |
| Fig. 104 | LMP 23057 A (1) .....   | 79 |
| Fig. 105 | LMP 23681 A (4) .....   | 79 |
| Fig. 106 | LMP 24305 A (7) .....   | 79 |
| Fig. 107 | LMP 23800 A (5) .....   | 80 |
| Fig. 108 | LMP 23253 A (2) .....   | 80 |
| Fig. 109 | LMP 23883 A (6) .....   | 80 |
| Fig. 110 | LMP 24513 A (8) .....   | 80 |
| Fig. 111 | Evolving of the sigma phase fraction area to LMP .....  | 81 |
| Fig. 112 | Evolving of the sigma phase fraction area to LMP for NA state .....   | 82 |
| Fig. 113 | Evolving of the sigma phase fraction area to LMP for A state .....  | 82 |
| Fig. 114 | Ductile fracture surface of as-received SUPER 304H steel.....   | 84 |
| Fig. 115 | Brittle fracture surface of exposed SUPER 3004H steel in E-NA state .....                                   | 84 |
| Fig. 116 | Ductile fracture surface of as-received HR3C steel [54].....  | 85 |
| Fig. 117 | Brittle fracture surface of exposed HR3C steel in E-NA state [54] .....                                     | 85 |
| Fig. 118 | Sigma phase with its chemical composition (Spectrum 1) on fracture surface<br>of SUPER 304H steel [54]..... | 85 |
| Fig. 119 | Sigma phase with its chemical composition (Spectrum 1) on fracture surface<br>of HR3C steel [54] .....      | 85 |
| Fig. 120 | Fracture surface of as-received state after long-term ageing [52].....                                      | 86 |
| Fig. 121 | Evolving of the sigma phase fraction area to LMP for SUPER 304H NA state ...                                | 95 |